Studies on Synthetic Methods and Physicochemical Properties of Various Rare Earth Phosphates

Onoda, Hiroaki

(Degree)
博士（工学）

(Date of Degree)
2002-03-31

(Date of Publication)
2013-04-24

(Resource Type)
doctoral thesis

(Report Number)
甲2541

(URL)
https://hdl.handle.net/20.500.14094/D1002541

博士論文

Studies on Synthetic Methods and Physicochemical Properties of Various Rare Earth Phosphates

- 種々の希土類リン酸塩の合成方法及び物理化学的性質の研究 -

平成14年1月

神戸大学大学院自然科学研究科

斧田　宏明

要旨

リン酸塩は加熱などにより脱水縮合反応や加水分解反応を起こし、種々のリン酸塩へと変化することが知られている。リン酸塩は単量体であるオルソリン酸塩と縮合リン酸塩とに大別される。縮合リン酸塩は正四面体構造のPO_4ユニットが鎖状、環状、層状、三次元網目状などに連結した構造を有する無機高分子である。それらの構造はそれぞれ特徴のある性質を持っており、種々のリン酸塩の合成とその性質の解明は利用にむけての第一歩として重要である。希土類オルソリン酸塩は、モナズ石やゼノタイムなどの希土類鉱石の主成分である。また、三次元網目状構造を有するウルトラリン酸塩は、一般的には容易に加水分解されるが、希土類塩では比較的安定に存在することが知られており、レーザー源等に用いられている。本研究では、種々の希土類リン酸塩の合成について、主に合成法の観点から検討するとともに、合成されたリン酸塩について熱挙動や触媒物性などについて評価した。

第1章では、希土類酸化物とリン酸水素二アンモニウムの混合物を加熱することによって、希土類リン酸塩を合成する過程での原料の混合条件について比較検討した。固体物質に摩砕等の機械的エネルギーを加えることにより、物質の物理化学的性質が変化したり、化学反応が起こることが知られており、これらの現象はメカノケミカル効果と総称されている。また、この効果を高めるため、種々の摩砕助剤の利用が報告されている。本実験系においても、機械的な処理により、原料混合物が均一化されるとともに活性化された。摩砕助剤として水やエタノールを用いると、生成する希土類リン酸塩の種類やその生成温度に影響が現れた。その際、希土類酸化物はリン酸水素二アンモニウムとの反応性に乏しく、希土類リン酸塩の生成温度が高く、そのため混合条件による変化が現れにくかった。そこで、より低温度での希土類リン酸塩の生成を目的として、種々の希土類化合物について比較検討することにした。

第2章では、リン酸水素二アンモニウムあるいはリン酸と、種々の希土類化合物(酸化物、硝酸塩、塩化物、炭酸塩、硫酸塩、シュウ酸塩及びフッ化物)とを混合し加熱することによって生成する希土類リン酸塩を調べた。酸化セリウムを原料とすると生成しないRhabdophane型オルソリン酸塩が、硝酸塩、塩化物あるいは炭酸塩を原料とした場合に生成した。また、他の希土類塩においても、希土類硝酸塩、塩化物あるいは炭酸塩を用いることにより、希土類リン酸塩の生成温度の低下や結晶性の向上が観察された。そこで、さらにこれらの系についてもメカノケミカル効果を調べることにした。

第3章では、リン酸水素二アンモニウムと希土類硝酸塩、塩化物あるいは炭酸塩との混合物を摩砕することにより起こるメカノケミカル効果について検討した。硝酸塩を用いた場合、摩砕によるRhabdophane型オルソリン酸塩の生成が確認された。また、塩化物を用いた場合では、摩砕することにより希土類リン酸塩の生成温度が低下した。エタノールを摩砕助剤として用いて摩砕した後、加熱すると表面積が大きなRhabdophane型オルソリン酸塩が得られた。

リン酸塩の加熱合成において、尿素あるいはビウレットを加えることにより、リン酸塩生成に影響が現れることが知られている。そこで第4章では、リン酸水素二アンモニウムあるいはリン酸と、希土類酸化物、硝酸塩、塩化物あるいは炭酸塩の混合物に、尿素あるいはビウレットをさらに混合し加熱した。尿素あるいはビウレットを加えることにより、加熱生成物が変化する場合が存在した。また、得られた希土類リン酸塩の表面積に影響が見られた。

以上より、種々の希土類リン酸塩の加熱合成に影響を及ぼす条件とその影響について明らかにした。

第5章では、希土類リン酸塩の熱挙動について調べた。Rhabdophane型(軽希土類塩)及びWeinshenkite型(重希土類塩)オルソリン酸塩は、加熱によりそれぞれMonazite型及びXenotime型オルソリン酸塩へと変化した。ポリリン酸塩(鎖状構造)及びウルトラリン酸塩は、700℃以上でP_2O_5を揮発し、Monazite型あるいは

Xenotime型オルソリン酸塩へと変化した。加熱による方法では、環状リン酸塩は生成しなかった。そこで水溶液中で調製した希土類リン酸塩についてもその熱挙動を調べた。水溶液中で調製されたポリリン酸塩及び環状リン酸塩は、200℃以下の加熱によりオルソ、ピロ(2量体)リン酸塩などの短鎖状リン酸塩へと一度加水分解され、その後、脱水縮合反応を起こしポリリン酸塩へと変化した。このポリリン酸塩は特定の温度において結晶化したが、その結晶化温度は希土類元素のイオン半径と関連性が見られた。

第6章では、5章で熱安定性が確認された希土類リン酸塩について、触媒的側面から表面物性を評価した。Rhabdophane型オルソリン酸塩は、比較的大きな表面積を有した。逆に、縮合リン酸塩は$5 m^2/g$以下であった。大部分の希土類リン酸塩表面の酸強度は、$+1.5 \geqq Ho \geqq -3.0$であり、酸性度は小さかった。酸点・塩基点評価の手段として、2-プロパノールの脱水/脱水素反応に、各種希土類リン酸塩を触媒として用いた。脱水素反応の生成物であるアセトンは検出されず、希土類リン酸塩が塩基触媒として働かないことが判明した。また、Brönsted/Lewis酸点評価の反応であるクメンのクラッキング/脱水素反応にも同様に触媒として用いた。得られた結果より、希土類リン酸塩にはBrönsted酸点が優位に存在することが分かった。また、4価セリウムリン酸塩は、この反応系に用いることによって還元され、3価セリウムリン酸塩へ変化することが明らかとなった。さらに、ブテンの異性化反応においても、各種希土類リン酸塩を触媒として用いた。希土類オルソリン酸塩が、高い触媒活性を示した。一方、縮合リン酸塩の触媒物性は低かったので、メカノケミカルな表面改質を施し、その変化を調べることにした。

第7章では、希土類ウルトラリン酸塩に摩砕処理を施し、その熱挙動や触媒作用を調べた。摩砕処理を施すことにより、希土類ウルトラリン酸塩は無定形化した。ウルトラリン酸塩のP-O-P結合は、水を吸収しながらP-OH結合へ開裂していた。このP-OH結合は、酸性度を増大させ、2-プロパノールの脱水反応における転化率を上昇させた。しかしながら、長時間摩砕すると、生成した多量のP-OH

結合が凝集に働くため、触媒活性は低下した。また、この生成したP-OH結合は、加熱により一部P-O-P結合へ変化した。また、水あるいはエタノールを摩砕助剤として用いると、表面改質の効果が増大した。

加熱による合成法で得た種々の希土類リン酸塩は、高温まで安定であり、その表面を触媒的側面から評価できた。しかしながら、希土類環状リン酸塩は、加熱による方法では合成されず、水溶液反応により調製した塩では、含まれる多くの結晶水により加熱によって加水分解されるため、6章では調べられなかった。そこで、第8章では加熱により環状構造が得られやすいリン酸塩を用い、その一部を希土類元素に置換することで、その加熱生成物や物性について評価した。銅塩では、希土類元素の存在によって、加熱生成物がシクロテトラリン酸塩からピロリン酸塩へと変化した。その変化に要する希土類元素の割合は、希土類元素の種類によって異なっていた。マグネシウム塩では、希土類元素を含んだシクロテトラリン酸塩の合成が可能であった。希土類元素を含んだ環状リン酸塩は、含まないリン酸塩よりも、大きな酸性度をもち高い酸触媒活性を示した。これらの結果は、希土類元素がマグネシウムよりも高い触媒活性を示すことを示し、さらに他の希土類縮合リン酸塩よりも高い活性を示すことから、環状構造がより希土類元素の表面活性を引き出していると考えられた。

以上、本研究では、種々の希土類リン酸塩の合成方法について、いくつかの観点から検討した。また、得られた種々の希土類リン酸塩の加熱変化及び触媒的な物性について明らかにした。

-Contents-

Part Ⅱ . Thermal Behavior of Rare Earth Phosphates

Part Ⅲ . Catalytic Properties of Rare Earth Phosphates

General Introduction

Phosphates have some characteristics; to be hydrophilic, to have the volatility at high temperature, to be corrosiveness, to have low melting point, to have relationship to organism, and so on. Phosphates have been used for ceramic materials, catalyst, fluorescent materials, dielectric substance, metal surface treatment, manure, detergent, food additives, fuel cells, etc.

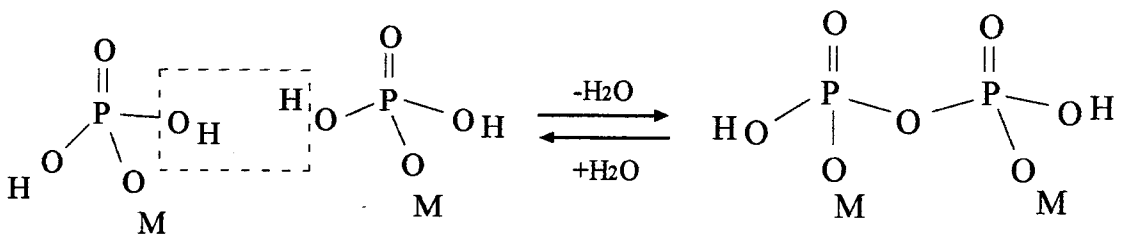

Fig.1. Scheme of condensation of phosphate.

Phosphates transform to various other phosphates with hydrolysis and dehydration reactions by heating (Fig.1) [1-12]. Phosphates are classified into orthophosphates and condensed phosphates. Condensed phosphates are a group of inorganic polymer, which are tetrahedral PO4 units linked at linear, cyclic, and network structure. Figure 2 shows typical structures of these condensed phosphates. Polyphosphate had linear structure and this is common condensed phosphate. Condensation degree varies from 2 (pyrophosphate), 3 (triphosphate) to large number. These polyphosphates had various properties depending on condensation degree. Polyphosphates are formed at high temperature in large amount of phosphates. *Cyclo*-phosphates are known to have condensation degree of 3 to 12. In these phosphates, *cyclo*-tri-, *cyclo*-tetra-, *cyclo*-hexa-, and *cyclo*-octaphosphate are relatively easy to prepare, however other

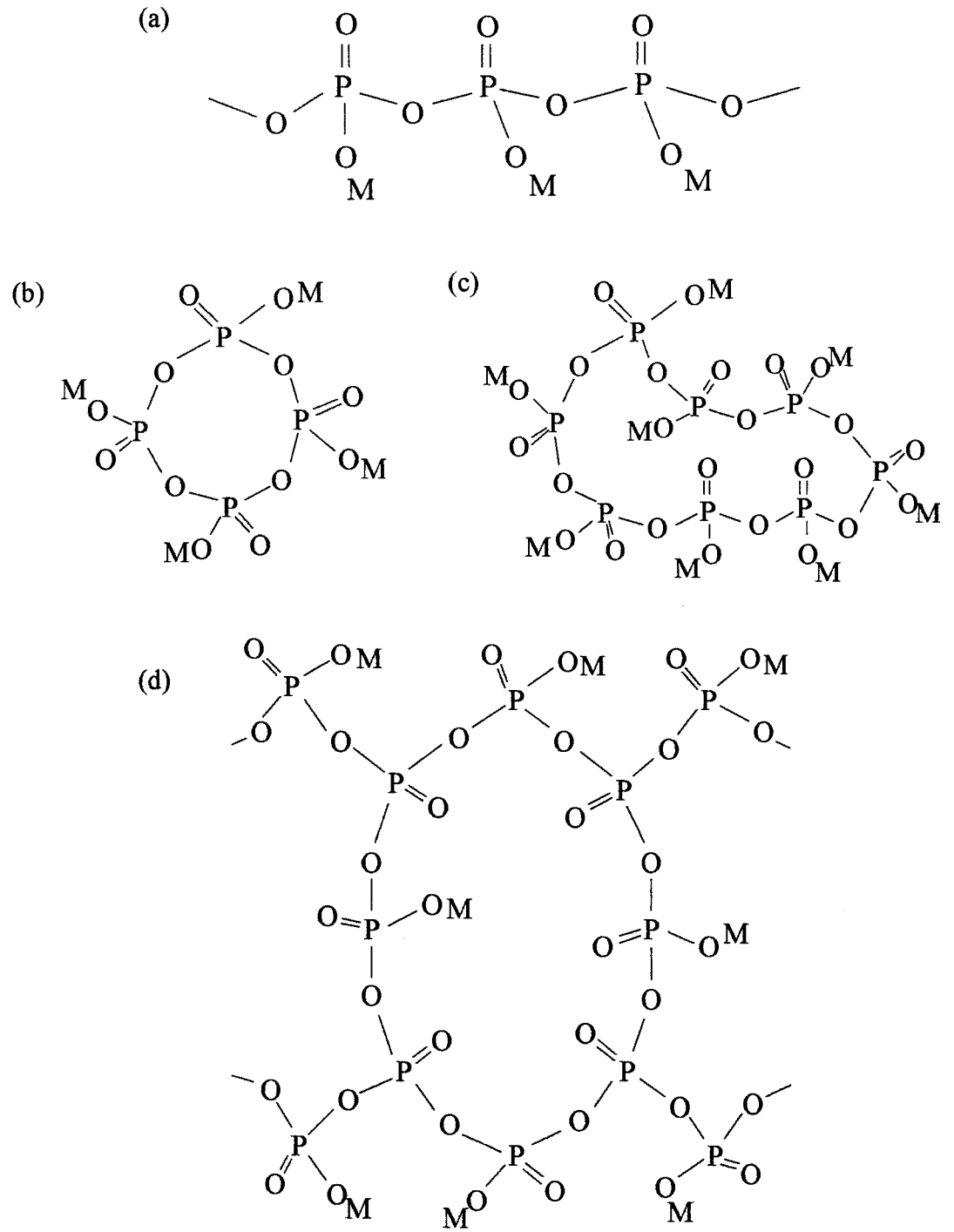

Fig. 2. Typical structures of condensed phosphates, (a) polyphosphate, (b) *cyclo*-tetraphosphate, (c) *cyclo*-octaphosphate, and (d) ultraphosphate.

cyclo-phosphates are much difficult to prepare. Ultraphosphate had the network structure in which PO4 tetrahedra linked to three PO4 units.

The formation and structure of phosphates depend on heating temperature, rate, and time, the cooling rate of melts, the atomosphere, kinds of cations in phosphate, and the ratio of phosphorus / cation. The ratio of phosphorus / cation varied in orthophosphate and various condensed phosphates. Thermal products depend severely on the ratio of phosphorus / cation [1,10-12].

Rare earth orthophosphate is the main component of natural Monazite and Xenotime which are rare earth elements ores. Monazite-type and Rhabdophane-type rare earth phosphates are mainly formed in light rare earth salts, on the other hand, Xenotime and Weinshenkite-type rare earth phosphates are chiefly formed in heavy rare earth salts. Generally, ultraphosphates are easily decomposed by hydration reaction. However, rare earth ultraphosphate is stable for hydrolysis reaction. On the whole, rare earth phosphates are poorly studied than other metal phosphates.

In this work, some factors are discussed on formation of various rare earth phosphates. Thermal behavior of these rare earth phosphates are investigated to support the knowledge of formation of the rare earth phosphates. Furthermore, thermostable rare earth phosphates are estimated for catalytic aspects.

References

[1] M. Tsuhako, S. Ikeuchi, T. Matsuo, I. Motooka, and M. Kobayashi, Bull. Chem. Soc. Jpn., **52**, 1034, (1979).

[2] H. Nariai, I. Motooka, M. Doi, and M. Tsuhako, Bull. Chem. Soc. Jpn., **58**, 379, (1985).

[3] H. Nariai, J. Suenaga, M. Tsuhako, and I. Motooka, Phosphorus Res. Bull, **4**, 99, (1994).

[4] H. Onoda, H. Nariai, H. Maki, and I. Motooka, Phosphorus Res. Bull., **9**, 69, (1999).

[5] H. Onoda, H. Nariai, H. Maki, and I. Motooka, Mem. Grad. School Sci. & Technol., Kobe Univ., **18-A**, 39, (2000).

[6] H. Onoda, H. Nariai, H. Maki, and I. Motooka, Phosphorus Res. Bull., **12**, 139, (2001).

[7] H. Onoda, H. Nariai, H. Maki, and I. Motooka, Mater. Chem. Phys., **73**, 19, (2002).

[8] I. L. Botto and E. J. Baran, Z. Anorg. Allg. Chem., **435**, 293, (1977).

[9] K. Byrappa and B. N. Litvin, J. Mater. Sci., **18(3)**, 703, (1983).

[10] A. Durif, "CRYSTAL CHEMISTRY OF CONDENSED PHOSPHATES", Plenum Publishing Corp., New York, 1995.

[11] M. T. Averbuch-Pouchat and A. Durif, "Topics in Phosphate Chemistry", World Scientific Publishing Co. Pte. Ltd., Shingapore, 1996.

[12] J. R. Van Wazer, "Phosphorus and Its Compound", Vol. I and II, Interscience Publishers Inc, New York, 1961.

Part I
Synthetic Methods of Rare Earth Phosphates

Chapter 1.
Mixing conditions of raw materials on formation of various rare earth phosphates

Abstract

The mixture of a rare earth oxide (CeO_2, Pr_6O_{11}, or Nd_2O_3) and diammonium hydrogenphosphate was treated mechanically, treated with water or ethanol. The mixtures and treated samples were analyzed by X-ray diffraction (XRD), Fourier transform infrared spectroscopy (FT-IR), and thermogravimetry - differential thermal analyses (TG-DTA). The mixtures and ground samples were heated at several temperatures and then thermal products were analyzed by XRD and FT-IR. From these results, these mixtures were indicated to be homogenized and activated by mechanical treatment. By mechanical treatment, $NdPO_4$ was easily formed on heating in P/Nd=1. The existence of water or ethanol as grinding media also gave influence on formation of $NdPO_4$. In P/Nd=3, 5, and 7, neodymium polyphosphate and ultraphosphate were formed. Mechanical treatment and grinding media also had the influence on formation of these condensed phosphates in the manner as orthophosphate. The formation of cerium salts was expected to differ from that of other rare earth phosphates because of tetravalent cerium salts. Samples in P/Ce=4 were the mixture of CeP_2O_7, $Ce(PO_3)_3$, $Ce(PO_3)_4$, and CeP_5O_{14}. Samples in P/Ce=7 were the mixture of $Ce(PO_3)_3$, $Ce(PO_3)_4$, and CeP_5O_{14}. The formation of these cerium phosphates was also affected by mixing conditions of raw materials.

1.1. Introduction

Phosphates transform to various other phosphates with hydrolysis and dehydration reactions by heating [1-6]. The formation and structure of phosphates depend on heating temperature, rate, and time, the cooling rate of melts, the atmosphere, kinds

of cations in phosphate, and the ratio of phosphorus / cation. Thermal products were depended highly on the ratio of phosphorus / cation [7].

Anhydrous rare earth orthophosphate (RPO_4) is the main component of natural Monazite and Xenotime which are rare earth elements ores. Rare earth polyphosphate ($R(PO_3)_3$) had chain structure that PO_4 unit ownership two oxygen atoms [8]. Rare earth ultraphosphate have the network structure which consists the anion represented by $P_5O_{14}^{3-}$. Furthermore, CeP_2O_7 and $Ce(PO_3)_4$ were known as tetravalent cerium phosphates. These phosphates were reported to be prepared from rare earth oxide and phosphoric acid by heating [1]. However, various rare earth phosphates were few reported to be prepared from rare earth oxide and diammonium hydrogenphosphate.

Physical and chemical properties of solid materials are changed by crusing, pressing, milling, and other mechanical treatments [9-14]. These phenomena are known as mechanochemical effects, which comprises of the increase of surface area, defects and strain, and the cleavage of chemical bonds. For these effects, mechanically treated materials were regarded as in an active state. These mechanical treatments have been applied to inorganic materials.

These mechanochemical phenomena largely depend on the conditions of the mechanical treatments, for example the apparatus, atmosphere, and period of treatment [15,16]. To improve the efficiency of the mechanical treatment, various grinding media were used. These media had effects to lower the surface energy, to enhance the degree of dispersion, and so on. Aceton, ethanol, benzene, triethanolamine, dodecylamine, and so on were reported much efficacious solvents as liquid grinding media [17]. On the other hand, some solvent works as a floccuating agent.

The uniformity of raw materials is important in solid state reaction. By mechanical treatment for this uniformity of raw materials, it could be expected that target

materials are synthesized at lower temperature and that higher yields of products are obtained. In this Chapter, the influence of mechanical treatment was investigated on formation of various rare earth phosphates.

1.2. Experimental

Rare earth oxide (CeO_2, Pr_6O_{11}, or Nd_2O_3) was mixed with diammonium hydrogenphosphate. These mixtures with various atomic ratios of P/R (R; rare earth element) were analyzed by XRD, FT-IR, and TG-DTA. Moreover, these mixtures were heated at several temperatures for 20 hours with Automatic Precision Maffle Furnace. Heated samples were also analyzed by XRD, and FT-IR.

In this Chapter, the influence of mixing condition of above raw materials was studied on formation of various rare earth phosphates. Mixing condition of raw materials varied as follows.

1. Raw materials were mixed manually in agate motar for about 5 minutes (mixed sample).
2. Raw materials were treated with grinding-mill for several hours (ground sample).
3. Raw materials were mixed with water manually in agate motar for about 5 minutes (sample mixed with water). The ratio of liquid (water) - solid (rare earth oxide and diammonium hydrogenphosphate) equaled about 5ml/g.
4. Raw materials were ground with water for 6 hours (sample ground with water).
5. Raw materials were mixed with ethanol manually in agate motar for about 5 minutes (sample mixed with ethanol). The ratio of liquid (ethanol) - solid (rare earth oxide and diammonium hydrogenphosphate) equaled about 5ml/g.
6. Raw materials were ground with ethanol for 6 hours (sample ground with

ethanol).

XRD patterns were recorded on a Rigaku Denki RINT 1200M X-Ray diffractometer using monochromated CuK α 1 radiation. IR spectra were recorded on a HORIBA FT-IR spectrometer FT-710 with a KBr disk method. TG-DTA were carried out at a heating rate of 10℃/min, using a Rigaku Denki Thermo Plus TG8120. The grinding apparatus was an Ishikawa's grinder equipped with an agate motar.

1.3. Results and discussion

1.3.1. Mechanochemical effects

Figure 1-1 shows TG-DTA curves of the mixtures of Pr6O11 and (NH4)2HPO4 in P/Pr=1 ground for several hours. Two endothermic peaks in DTA curves were caused from volatilization of two molar of ammonia. These peaks shifted at lower temperature by mechanical treatment. TG curves of ground mixtures had two steps of weight loss. Since the mixture was homogenized and activated by mechanical treatment, the reaction occurred at lower specified temperature. Furthermore, mixtures were suggested to became homogeneous by grinding from sharp IR absorption peaks.

In P/R=1, mechanochemical effect was observed before formation of Monazite-type rare earth orthophosphate. Figure 1-2 shows XRD patterns of the mixtures of Pr6O11 and (NH4)2HPO4 ground for several hours and then heated at 250℃ for 20 hours. The peaks of PrO2 were observed with the peaks of Pr6O11. The peaks of Pr6O11 were stronger than the peaks of PrO2 in XRD pattern of the non-treated mixture. Whereas, treated samples had stronger peaks of PrO2 than those of Pr6O11.

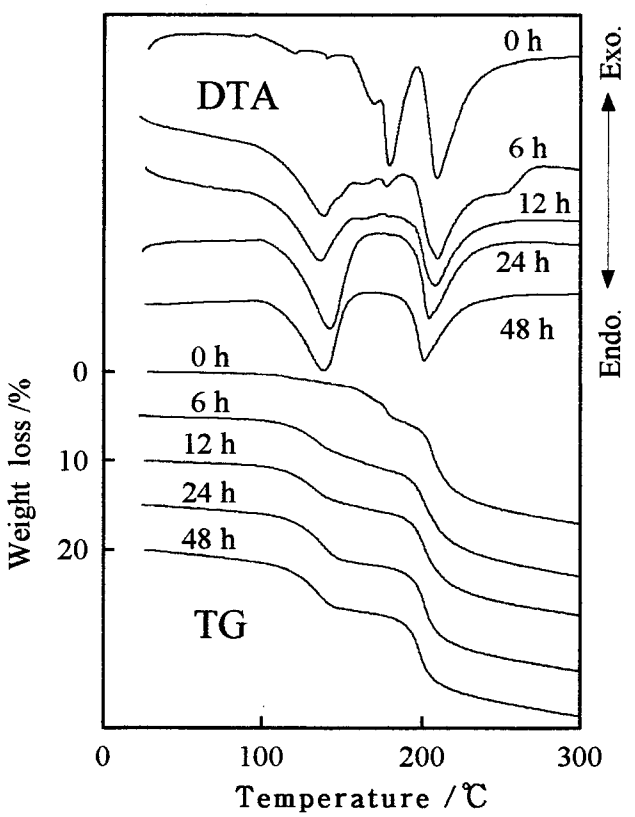

Fig. 1-1. TG-DTA curves of samples of Pr6O11 and (NH4)2HPO4 ground for several hours.

By grinding, Pr6O11 transformed to PrO2 which was higher energy state than Pr6O11. This phenomena was also observed in the results obtained by grinding only Pr6O11.

1.3.2. Influence of water or ethanol

Figure 1-3 shows XRD patterns of samples of Nd2O3 and (NH4)2HPO4 in P/Nd=1 heated at 600℃ for 20 hours. Samples had the peaks of Nd2O3 and NdPO4. Figure 1-3 (a) is XRD pattern of sample mixed manually. Figure 1-3 (b) is that of sample ground for 6 hours mechanically. Monazite-type NdPO4 was formed in some

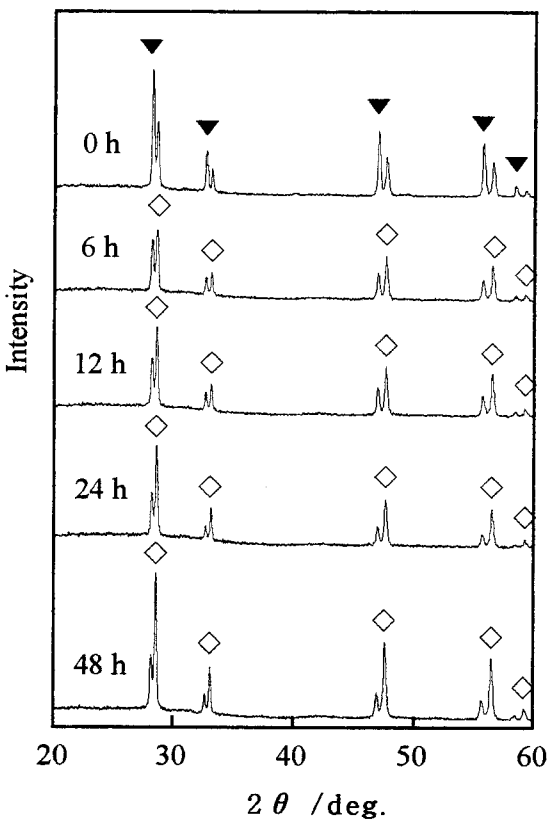

Fig. 1-2. XRD patterns of samples of Pr6O11 and (NH4)2HPO4 ground for several hours and then heated at 250℃ for 20 hours, ▼; Pr6O11 and ◇; PrO2.

degree by grinding. Figure 1-3 (c) is XRD pattern of sample mixed with water in the ratio of liquid (water) - solid (Nd2O3 and (NH4)2HPO4) equal about 5 ml/g. Figure 1-3 (d) is that of sample ground with water for 6 hours in the same ratio of liqiud - solid. By mixing with water, the reaction between Nd2O3 and (NH4)2HPO4 easily occurred. Grinding with water was the effective pretreatment on thermal formation of Monazite-type NdPO4. Figure 1-3 (e) is XRD pattern of sample mixed with ethanol in the ratio of liquid (ethanol) - solid (Nd2O3 and (NH4)2HPO4) equal

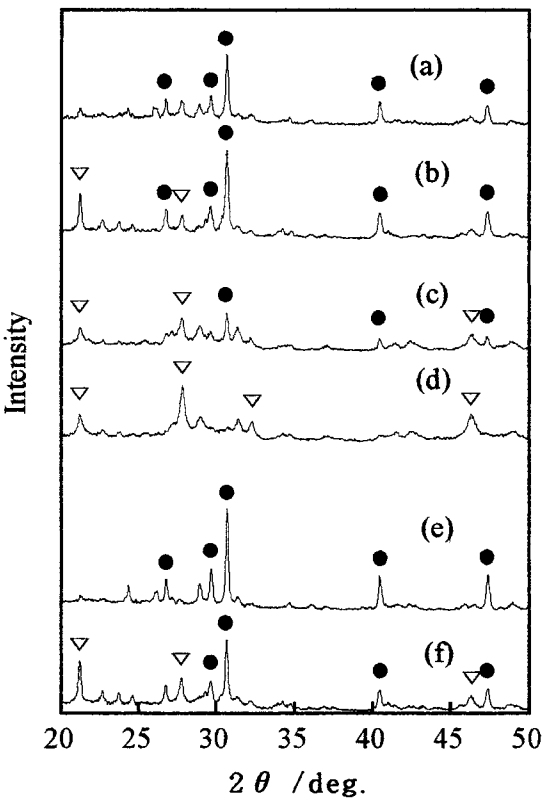

Fig. 1-3. XRD patterns of samples of Nd_2O_3 and $(NH_4)_2HPO_4$ in P/Nd=1 heated at 600℃ for 20 hours, (a) mixed, (b) ground for 6 hours, (c) mixed with water, (d) ground with water for 6 hours, (e) mixed with ethanol, and (f) ground with ethanol for 6 hours, ▽; Monazite-type $NdPO_4$ and ●; Nd_2O_3.

about 5 ml/g. Figure 1-3 (f) is that of sample ground with ethanol for 6 hours in the same ratio of liquid - solid. By grinding with ethanol, $NdPO_4$ was formed. Water and ethanol worked as efficacious grinding media on formation of Monazite-type $NdPO_4$.

1.3.3. Rare earth polyphosphate and ultraphosphate

In P/Nd=3, neodymium polyphosphate was formed in all mixing conditions.

Figure 1-4 shows IR spectra of samples of Nd2O3 and (NH4)2HPO4 in P/Nd=3 heated at 400℃ for 20 hours. The mixing conditions of (a)-(f) in Figs 1-4 and 1-5 were the same with those in Fig. 1-3. By mechanical treatment, the absorption peaks became sharp (Fig. 1-4 (b)(d)(f)). Neodymium polyphosphate was homogeneously formed by grinding of raw materials. This mechanochemical effect clearly appeared in sample ground with ethanol. Grinding with ethanol before heating was the effective way to prepare thermal product homogeneously.

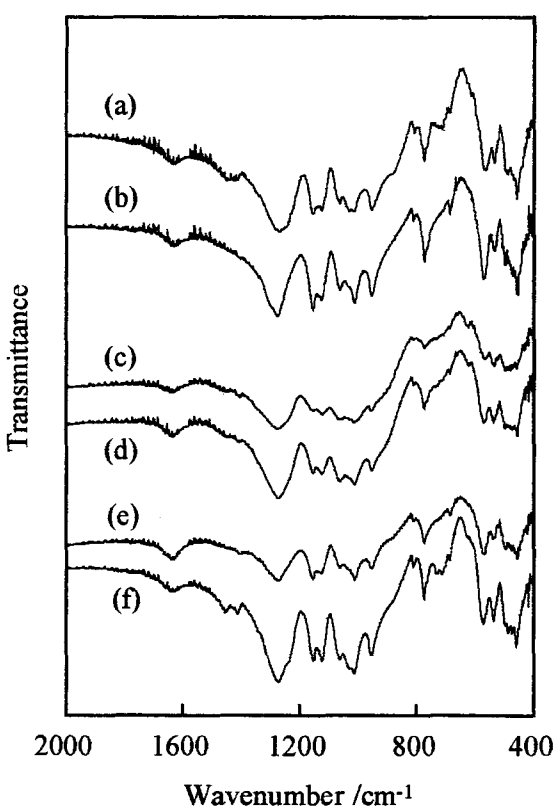

Fig. 1-4. IR spectra of samples of Nd2O3 and (NH4)2HPO4 in P/Nd=3 heated at 400℃ for 20 hours, (a) mixed, (b) ground for 6 hours, (c) mixed with water, (d) ground with water for 6 hours, (e) mixed with ethanol, and (f) ground with ethanol for 6 hours.

The ratio of P/Nd in neodymium ultraphosphate is 5. However, neodymium ultraphosphate was formed with neodymium polyphosphate in P/Nd=5 and 7. In P/Nd=10, NdP_5O_{14} was formed without $Nd(PO_3)_3$ [4]. Samples in P/Nd=5 were concerned here to clarify the influence of mechanical treatment and grinding media on formation of rare earth ultraphosphate. Figure 1-5 shows XRD patterns of samples of Nd_2O_3 and $(NH_4)_2HPO_4$ in P/Nd=5 heated at 500℃ for 20 hours.

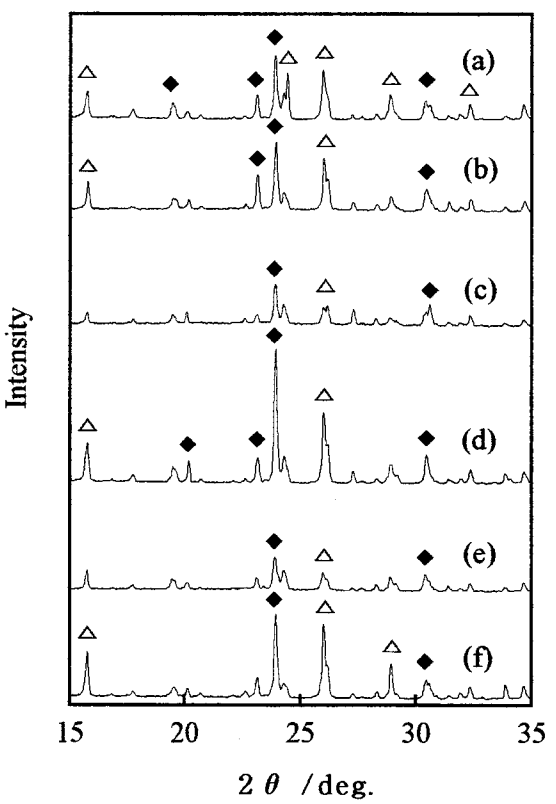

Fig. 1-5. XRD patterns of samples of Nd_2O_3 and $(NH_4)_2HPO_4$ in P/Nd=5 heated at 500℃ for 20 hours, (a) mixed, (b) ground for 6 hours, (c) mixed with water, (d) ground with water for 6 hours, (e) mixed with ethanol, and (f) ground with ethanol for 6 hours, △; $Nd(PO_3)_3$ and ◆; NdP_5O_{14}.

Mechanochemical treatment gave advantage on formation of neodymium ultraphosphate (Fig.1-5 (a)(b)). Neodymium ultraphosphate was richly formed in sample ground with water (Fig.1-5 (d)). On the other hand, sample ground with ethanol contained large amount of neodymium polyphosphate (Fig.1-5 (f)).

1.3.4. Cerium phosphates

Because tetravalent cerium cation is stable, there are CeP_2O_7, $Ce(PO_3)_4$, and so on as exceptional rare earth phosphate. Therefore, formation of cerium salts was expected to differ from that of other rare earth phosphates. Cerium salt was concerned here as a group of exceptional rare earth phosphates.

In P/Ce=1, XRD peaks of CeO_2 and Monazite-type $CePO_4$ were observed in all mixing conditions. Mixing conditions had little influence on formation of $CePO_4$.

Figure 1-6 shows XRD patterns of samples from CeO_2 and $(NH_4)_2HPO_4$ in P/Ce=4 heated at 500℃ for 20 hours. The mixing conditions of (a)-(f) in Figs 1-6 and 1-7 were the same with those in Fig. 1-3. All samples were the mixture of CeP_2O_7, $Ce(PO_3)_3$, $Ce(PO_3)_4$, and CeP_5O_{14}. CeP_2O_7 was richly formed in mixed sample and sample ground with water (Fig. 1-6 (a)(d)). $Ce(PO_3)_3$ was formed in some degree in mixed sample and sample ground with ethanol (Fig. 1-6 (a)(f)). $Ce(PO_3)_4$ was chiefly formed in samples ground with water and ethanol (Fig. 1-6 (d)(f)). CeP_5O_{14} was mainly formed in samples except for mixed sample (Fig. 1-6 (b)-(f)).

Figure 1-7 shows XRD patterns of samples of CeO_2 and $(NH_4)_2HPO_4$ in P/Ce=7 heated at 800℃ for 20 hours. Samples were the mixture of $Ce(PO_3)_3$, $Ce(PO_3)_4$, and CeP_5O_{14}. $Ce(PO_3)_3$ was chiefly formed in ground sample, sample mixed with water, and sample ground with water (Fig. 1-7 (b)-(d)). $Ce(PO_3)_4$ was formed in some degree in ground sample and sample mixed with ethanol (Fig. 1-7 (b)(e)). CeP_5O_{14} was mainly formed in mixed sample, sample mixed with ethanol, and

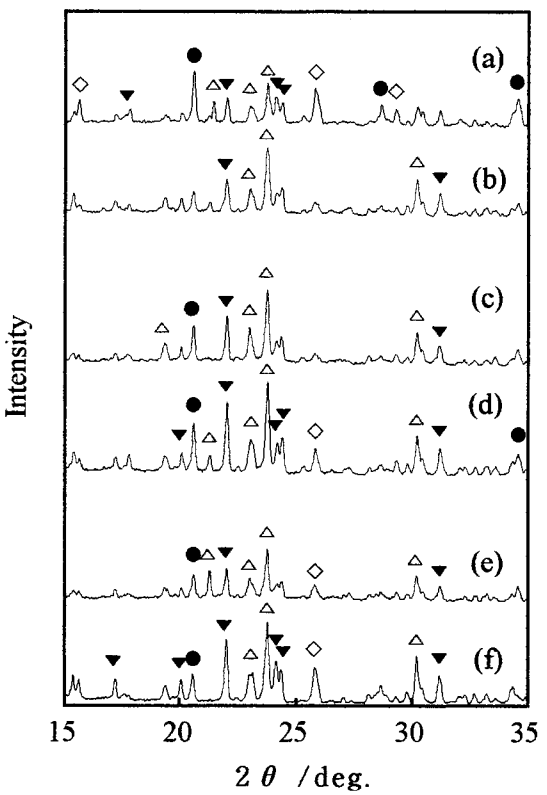

Fig. 1-6. XRD patterns of samples of CeO_2 and $(NH_4)_2HPO_4$ in P/Ce=4 heated at 500℃ for 20 hours, (a) mixed, (b) ground for 6 hours, (c) mixed with water, (d) ground with water for 6 hours, (e) mixed with ethanol, and (f) ground with ethanol for 6 hours, ●; CeP_2O_7, ◇; $Ce(PO_3)_3$, ▼; $Ce(PO_3)_4$, and △; CeP_5O_{14}.

sample ground with ethanol (Fig. 1-7 (a)(e)(f)).

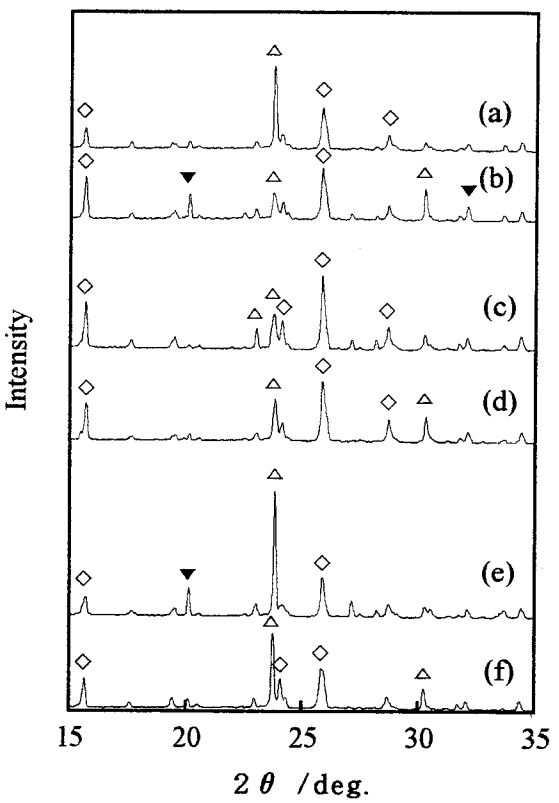

Fig. 1-7. XRD patterns of samples of CeO_2 and $(NH_4)_2HPO_4$ in P/Ce=7 heated at 800℃ for 20 hours, (a) mixed, (b) ground for 6 hours, (c) mixed with water, (d) ground with water for 6 hours, (e) mixed with ethanol, and (f) ground with ethanol for 6 hours, ◇; $Ce(PO_3)_3$, ▼; $Ce(PO_3)_4$, and △; CeP_5O_{14}.

1.4. Conclusion

The experimental results obtained in this Chapter are summarized as follows.

1. The mixture of rare earth oxide and diammonium hydrogenphosphate was

homogenized and activated by mechanical treatment.

2. Water and ethanol worked as effective grinding media in mixing process of raw materials on formation of Monazite-type rare earth orthophosphate.

3. Mechanical treatment and grinding media had the influence on formation of rare earth condensed phosphates in the manner as Monazite-type rare earth orthophosphate.

1.5. References

[1] M. Tsuhako, S. Ikeuchi, T. Matsuo, I. Motooka, and M. Kobayashi, Bull. Chem. Soc. Jpn., **52**, 1034, (1979).

[2] H. Nariai, I. Motooka, M. Doi, and M. Tsuhako, Bull. Chem. Soc. Jpn., **58**, 379, (1985).

[3] H. Nariai, J. Suenaga, M. Tsuhako, and I. Motooka, Phosphorus Res. Bull., **4**, 99, (1994).

[4] H. Onoda, H. Nariai, H. Maki, and I. Motooka, Phosphorus Res. Bull., **9**, 69, (1999).

[5] I. L. Botto and E. J. Baran, Z. Anorg. Allg. Chem., **435**, 293, (1977).

[6] K. Byrappa and B. N. Litvin, J. Mater. Sci., **18(3)**, 703, (1983).

[7] J. R. Van Wazer, "Phosphorus and Its Compound", Vol. I and II, Interscience Publishers Inc, New York, 1961.

[8] H. Y-P. Hong, Acta Cryst., **B30**, 468, (1974).

[9] F. Cardellini, V. Contini, and G. Mazzone, J. Mater. Sci., **31**, 4175, (1996).

[10] P. Balaz, T. Havlik, Z. Bastl, J. Briancin, and R. Kammel, J. Mater. Sci. Letters,

15, 1161, (1996).

[11] E. G. Avvakumov, E. T. Devyatkina, and N. V. Kosova, J. Solid State Chem., **113**, 379, (1994).

[12] N. Hashimoto, H. Yoden, and S. Deki, J. Am. Ceram. Soc., **76**, 438, (1993).

[13] W. Kim, Q. Zhang, and F. Saito, J. Mater. Sci., **35**, 5401, (2000).

[14] K. Kudaka, K. Iizuka, T. Sasaki, and H. Izumi, J. Am. Ceram. Soc., **83**, 2887, (2000).

[15] H. Nariai, M. Tada, M. Tsuhako, and I. Motooka, Phosphorus Res. Bull., **5**, 125, (1995).

[16] H. Nariai, S. Shibamoto, H. Maki, and I. Motooka, Phosphorus Res. Bull., **8**, 101, (1998).

[17] T. Kubo, "Mechanochemistry gairon", p.134, Tokyo Kagaku Dojin Ltd., Tokyo, 1978.

Chapter 2.
Syntheses of various rare earth phosphates from some rare earth compounds

Abstract

Each rare earth compound (rare earth element; R=La, Ce, and Nd, anion; oxide, carbonate, chloride, nitrate, sulfate, oxalate, and fluoride) was mixed with $(NH_4)_2HPO_4$ or H_3PO_4 in P/R=1, 3, and 5, and heated in air. The resulting salts were analyzed by TG-DTA, XRD and FT-IR. Rhabdophane-type $CePO_4$ was not formed in the system of CeO_2-H_3PO_4. However, this phosphate was synthesized in the systems of $Ce(NO_3)_3 \cdot 6H_2O$-$(NH_4)_2HPO_4$, $Ce_2(CO_3)_3 \cdot 8H_2O$-H_3PO_4, $CeCl_3 \cdot 7H_2O$-H_3PO_4, and $Ce(NO_3)_3 \cdot 6H_2O$-H_3PO_4. The crystallinity of Rhabdophane-type $CePO_4$ was high in the systems of $CeCl_3 \cdot 7H_2O$-H_3PO_4 and $Ce(NO_3)_3 \cdot 6H_2O$-H_3PO_4. In P/Ce=1, formation of CeO_2 was observed in the systems of $Ce_2(CO_3)_3 \cdot 8H_2O$-$(NH_4)_2HPO_4$, $CeCl_3 \cdot 7H_2O$-$(NH_4)_2HPO_4$, and $Ce_2(C_2O_4)_3 \cdot 9H_2O$-$(NH_4)_2HPO_4$.

2.1. Introduction

Anhydrous rare earth orthophosphate (RPO_4) is the main component of natural Monazite and Xenotime which are rare earth elements ores. Rhabdophane-type rare earth orthophosphate hydrate ($RPO_4 \cdot nH_2O$, R=La, Ce or Nd, n; ~2) had the specific structure with vacant spaces [1]. Rare earth polyphosphate ($R(PO_3)_3$) had chain structure that PO_4 unit ownership two oxygen atoms. Rare earth ultraphosphate have the network structure which consists the anion represented by $P_5O_{14}^{3-}$.

As phosphorus resource to prepare various rare earth phosphates, phosphoric acid is widely used, whereas diammonium hydrogenphosphate is little used [2-8]. Using diammonium hydrogenphosphate has some merits, for example, to react slowly and

mildly, to be easy to get rid of non-target cation by heating, to be easy to treat with as solid state etc. Syntheses of lanthanum phosphates were explored from various compounds [9]. It was reported that new Rhabdophane-type $TmPO_4$ and $TbPO_4$ were synthesized under presence of coexistent salts [10]. By changing raw materials, new materials has tried to be synthesized, higher yields of products and sintering effect at lower temperature could be expected. In this work, various rare earth compounds were studied for syntheses of rare earth phosphates using $(NH_4)_2HPO_4$ and H_3PO_4 as phosphorus resource.

2.2. Experimental

Each rare earth compound (rare earth element; R=La, Ce, and Nd, anion; oxide, carbonate, chloride, nitrate, sulfate, oxalate, and fluoride) was mixed with diammonium hydrogenphosphate or phosphoric acid at various ratio of phosphorus and rare earth element (P/R). Then the mixtures were heated with Automatic Precision Maffle Furnace from Thomas Scientific Co., Ltd. Samples were analyzed by thermogravimetry - differential thermal analysis (TG-DTA), X-Ray diffractometry (XRD), and fourier transform infrared spectroscopy (FT-IR). TG-DTA were measured with a Rigaku Denki Thermo Plus TG8120. 15 ~ 20mg of sample was placed in a platinum pan. Thermal analyses were carried out at 10℃/min. X-ray diffraction patterns were recorded on a Rigaku Denki RINT1200M X-Ray diffractometer using monochromated CuK α 1 radiation. The IR spectra were recorded on a HORIBA FT-IR spectrometer, FT-710 with a KBr disk method. The samples heated with TG-DTA apparatus were also analyzed by XRD and FT-IR. All reagent were of analytical-reagent grade and used without further purification.

2.3. Results and Discussion

2.3.1. In P/R=1

Figure 2-1 shows a part of XRD patterns of samples in P/La=1. XRD pattern of Fig. 2-1 (a) was due to lanthanum orthophosphate anhydrate, $LaPO_4$ (Monazite-type). High temperature was needed for preparation in the system of La_2O_3-$(NH_4)_2HPO_4$, because rare earth oxide are thermostable [11]. At 300℃, $LaPO_4$ was formed in the system of $La(NO_3)_3 \cdot 9H_2O$-$(NH_4)_2HPO_4$ (Fig. 2-1 (b)). XRD pattern of Fig. 2-1 (c) shows Rhabdophane-type lanthanum orthophosphate, $LaPO_4$. And sample of Fig. 2-1 (d) was Monazite-type $LaPO_4$. By heating at 700℃ for a long time, Monazite-type $LaPO_4$ was formed in the system of La_2O_3-H_3PO_4, while $LaPO_4$ was formed

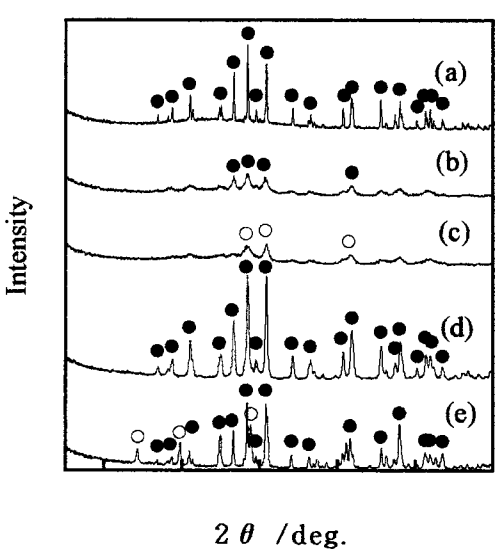

Fig. 2-1. XRD patterns of samples in P/La=1; (a) La_2O_3-$(NH_4)_2HPO_4$ 1200℃, (b) $La(NO_3)_3 \cdot 9H_2O$-$(NH_4)_2HPO_4$ 300℃, (c) La_2O_3-H_3PO_4 700℃, (d) La_2O_3-H_3PO_4 700℃ 20 hours, and (e) $La(NO_3)_3 \cdot 9H_2O$-H_3PO_4 150℃ 20 hours, ●; Monazite-type $LaPO_4$ and ○; Rhabdophane-type $LaPO_4$.

at 150℃ for 20 hours in the system of $La(NO_3)_3 \cdot 9H_2O$-H_3PO_4 (Fig. 2-1 (e)). Lanthanum nitrate gave the guide to Monazite-type $LaPO_4$. Monazite-type lanthanum orthophosphate was possible to synthesize at lower temperature in this report than in the method of La_2O_3-H_3PO_4. Monazite-type $LaPO_4$ was also formed in all systems except for LaF_3-H_3PO_4.

Figure 2-2 shows a part of TG-DTA curves of samples in P/La=1. Rhabdophane-type lanthanum orthophosphate is synthesized by mixing La_2O_3 and H_3PO_4. This phosphate, $LaPO_4$, loses the water of crystalline at about 240℃ with its structure maintained (Fig. 2-2 (a)). Rhabdophane-type lanthanum orthophosphate changed to Monazite-type lanthanum orthophosphate at 700℃ for a long time (Fig. 2-1 (c)(d)). Rhabdophane-type $LaPO_4$ was not formed in the system of La_2O_3-$(NH_4)_2HPO_4$.

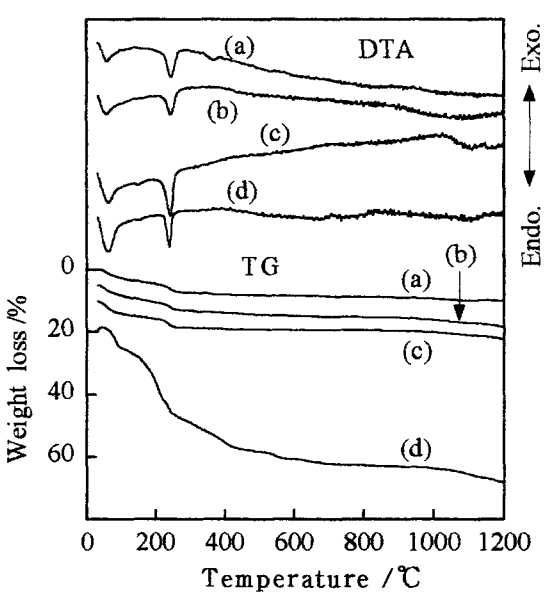

Fig. 2-2. TG-DTA curves of samples in P/La=1 at 150℃ for 20 hours, (a) La_2O_3-H_3PO_4, (b) $La_2(CO_3)_3$-H_3PO_4, (c) $LaCl_3 \cdot 7H_2O$-H_3PO_4, and (d) $La(NO_3)_3 \cdot 9H_2O$-H_3PO_4.

Rhabdophane-type $LaPO_4$ was neither formed from other lanthanum compounds in the condition using $(NH_4)_2HPO_4$.

$La_2(CO_3)_3$ or $LaCl_3 \cdot 7H_2O$ was reacted with H_3PO_4 to Rhabdophane-type $LaPO_4$. Thermal behavior of Rhabdophane-type $LaPO_4$ prepared from $La_2(CO_3)_3$ or $LaCl_3 \cdot 7H_2O$ was the same with that of Rhabdophane-type $LaPO_4$ prepared from La_2O_3 (Fig. 2-2 (a)-(c)). XRD pattern of sample in the system of $La(NO_3)_3 \cdot 9H_2O$-H_3PO_4 indicates the mixture of peaks of Monazite-type and Rhabdophane-type lanthanum orthophosphates. Figure 2-3 shows typical IR spectra. IR spectrum of this sample (Fig. 2-3 (c)) had new peak at about $1400cm^{-1}$ which was not observed in spectra of Monazite-type and Rhabdophane-type lanthanum orthophosphates (Fig. 2-3 (a)(b)). This peak is considered to be due to unreacted NO_3^-. The peak became

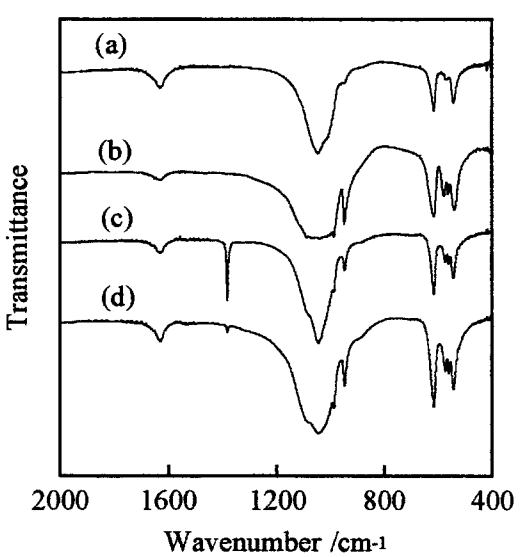

Fig. 2-3. IR spectra, (a) Rhabdophane-type $LaPO_4$, (b) Monazite-type $LaPO_4$, (c) sample prepared from $La(NO_3)_3 \cdot 9H_2O$-H_3PO_4 in P/La=1 at 150℃, and (d) sample prepared from $La(NO_3)_3 \cdot 9H_2O$-H_3PO_4 in P/La=1 at 300℃.

became smaller by heating at 300℃ (Fig. 2-3 (d)). Sample prepared from $La(NO_3)_3 \cdot 9H_2O$ and H_3PO_4 had larger weight loss in TG curve than Rhabdophane-type $LaPO_4$ (Fig.2-2 (d)). $LaPO_4 \cdot nH_2O$ was not formed in the systems using $La_2(SO_4)_3 \cdot 9H_2O$, $La_2(C_2O_4)_3 \cdot 9H_2O$, and LaF_3.

Figure 2-4 shows a part of XRD patterns of samples in P/Nd=1. Rhabdophane-type neodymium orthophosphate, $NdPO_4$, was formed in the systems of $Nd(NO_3)_3 \cdot 6H_2O$-$(NH_4)_2HPO_4$, Nd_2O_3-H_3PO_4, $Nd_2(CO_3)_3 \cdot 8H_2O$-H_3PO_4, $NdCl_3 \cdot 6H_2O$-H_3PO_4, and $Nd(NO_3)_3 \cdot 6H_2O$-H_3PO_4. Sample in the system of Nd_2O_3-H_3PO_4 was the mixture of Rhabdophane-type $NdPO_4$ and Nd_2O_3 (Fig. 2-4 (b)). The crystallinity of Rhabdophane-type $NdPO_4$ prepared from $NdCl_3 \cdot 6H_2O$ or $Nd(NO_3)_3 \cdot 6H_2O$ was higher than that prepared from Nd_2O_3 or $Nd_2(CO_3)_3 \cdot 8H_2O$. An adsorption peak at

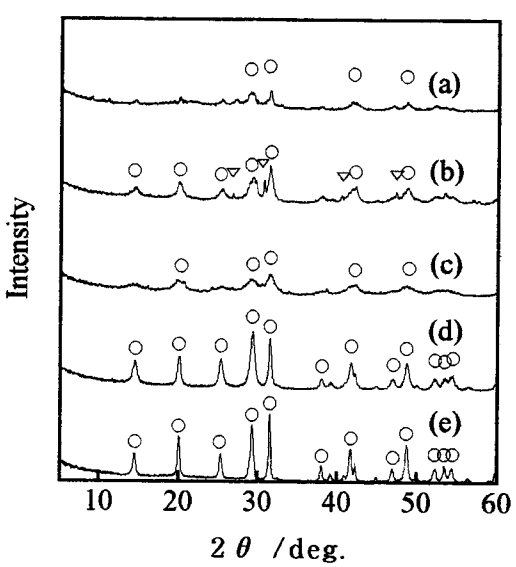

Fig. 2-4. XRD patterns of samples in P/Nd=1 at 150℃ for 20 hours, (a) $Nd(NO_3)_3 \cdot 6H_2O$-$(NH_4)_2HPO_4$, (b) Nd_2O_3-H_3PO_4, (c) $Nd_2(CO_3)_3 \cdot 8H_2O$-H_3PO_4, (d) $NdCl_3 \cdot 6H_2O$-H_3PO_4, and (e) $Nd(NO_3)_3 \cdot 6H_2O$-H_3PO_4, ○; Rhabdophane-type $NdPO_4$ and ▽; Nd_2O_3.

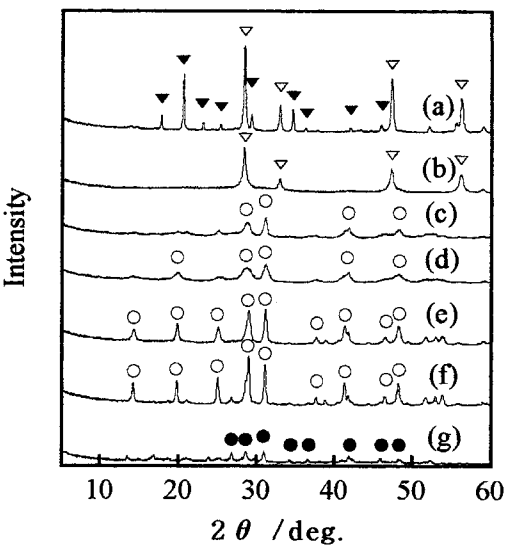

Fig. 2-5. XRD patterns of samples in P/Ce=1 at 300℃ for 20 hours; (a) CeO_2-$(NH_4)_2HPO_4$, (b) $CeCl_3 \cdot 7H_2O$-$(NH_4)_2HPO_4$, (c) $Ce(NO_3)_3 \cdot 6H_2O$-$(NH_4)_2HPO_4$, (d) $Ce_2(CO_3)_3 \cdot 8H_2O$-H_3PO_4, (e) $CeCl_3 \cdot 7H_2O$-H_3PO_4, (f) $Ce(NO_3)_3 \cdot 6H_2O$-H_3PO_4, and (g) $Ce_2(C_2O_4)_3 \cdot 9H_2O$-$H_3PO_4$, ●; Monazite-type $CePO_4$, ○; Rhabdophane-type $CePO_4$, ▼; CeP_2O_7, and ▽; CeO_2.

about 1400cm^{-1} of unreacted NO_3^- was observed in IR spectrum of samples prepared from $Nd(NO_3)_3 \cdot 6H_2O$. This peak became smaller by heating at 300℃.

Figure 2-5 shows a part of XRD patterns of samples in P/Ce=1. In spite of P/Ce=1, samples in the systems of CeO_2-$(NH_4)_2HPO_4$ and CeO_2-H_3PO_4 changed to the mixture of cerium pyrophosphate, CeP_2O_7, and CeO_2 (Fig. 2-5 (a)). IR spectrum of this sample was due to CeP_2O_7. Samples in these systems at 1200℃ was Monazite-type $CePO_4$. The reduction reaction occurred at high temperature, and thermostable trivalent Monazite-type cerium orthophosphate, $CePO_4$, was formed.

CeO_2 was formed in the systems of $Ce_2(CO_3)_3 \cdot 8H_2O$-$(NH_4)_2HPO_4$, $CeCl_3 \cdot 7H_2O$-

$(NH_4)_2HPO_4$, and $Ce_2(C_2O_4)_3 \cdot 9H_2O$-$(NH_4)_2HPO_4$ (Fig. 2-5 (b)). It was considered that $Ce_2(CO_3)_3 \cdot 8H_2O$, $CeCl_3 \cdot 7H_2O$, and $Ce_2(C_2O_4)_3 \cdot 9H_2O$ transformed to CeO_2 and then reacted with $(NH_4)_2HPO_4$ to Monazite-type $CePO_4$. CeO_2 wasn't formed in the systems using H_3PO_4. Since H_3PO_4 was much reactive than $(NH_4)_2HPO_4$, trivalent cerium compounds reacted directly with H_3PO_4.

Rhabdophane-type cerium orthophosphate was formed in the systems of $Ce(NO_3)_3 \cdot 6H_2O$-$(NH_4)_2HPO_4$, $Ce_2(CO_3)_3 \cdot 8H_2O$-H_3PO_4, $CeCl_3 \cdot 7H_2O$-H_3PO_4, and $Ce(NO_3)_3 \cdot 6H_2O$-H_3PO_4 (Fig. 2-5 (c)-(f)). $Ce(NO_3)_3 \cdot 6H_2O$ was considered to be the most reactive cerium compound in this work. The crystallinity of Rhabdophane-type $CePO_4$ in the systems of $CeCl_3 \cdot 7H_2O$-H_3PO_4 and $Ce(NO_3)_3 \cdot 6H_2O$-H_3PO_4 was higher than that of Rhabdophane-type $CePO_4$ in the system of $Ce_2(CO_3)_3 \cdot 8H_2O$-H_3PO_4.

Sample prepared from $Ce_2(C_2O_4)_3 \cdot 9H_2O$ signed the weak peaks of Monazite-type $CePO_4$ in XRD result at 300℃ (Fig. 2-5 (g)). Monazite-type $CePO_4$ was formed in all systems except for CeF_3-H_3PO_4 at 1200℃.

2.3.2. In P/R=3

Lanthanum polyphosphate, $La(PO_3)_3$, was formed in the system of La_2O_3 and $(NH_4)_2HPO_4$ at 500℃ in P/La=3. $La_2(CO_3)_3$, $LaCl_3 \cdot 7H_2O$, $La(NO_3)_3 \cdot 9H_2O$, and $La_2(SO_4)_3 \cdot 9H_2O$ also gave $La(PO_3)_3$ with $(NH_4)_2HPO_4$ at 500℃. $La(PO_3)_3$ was formed in the systems of $La_2(C_2O_4)_3 \cdot 9H_2O$-$(NH_4)_2HPO_4$ and LaF_3-$(NH_4)_2HPO_4$ at 700℃. The crystallinity of $La(PO_3)_3$ in the systems of $La_2(CO_3)_3$-$(NH_4)_2HPO_4$, $LaCl_3 \cdot 7H_2O$-$(NH_4)_2HPO_4$, $La(NO_3)_3 \cdot 9H_2O$-$(NH_4)_2HPO_4$, $La_2(SO_4)_3 \cdot 9H_2O$-$(NH_4)_2HPO_4$, and $La_2(C_2O_4)_3 \cdot 9H_2O$-$(NH_4)_2HPO_4$ at 700℃ was higher than that of $La(PO_3)_3$ in the system of La_2O_3-$(NH_4)_2HPO_4$. These coexistent anions assisted the crystal growth of $La(PO_3)_3$. The weak peaks of LaF_3 and $La(PO_3)_3$ were observed

in XRD pattern of sample prepared from LaF_3.

The mixture of La_2O_3 and H_3PO_4 in P/La=3 transformed to $La(PO_3)_3$ by heating at 300℃ for 20 hours. $La(PO_3)_3$ was also formed at 300℃ for 20 hours in the condition using other lanthanum compounds except for LaF_3 with H_3PO_4.

Neodymium polyphosphate, $Nd(PO_3)_3$, was formed in the systems using neodymium compounds except for NdF_3 with either $(NH_4)_2HPO_4$ or H_3PO_4 in P/Nd=3. The mixture of $Nd(PO_3)_3$ and Monazite-type $NdPO_4$ was produced in the system of NdF_3-$(NH_4)_2HPO_4$.

Figure 2-6 shows a part of XRD results in P/Ce=3. The mixture of CeP_2O_7 and

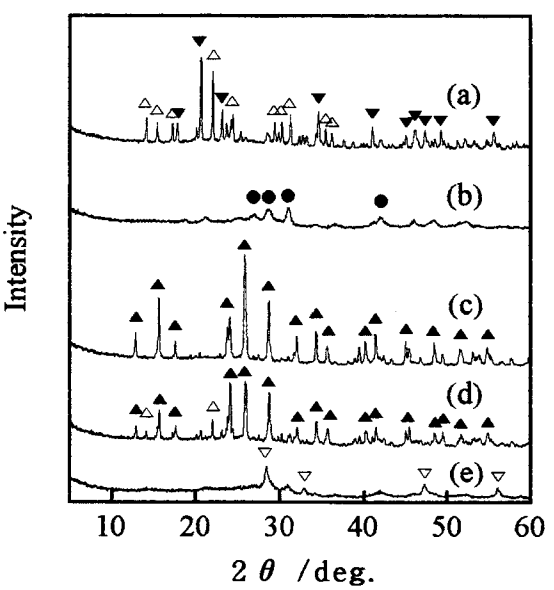

Fig. 2-6. XRD patterns of samples in P/Ce=3; (a) CeO_2-$(NH_4)_2HPO_4$ 700℃, (b) $Ce_2(CO_3)_3 \cdot 8H_2O$-$(NH_4)_2HPO_4$ 300℃ 20 hours, (c) $Ce_2(CO_3)_3 \cdot 8H_2O$-$(NH_4)_2HPO_4$ 700℃, (d) $Ce(NO_3)_3 \cdot 6H_2O$-$(NH_4)_2HPO_4$ 700℃, (e) $CeCl_3 \cdot 7H_2O$-$(NH_4)_2HPO_4$ 300℃ 20 hours, ●; Monazite-type $CePO_4$, ▲; $Ce(PO_3)_3$, △; $Ce(PO_3)_4$, ▼; CeP_2O_7, and ▽; CeO_2.

tetravalent cerium polyphosphate, $Ce(PO_3)_4$, was formed in the systems of CeO_2-$(NH_4)_2HPO_4$ and CeO_2-H_3PO_4 (Fig. 2-6 (a)). Monazite-type $CePO_4$ was formed in the systems of $Ce_2(CO_3)_3 \cdot 8H_2O$-$(NH_4)_2HPO_4$, $Ce_2(CO_3)_3 \cdot 8H_2O$-H_3PO_4, $CeCl_3 \cdot 7H_2O$-H_3PO_4, $Ce(NO_3)_3 \cdot 6H_2O$-H_3PO_4, and $Ce_2(C_2O_4)_3 \cdot 9H_2O$-$H_3PO_4$ at 300℃ (Fig. 2-6 (b)). Trivalent cerium polyphosphate, $Ce(PO_3)_3$, was formed in the systems using $Ce_2(CO_3)_3 \cdot 8H_2O$, $CeCl_3 \cdot 7H_2O$, $Ce(NO_3)_3 \cdot 6H_2O$, and $Ce_2(C_2O_4)_3 \cdot 9H_2O$ heated at 500℃ and 700℃ (Fig. 2-6 (c)(d)). $Ce(PO_3)_3$ was considered to be synthesized by way of Monazite-type $CePO_4$. $Ce(PO_3)_4$ was also formed in sample prepared from nitrate (Fig. 2-6 (d)). CeO_2 was formed in the system of $CeCl_3 \cdot 7H_2O$-$(NH_4)_2HPO_4$ at 300℃ (Fig. 2-6 (e)). $CeCl_3 \cdot 7H_2O$ was considered to transform to CeO_2 and then reacted with $(NH_4)_2HPO_4$ to $Ce(PO_3)_3$ by way of Monazite-type $CePO_4$.

2.3.3. In P/R=5

The ratio of phosphorus and rare earth element (P/R) in ultraphosphate, RP_5O_{14}, is 5. The mixture of rare earth oxide and H_3PO_4 in P/R=5 changed to the mixture of ultraphosphate and polyphosphate by heating at 700℃ for 20 hours. Synthetic method of ultraphosphate without polyphosphate is heating the mixture in P/R=10 at 700℃ for 20 hours. In the systems of $La_2(C_2O_4)_3 \cdot 9H_2O$-$(NH_4)_2HPO_4$, LaF_3-$(NH_4)_2HPO_4$, $La_2(SO_4)_3 \cdot 9H_2O$-H_3PO_4, $La_2(C_2O_4)_3 \cdot 9H_2O$-$H_3PO_4$, and LaF_3-H_3PO_4 in P/La=5, the crystallinity of LaP_5O_{14} was high and that of $La(PO_3)_3$ was low. The systems of $Nd_2(C_2O_4)_3 \cdot 6H_2O$-$(NH_4)_2HPO_4$, NdF_3-$(NH_4)_2HPO_4$, $Nd(NO_3)_3 \cdot 6H_2O$-H_3PO_4, and NdF_3-H_3PO_4 showed the same tendency.

Figure 2-7 shows XRD patterns of samples prepared from CeO_2 and $Ce_2(CO_3)_3 \cdot 8H_2O$ in P/Ce=5 heated at 700℃ for 20 hours. Samples prepared from CeO_2 were the mixture of CeP_5O_{14}, $Ce(PO_3)_4$, and $Ce(PO_3)_3$ (Fig. 2-7 (a)(b)). Samples prepared from $Ce_2(CO_3)_3 \cdot 8H_2O$ were the mixture of CeP_5O_{14} and $Ce(PO_3)_3$

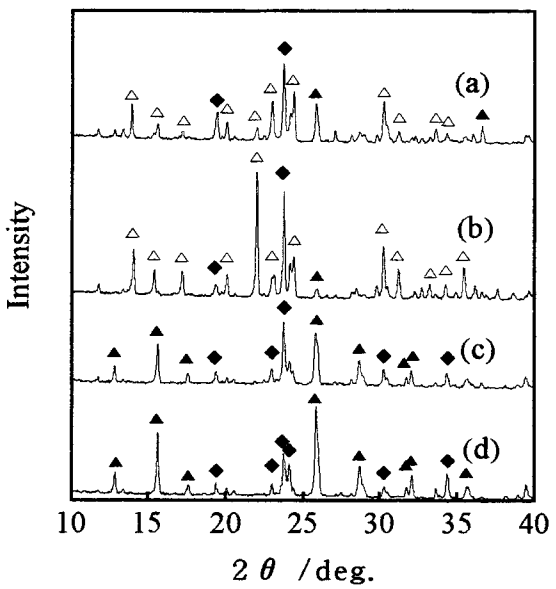

Fig. 2-7. XRD patterns of samples in P/Ce=5 heated at 700℃ for 20 hours, (a) CeO_2-$(NH_4)_2HPO_4$, (b) CeO_2-H_3PO_4, (c) $Ce_2(CO_3)_3 \cdot 8H_2O$-$(NH_4)_2HPO_4$, and (d) $Ce_2(CO_3)_3 \cdot 8H_2O$-H_3PO_4, ▲; $Ce(PO_3)_3$, △; $Ce(PO_3)_4$, and ◆; CeP_5O_{14}.

(Fig. 2-7 (c)(d)). The materials prepared from other trivalent cerium compounds were the mixture of CeP_5O_{14} and $Ce(PO_3)_3$. In the systems of $CeCl_3 \cdot 7H_2O$-H_3PO_4, $Ce_2(C_2O_4)_3 \cdot 9H_2O$-$H_3PO_4$, and CeF_3-H_3PO_4, XRD peak intensity of CeP_5O_{14} was strong and that of $Ce(PO_3)_3$ was weak. Samples prepared from $(NH_4)_2HPO_4$ had stronger peaks of CeP_5O_{14} than those prepared from H_3PO_4.

2.3.4. Rare earth cation and coexistent anion

Rhabdophane-type RPO_4 was formed in the systems of $Ce(NO_3)_3 \cdot 6H_2O$-$(NH_4)_2HPO_4$ and $Nd(NO_3)_3 \cdot 6H_2O$-$(NH_4)_2HPO_4$. However, in the system of

$La(NO_3)_3 \cdot 6H_2O$-H_3PO_4, Monazite-type $LaPO_4$ was formed at same temperature.

CeP_2O_7 and $Ce(PO_3)_4$ were formed in the system using CeO_2, however Rhabdophane-type $CePO_4$ wasn't formed. Formation of CeO_2 was observed in the systems of $Ce_2(CO_3)_3 \cdot 8H_2O$-$(NH_4)_2HPO_4$, $CeCl_3 \cdot 7H_2O$-$(NH_4)_2HPO_4$, and $Ce_2(C_2O_4)_3 \cdot 9H_2O$-$(NH_4)_2HPO_4$ in P/Ce=1. A part of $Ce_2(CO_3)_3 \cdot 8H_2O$, $CeCl_3 \cdot 7H_2O$, and $Ce_2(C_2O_4)_3 \cdot 9H_2O$ were transformed to CeO_2 and then reacted with $(NH_4)_2HPO_4$.

From the standpoint of coexistent anions, rare earth nitrates were easy to react with $(NH_4)_2HPO_4$ and H_3PO_4. However, samples prepared from rare earth nitrates were considered to contain nitrate anion from IR and TG-DTA results. The systems of $R_2(CO_3)_3$-H_3PO_4 and RCl_3-H_3PO_4 in P/R=1 also produced Rhabdophane-type RPO_4. The crystallinity of this salt prepared from rare earth chloride was higher than that prepared from rare earth carbonate. RF_3 was difficult to react with $(NH_4)_2HPO_4$ and H_3PO_4. In P/R=5, oxalate and fluoride anions assisted the crystal growth of RP_5O_{14}.

2.4. References

[1] R. C. L. Mooney, Acta Cryst., **3**, 337, (1950).

[2] M. Tsuhako, S. Ikeuchi, T. Matsuo, I. Motooka, and M. Kobayashi, Bull. Chem. Soc. Jpn., **52**, 1034, (1979).

[3] H. Nariai, I. Motooka, M. Doi, and M. Tsuhako, Bull. Chem. Soc. Jpn., **58**, 379, (1985).

[4] H. Nariai, J. Suenaga, M. Tsuhako, and I. Motooka, Phosphorus Res. Bull., **4**, 99, (1994).

[5] H. Onoda, H. Nariai, H. Maki, and I. Motooka, Phosphorus Res. Bull., **9**, 69, (1999).

[6] I. L. Botto and E. J. Baran, Z. Anorg. Allg. Chem., **435**, 293, (1977).

[7] K. Byrappa and B. N. Litvin, J. Mater. Sci., **18(3)**, 703, (1983).

[8] J. R. Van Wazer, "Phosphorus and Its Compound", Vol. I and II, Interscience Publishers Inc, New York, 1961.

[9] P. Chen and T. Mah, J. Mater. Sci., **32**, 3863, (1997).

[10] N. Nishida, N.Yonetani, T. Yoshioka, and A. Okuwaki, Rare Earth, **32**, 250, (1998).

[11] G. Adachi, "Kidorui no Kagaku", Chap. 14, Sec. 1-4, pp. 270-369, Kagaku dojin Ltd., Kyoto, 1999.

Chapter 3.
Mechanochemical effects on synthesis of Rhabdophane-type rare earth phosphates

Abstract

Mechanochemical effects were investigated in the mixture of a rare earth compound ($Nd(NO_3)_3 \cdot 6H_2O$, $NdCl_3 \cdot 6H_2O$, $Nd_2(CO_3)_3 \cdot 8H_2O$, $Ce(NO_3)_3 \cdot 6H_2O$, $CeCl_3 \cdot 7H_2O$, or $Ce_2(CO_3)_2 \cdot 8H_2O$) and $(NH_4)_2HPO_4$. The mixture was ground and then heated. These ground mixtures and thermal products were characterized by X-ray diffraction (XRD), Fourier transform infrared spectroscopy (FT-IR), thermogravimetry - differential thermal analyses (TG-DTA), and adsorption of nitrogen. By grinding, Rhabdophane-type rare earth (Nd or Ce) phosphate was formed in the mixture of $Nd(NO_3)_3 \cdot 6H_2O$-$(NH_4)_2HPO_4$ or $Ce(NO_3)_3 \cdot 6H_2O$-$(NH_4)_2HPO_4$. By mechanical treatment, Rhabdophane-type neodymium phosphate was formed at lower temperature in the mixture of $NdCl_3 \cdot 6H_2O$-$(NH_4)_2HPO_4$. The mixture of $CeCl_3 \cdot 7H_2O$-$(NH_4)_2HPO_4$ indicated XRD peaks of CeO_2 by heating, whereas ground mixtures transformed to Rhabdophane-type cerium phosphate. Specific surface areas of Rhabdophane-type neodymium and cerium phosphates verified from 0.1 m^2/g to 120 m^2/g depending on various synthetic conditions. Rhabdophane-type neodymium and cerium phosphates which had large specific surface area were obtained by grinding with ethanol and then heating.

3.1. Introduction

Physical and chemical properties of solid materials are changed by crusing, pressing, milling, and other mechanical treatments [1-6]. These phenomena are known as mechanochemical effects, which comprises of the increase of specific

surface area, defects and strain, and the cleavage of chemical bonds, and so on. For these effects, mechanically treated materials were regarded as in an active state. These mechanical treatments have been applied to inorganic materials. By using these mechanical treatments, new materials has tried to be synthesized, higher yields of products and sintering effect at lower temperature could be expected.

These mechanochemical phenomena largely depend on the conditions of the mechanical treatments, for example the apparatus, atmosphere, and period of treatment [7,8]. By the kind of apparatus, for example ball-mill, vibration-mill, planetary-mill, and so on, materials obtained activation energy in different methods. Therefore, the field of mechanochemical effects was large and needed much studies. To improve the efficiency of the mechanical treatment, various grinding media were used. Aceton, ethanol, benzene, triethanolamine, dodecylamine, and so on were reported much efficacious solvents as a liquid grinding media [9]. These media had effects to lower the surface energy, to enhance the degree of dispersion, and so on. On the other hand, some solvent works as a floccuating agent. By the period of treatment increasing, the effective phenomena, for example the increase of specific surface area and so on, occurred larger. However, the phenomena which contradicted these mechanochemical effects, for example floccuation, also happened. Therefore, materials treated mechanically reached an equilibrium state at a certain period of treatment.

Then, Rhabdophane-type rare earth phosphate had the specific structure with vacant spaces in the crystal lattice [10-12]. Rare earth phosphates were reported to be formed from phosphoric acid and rare earth oxides in previous reports [13-15]. However, other synthetic method of them was few reported.

The author investigated mechanochemical effect in the mixture of Nd_2O_3-$(NH_4)_2HPO_4$ or CeO_2-$(NH_4)_2HPO_4$ (Chap. 1). Formation temperature of Monazite-

type neodymium and cerium orthophosphates shifted lower by mechanochemical treatment and grinding media (water and ethanol). However, as a whole, mechanochemical effects appeared a little in the mixtures of Nd_2O_3-$(NH_4)_2HPO_4$ and CeO_2-$(NH_4)_2HPO_4$. Neodymium and cerium oxides reacted with diammonium hydrogenphosphate to Monazite-type neodymium and cerium orthophosphates at above 800℃, respectively. The energy needed for this reaction was large. The energy which raw materials obtained by mechanochemical treatment was considered to be much smaller than the energy needed for this reaction.

The author also studied on some rare earth compounds (rare earth element; lanthanum, cerium, and neodymium, anion; oxide, carbonate, chloride, nitrate, sulfate, oxalate, and fluoride) for synthesis of various rare earth phosphates (orthophosphate, polyphosphate, and ultraphosphate) (Chap. 2). Each of rare earth compounds ($La(NO_3)_3 \cdot 6H_2O$, $LaCl_3 \cdot 7H_2O$, $La_2(CO_3)_3$, $Ce(NO_3)_3 \cdot 6H_2O$, $CeCl_3 \cdot 7H_2O$, $Ce_2(CO_3)_3 \cdot 8H_2O$, $Nd(NO_3)_3 \cdot 6H_2O$, $NdCl_3 \cdot 6H_2O$, and $Nd_2(CO_3)_3 \cdot 8H_2O$) reacted with $(NH_4)_2HPO_4$ at lower temperature than each rare earth oxide.

In this Chapter, mechanochemical effects were studied on the systems of a rare earth compound ($Nd(NO_3)_3 \cdot 6H_2O$, $NdCl_3 \cdot 6H_2O$, $Nd_2(CO_3)_3 \cdot 8H_2O$, $Ce(NO_3)_3 \cdot 6H_2O$, $CeCl_3 \cdot 7H_2O$, or $Ce_2(CO_3)_2 \cdot 8H_2O$) and $(NH_4)_2HPO_4$.

3.2. Experimental

Figure 3-1 shows a schematic diagram of experimental procedure. Each of rare earth compounds ($Nd(NO_3)_3 \cdot 6H_2O$, $NdCl_3 \cdot 6H_2O$, $Nd_2(CO_3)_3 \cdot 8H_2O$, $Ce(NO_3)_3 \cdot 6H_2O$, $CeCl_3 \cdot 7H_2O$, and $Ce_2(CO_3)_2 \cdot 8H_2O$) was treated with $(NH_4)_2HPO_4$ with grinding-

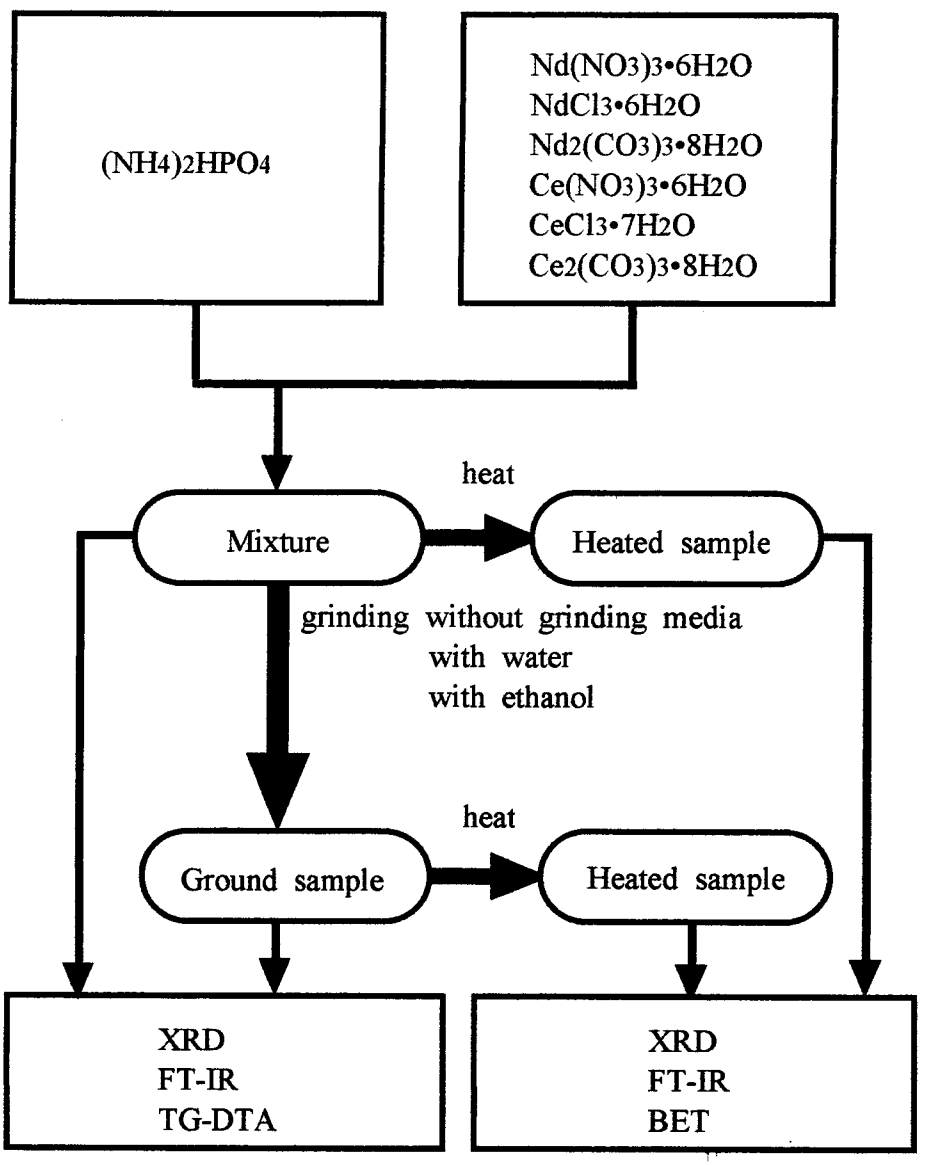

Fig. 3-1. Experimental procedure.

mill from Ishikawa-kojyo Ltd. for 6 hours. Mixtures were also ground with water or ethanol in the ratio of liquid / solid equal about 5 ml/g. Resulting products were dried at 50℃, then analyzed by XRD, FT-IR, and TG-DTA. XRD patterns were recorded on a Rigaku Denki RINT 1200M X-Ray diffractometer using monochromated

CuK α radiation. The IR spectra were recorded on a HORIBA FT-IR spectrometer spectrometer FT-710 with a KBr disk method. TG-DTA were carried out at a heating rate of 10℃/min, using a Rigaku Denki Thermo Plus TG8120. Specific surface areas of Rhabdophane-type neodymium and cerium phosphates were calculated from the amount of nitrogen gas adsorbed at the temperature of liquid nitrogen by five-points BET method (P/Po=0.10, 0.15, 0.20, 0.25, and 0.30) with Gemini-Micromeritics 2360 from Shimadzu Corp. Ltd.

3. Results and discussion

3.1. Mechanochemical reactions

The period of mechanical treatment is an important factor on mechanochemical reaction. In previous study (Chap. 1), sample ground for 6 hours had similar results with long-time-ground sample. Then, the period of mechanical treatment was 6 hours in this Chapter.

Figure 3-2 shows XRD results of samples prepared from $Nd(NO_3)_3 \cdot 6H_2O$-$(NH_4)_2HPO_4$. The mixture(non-ground, (a)) had unknown peaks. The peaks of Rhabdophane-type neodymium phosphate and ammonium nitrate appeared in XRD patterns of ground samples (b)-(d). All the samples heated at 150℃ indicated single phase pattern of Rhabdophane-type neodymium phosphate from XRD analyses. However, IR spectra indicated the existence of nitrate anion in samples heated at 150℃. The absorptions of nitrate ion at about 1400cm^{-1} and 830cm^{-1} in IR spectra became smaller in samples heated at 300℃.

Figure 3-3 shows XRD patterns of samples prepared from $Ce(NO_3)_3 \cdot 6H_2O$-

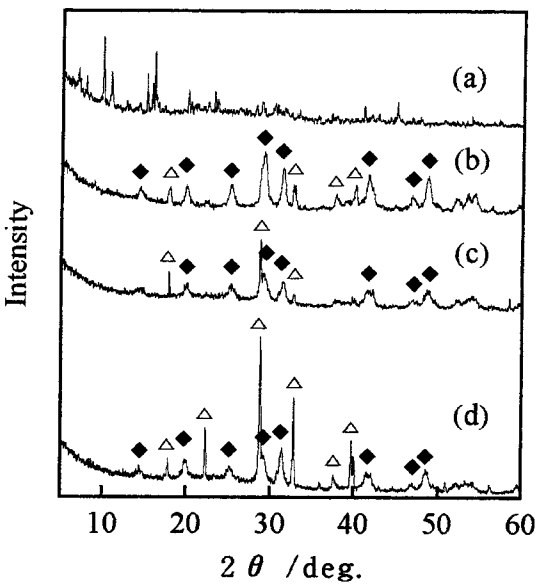

Fig. 3-2. XRD patterns of samples prepared from $Nd(NO_3)_3 \cdot 6H_2O$-$(NH_4)_2HPO_4$, (a) mixture (non-ground), (b) sample ground without grinding media, (c) sample ground with water, and (d) sample ground with ethanol, ◆; Rhabdophane-type neodymium phosphate and △; ammonium nitrate.

$(NH_4)_2HPO_4$. The ground samples (b)-(d) had the peaks of Rhabdophane-type cerium phosphate and ammonium nitrate. Sample (c) had stronger peaks of ammonium nitrate than samples (b) and (d). Both $Ce(NO_3)_3 \cdot 6H_2O$ and $(NH_4)_2HPO_4$ are soluble in water. The surface of them was activated by grinding, therefore the solubility of the materials in water increased [16]. Generally, ionic bond inorganic materials tend to ionize by grinding [19]. The coexist water promoted this ionization reaction. In the systems of $NdCl_3 \cdot 6H_2O$-$(NH_4)_2HPO_4$ and $CeCl_3 \cdot 7H_2O$-$(NH_4)_2HPO_4$, sample ground with water also had strong XRD peaks. At 150℃, all samples indicated Rhabdophane-type cerium phosphate. The absorptions of nitrate ion were observed in IR spectra of all samples heated at 150℃. At 300℃, these absorptions

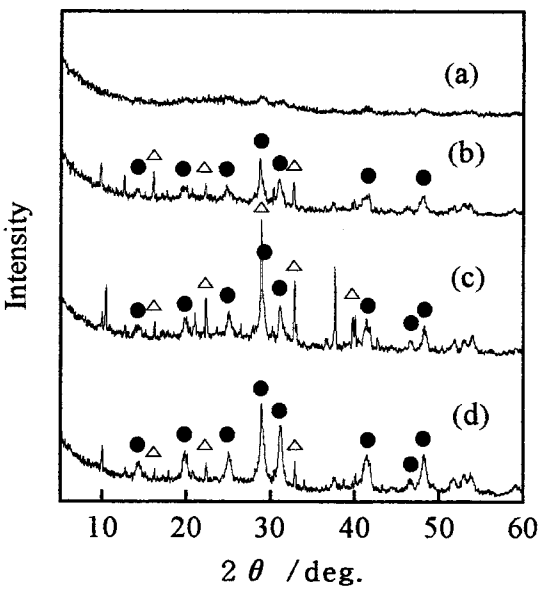

Fig. 3-3. XRD patterns of samples prepared from $Ce(NO_3)_3 \cdot 6H_2O$-$(NH_4)_2HPO_4$, (a) mixture (non-ground), (b) sample ground without grinding media, (c) sample ground with water, and (d) sample ground with ethanol, ●; Rhabdophane-type cerium phosphate and △; ammonium nitrate.

disappeared in all samples.

In the system using neodymium chloride, all non-heated samples (mixture, sample ground without grinding media, sample ground with water, and sample ground with ethanol) had the peaks of ammonium chloride in XRD patterns. XRD results of samples heated at 150℃ are shown in Fig. 3-4. The mixture (a) had the unknown peaks, whereas ground samples (b)-(d) had the peaks of Rhabdophane-type neodymium phosphate and ammonium chloride. The strong peaks of Rhabdophane-type neodymium phosphate and ammonium chloride were observed in XRD pattern of sample (c). All samples heated at 300℃ disappeared the peaks of ammonium

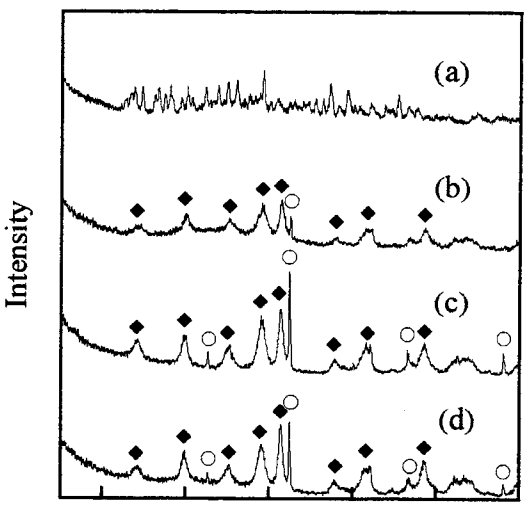

Fig. 3-4. XRD patterns of samples prepared from $NdCl_3 \cdot 6H_2O$-$(NH_4)_2HPO_4$ heated at 150℃ for 20 hours, (a) mixture (non-ground), (b) sample ground without grinding media, (c) sample ground with water, and (d) sample ground with ethanol, ◆; Rhabdophane-type neodymium phosphate and ○; ammonium chloride.

chloride. Mechanochemical effects in the system using chloride were smaller than those in the system using nitrate. These mechanochemical effects followed previous report that mechanochemical effects are related with three-dimentional structure of anion [20].

Figure 3-5 shows TG-DTA curves of samples prepared from $NdCl_3 \cdot 6H_2O$-$(NH_4)_2HPO_4$. In DTA curve of the mixture (non-ground, (a)), some endothermic peaks were observed below 400℃. TG curve of the mixture had continuous weight loss up to 400℃. DTA curves of ground samples (b)-(d) had two large endothermic

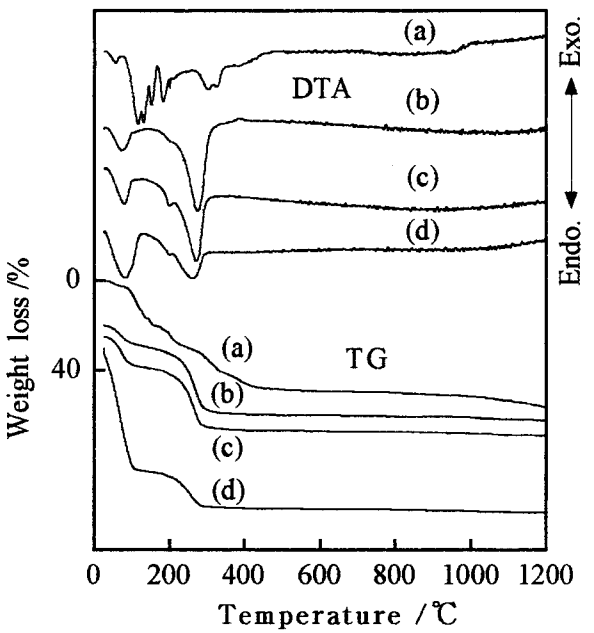

Fig. 3-5. TG-DTA curves of samples prepared from $NdCl_3 \cdot 6H_2O$-$(NH_4)_2HPO_4$, (a) mixture (non-ground), (b) sample ground without grinding media, (c) sample ground with water, and (d) sample ground with ethanol.

peaks at about 70℃ and 280℃. The peak at about 70℃ was due to volatilization of water or ethanol. The weight loss at about 280℃ in TG curve was small in sample (d) and large in samples (b) and (c). The peak at about 280℃ was due to volatilization of ammonia and hydrogen chloride. Ammonium chloride decomposed at high temperature, because Rhabdophane-type rare earth phosphate had vacancies. DTA curves of sample (d) had smaller endothermic peak at about 280℃ than samples (b) and (c), and TG curve of sample (d) had small weight loss. It was considered that the decomposition of ammonium chloride occurred in grinding with ethanol. The results supported the idea that the reaction between $NdCl_3 \cdot 6H_2O$ and

$(NH_4)_2HPO_4$ occurred at particular temperatures because of uniformity of the samples by mechanical treatment.

In the system using cerium chloride, the remarkable difference appeared in products at 300℃. Figure 3-6 shows XRD patterns of samples prepared from $CeCl_3 \cdot 7H_2O$-$(NH_4)_2HPO_4$ heated at 300℃ for 20 hours. The mixture (a) had the peaks of cerium oxide, whereas ground samples (b)-(d) indicated XRD pattern of Rhabdophane-type cerium phosphate. The peaks of sample (c) were stronger than those of others.

However, Rhabdophane-type neodymium and cerium phosphates were not formed by heating the two mixtures of $Nd_2(CO_3)_3 \cdot 8H_2O$-$(NH_4)_2HPO_4$ and $Ce_2(CO_3)_3 \cdot 8H_2O$-

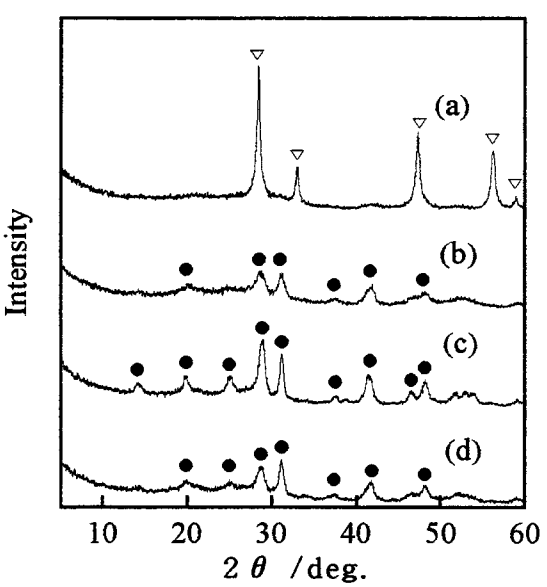

Fig. 3-6. XRD patterns of samples prepared from $CeCl_3 \cdot 7H_2O$-$(NH_4)_2HPO_4$ heated at 150℃ for 20 hours, (a) mixture (non-ground), (b) sample ground without grinding media, (c) sample ground with water, and (d) sample ground with ethanol, ●; Rhabdophane-type cerium phosphate and ▽; cerium oxide.

$(NH_4)_2HPO_4$, respectively. The ground samples didn't also form Rhabdophane-type neodymium and cerium phosphates by heating.

3.3.2. Specific surface areas

Table 3-1 shows specific surface areas of Rhabdophane-type neodymium and cerium phosphates synthesized in various conditions. As mentioned above, samples heated at 150℃ in the systems of $Nd(NO_3)_3 \cdot 6H_2O$-$(NH_4)_2HPO_4$ and $Ce(NO_3)_3 \cdot 6H_2O$-$(NH_4)_2HPO_4$ indicated the existence of ammonium nitrate from XRD and IR analyses. In the same way, samples heated at 150℃ in the systems of $NdCl_3 \cdot 6H_2O$-$(NH_4)_2HPO_4$ and $Ce(NO_3)_3 \cdot 6H_2O$-$(NH_4)_2HPO_4$ indicated the existence of ammonium chloride. Therefore, samples were washed with water to remove ammonium nitrate or ammonium chloride, and then specific surface areas of samples were measured by adsorption of nitrogen. Large increase of specific surface areas were observed on these washed samples at 150℃. Ammonium nitrate and ammonium chloride made specific surface areas of thermal products small. Specific surface areas at 300℃ had less change than those at 150℃. Samples heated at 300 ℃ had less ammonium nitrate and ammonium chloride.

In samples heated at 300℃, ground samples had larger specific surface areas than the mixture (non-ground, (a)). Especially, samples (d) had much larger ones. The factor which made specific surface area larger is to mix in minuteness by grinding and then to react much throughly in heating process. The factor which made specific surface areas smaller is to be flocculated in grinding procedure. Specific surface areas of Rhabdophane-type neodymium and cerium phosphates depended on these factors. Since grinding with ethanol prevented the flocculation of materials, samples ground with ethanol had larger specific surface areas than others.

Table 3-1 Specific surface areas of Rhabdophane-type rare earth phosphates /$m^2 \cdot g^{-1}$

rare earth anion	condition	Ce		Nd	
		150℃ 20h	300℃ 20h	150℃ 20h	300℃ 20h
Nitrate	(a)	34.0	81.1	0.4	30.1
	(b)	0.1	86.7	0.5	96.9
	(c)	0.1	87.6	36.8	95.6
	(d)	7.6	114.0	20.5	119.0
	(e)	77.6	106.4	89.3	114.2
Chloride	(a)	×	×	×	61.9
	(b)	4.6	52.5	5.3	69.9
	(c)	12.1	46.1	16.3	67.6
	(d)	24.9	64.8	38.6	82.1
	(e)	86.8	77.5	108.5	87.7

× represented this condition had not produced Rhabdophane-type rare earth phosphate, (a); the mixture (non-ground), (b); sample ground without grinding media, (c); samples ground with water, (d); sample ground with ethanol, and (e); sample washed with water after grinding with ethanol and then heating.

Rhabdophane-type rare earth phosphate is known to have vacancies [10-12]. Figure 3-7 shows pore size distribution of samples prepared from Nd(NO3)3•6H2O-(NH4)2HPO4 at 300℃ by Barett - Joyner - Halenda method [19]. Pretreatment by grinding gave the difference of pore surface areas of products, however didn't give the difference of pore size distribution.

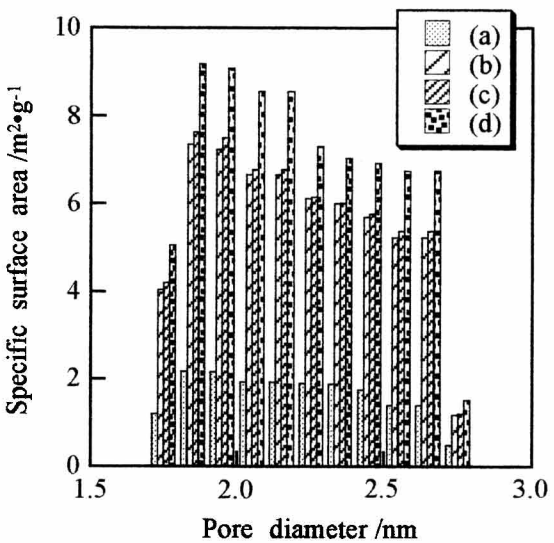

Fig. 3-7. Pore size distribution of samples prepared from $Nd(NO_3)_3 \cdot 6H_2O$-$(NH_4)_2HPO_4$ at 300℃, (a) mixture (non-ground), (b) sample ground without grinding media, (c) sample ground with water, and (d) sample ground with ethanol.

3.4. Conclusion

Rhabdophane-type rare earth (Nd or Ce) phosphate was produced in mechanochemical reaction between $Nd(NO_3)_3 \cdot 6H_2O$-$(NH_4)_2HPO_4$ or $Ce(NO_3)_3 \cdot 6H_2O$-$(NH_4)_2HPO_4$. Rhabdophane-type neodymium phosphate was formed at lower temperature in the mixture of $NdCl_3 \cdot 6H_2O$-$(NH_4)_2HPO_4$. In the system of $CeCl_3 \cdot 7H_2O$-$(NH_4)_2HPO_4$, the pretreatment of grinding changed thermal product from cerium

oxide to Rhabdophane-type cerium phosphate. XRD peaks of Rhabdophane-type neodymium or cerium phosphate were strong in samples ground with water. Samples ground with ethanol had large specific surface areas.

3.5. References

[1] F. Cardellini, V. Contini, and G. Mazzone, J. Mater. Sci., **31**, 4175, (1996).

[2] P. Balaz, T. Havlik, Z. Bastl, J. Briancin, and R. Kammel, J. Mater. Sci. Letters, **15**, 1161, (1996).

[3] E. G. Avvakumov, E. T. Devyatkina, and N. V. Kosova, J. Solid State Chem., **113**, 379, (1994).

[4] N. Hashimoto, H. Yoden, and S. Deki, J. Am. Ceram. Soc., **76**, 438, (1993).

[5] W. Kim, Q. Zhang, and F. Saito, J. Mater. Sci., **35**, 5401, (2000).

[6] K. Kudaka, K. Iizuka, T. Sasaki, and H. Izumi, J. Am. Ceram. Soc., **83**, 2887, (2000).

[7] H. Nariai, M. Tada, M. Tsuhako, and I. Motooka, Phosphorus Res. Bull., **5**, 125, (1995).

[8] H. Nariai, S. Shibamoto, H. Maki, and I. Motooka, Phosphorus Res. Bull., **8**, 101, (1998).

[9] T. Kubo, "Mechanochemistry gairon", p.134, Tokyo Kagaku Dojin Ltd., Tokyo, 1978.

[10] H. Nariai, I. Motooka, M. Doi, and M. Tsuhako, Bull. Chem. Soc. Jpn., **58**, 379, (1985).

[11] Y. Hikichi, T. Sasaki, K. Murayama, T. Nomura, and M. Miyamoto, J. Am. Ceram. Soc., **72**, 1073, (1989).

[12] R. C. L. Mooney, Acta Cryst., **3**, 337, (1950).

[13] M. Tsuhako, S. Ikeuchi, T. Matsuo, I. Motooka, and M. Kobayashi, Bull. Chem. Soc. Jpn., **52**, 1034, (1979).

[14] P. Chen and T. Mah, J. Mater. Sci., **32**, 3863, (1997).

[15] H. Onoda, H. Nariai, H. Maki, and I. Motooka, Phosphorus Res. Bull., **9**, 69, (1999).

[16] T. Kubo and T. Miyazaki, Kogyo Kagaku Shi, **71**, 1301, (1968).

[17] T. Kubo, "Yuukibutu no mechanochemistry", p.135, Sougou Kouhan Ltd., Tokyo, 1985.

[18] M. Quatinetz, R. J. Schafer, C. R. Smeal, NASA Tech. Note, D-879 (1962).

[19] E. P. Barrett, L. G. Joyner, and P. P. Halenda, J. Am. Chem. Soc., **73**, 373, (1951).

Chapter 4.
Addition of urea or biuret on synthesis of Rhabdophane-type rare earth phosphates

Abstract

Urea or biuret was added into the thermal synthetic system of Rhabdophane-type neodymium and cerium phosphates. The mixture of a rare earth compound, a phosphorus compound, and an additive ($CO(NH_2)_2$ or $NH(CONH_2)_2$) was heated at 150℃ or 300℃ for 20 hours, and the thermal products were analyzed by XRD, FT-IR, and BET method. H_3PO_4 and $(NH_4)_2HPO_4$ were used as for phosphorus compounds, and for rare earth compounds, Nd_2O_3, $Nd(NO_3)_3 \cdot 6H_2O$, $NdCl_3 \cdot 6H_2O$, $Nd_2(CO_3)_3 \cdot 8H_2O$, CeO_2, $Ce(NO_3)_3 \cdot 6H_2O$, $CeCl_3 \cdot 7H_2O$, and $Ce_2(CO_3)_3 \cdot 8H_2O$ were used. Urea and biuret worked not only as a dispersing agent but also as a reactant. By the addition of biuret, the thermal products changed from cerium oxide to Rhabdophane-type cerium phosphate in the system using $CeCl_3 \cdot 7H_2O$ and $(NH_4)_2HPO_4$. Addition of urea or biuret had influence on specific surface area of Rhabdophane-type neodymium and cerium phosphates. Furthermore, to increase the uniformity of the raw solid materials, mechanical treatment was performed. The mixture of diammonium hydrogenphosphate and a rare earth compound was ground with water or ethanol, and then heated. The influence by the addition of urea or biuret was also studied in these systems.

4.1. Introduction

Phosphates have been used for ceramic materials, catalysts, fluorescent materials, dielectric substances, metal surface treatment, manure, detergent, food additives, fuel cells, etc. In general, phosphates transform to various other phosphates with hydrolysis and dehydration reactions by heating [1,2]. The formation and structure of

phosphates depend on heating temperature, rate, and time, the cooling rate of melts, the atmosphere, and kinds of cations in phosphate [3,4]. Anhydrous rare earth orthophosphate is the main component of natural Monazite and Xenotime which are rare earth element ores. Rhabdophane-type rare earth orthophosphates have a specific structure with vacant spaces [5]. Rhabdophane-type rare earth phosphate had larger specific surface area than other rare earth phosphates [6].

Thermal syntheses of phosphates were widely studied. The effects of addition of organic nitrogen compounds on synthesis of various phosphates were reported. Urea, biuret, cyanuic acid, and melamine were added on synthesis of sodium *cyclo*-triphosphate from sodium dihydrogenphosphate [7]. The addition of urea and biuret brought about the high yield of sodium *cyclo*-triphosphate. The addition of urea into lithium phosphate made to change the thermal product from *cyclo*-hexaphosphate to *cyclo*-triphosphate [8]. A novel *cyclo*-octaphosphate was formed in the mixture of copper (Ⅱ) oxide - ammonium dihydrogenphosphate - urea [9]. Furthermore, an addition of urea supported the formation of *cyclo*-triphosphate in the mixture of lead (Ⅱ) oxide - ammonium dihydrogenphosphate - urea [10].

The uniformity of raw materials is important in solid state reaction. Physical and chemical properties of solid materials are changed by crusing, pressing, milling, and other mechanical treatments [11-16]. These phenomena are known as mechanochemical effects, which comprises of the increase of surface area, defects and strain, and the cleavage of chemical bonds, and so on. These mechanochemical phenomena remarkably depend on the conditions of the mechanical treatment [17,18]. To improve the efficiency of the mechanical treatment, various liqiud and solid compounds were reported as grinding media. These grinding media had effects to lower the surface energy, to enhance the degree of dispersion, and so on. Mechanochemical treatment with water or ethanol as a pretreatment was effective method to obtain

Rhabdophane-type neodymium and cerium phosphates which have large specific surface area (Chap.3).

In this Chapter, the influence by the addition of urea or biuret was investigated on synthesis of Rhabdophane-type neodymium and cerium phosphates. Furthermore, mechanochemical effects were also studied in synthesis of these phosphates.

4.2. Experimental

4.2.1. Sample preparation

Figure 4-1 shows schematic diagram of experimental procedure. Urea was mixed with phosphoric acid and a rare earth compound in the molecular ratio of $CO(NH_2)_2$ / H_3PO_4 / rare earth element = 0 / 1 / 1, 1 / 1 / 1, or 3 / 1 / 1. As for rare earth compounds, Nd_2O_3, $Nd(NO_3)_3 \cdot 6H_2O$, $NdCl_3 \cdot 6H_2O$, $Nd_2(CO_3)_3 \cdot 8H_2O$, CeO_2, $Ce(NO_3)_3 \cdot 6H_2O$, $CeCl_3 \cdot 7H_2O$, and $Ce_2(CO_3)_3 \cdot 8H_2O$ were used. Biuret was used in the same manner as urea. Diammonium hydrogenphosphate replaced with phosphoric acid in the above mixtures.

The mixture of an additive (urea or biuret), diammonium hydrogenphosphate, and a rare earth compound was also ground with water or ethanol for 6 hours in the liquid - solid ratio of about 5 ml/g. This mixture was heated at 150℃ or 300℃ for 20 hours.

In this Chapter, NA, U1, and U3 samples are defined as the materials prepared in $CO(NH_2)_2$ / phosphorus / rare earth element = 0 / 1 / 1, 1 / 1 / 1, and 3 / 1 / 1, respectively. In the same way, B1 and B3 samples are defined as the materials prepared in $NH(CONH_2)_2$ / phosphorus / rare earth element = 1 / 1 / 1 and 3 / 1 / 1,

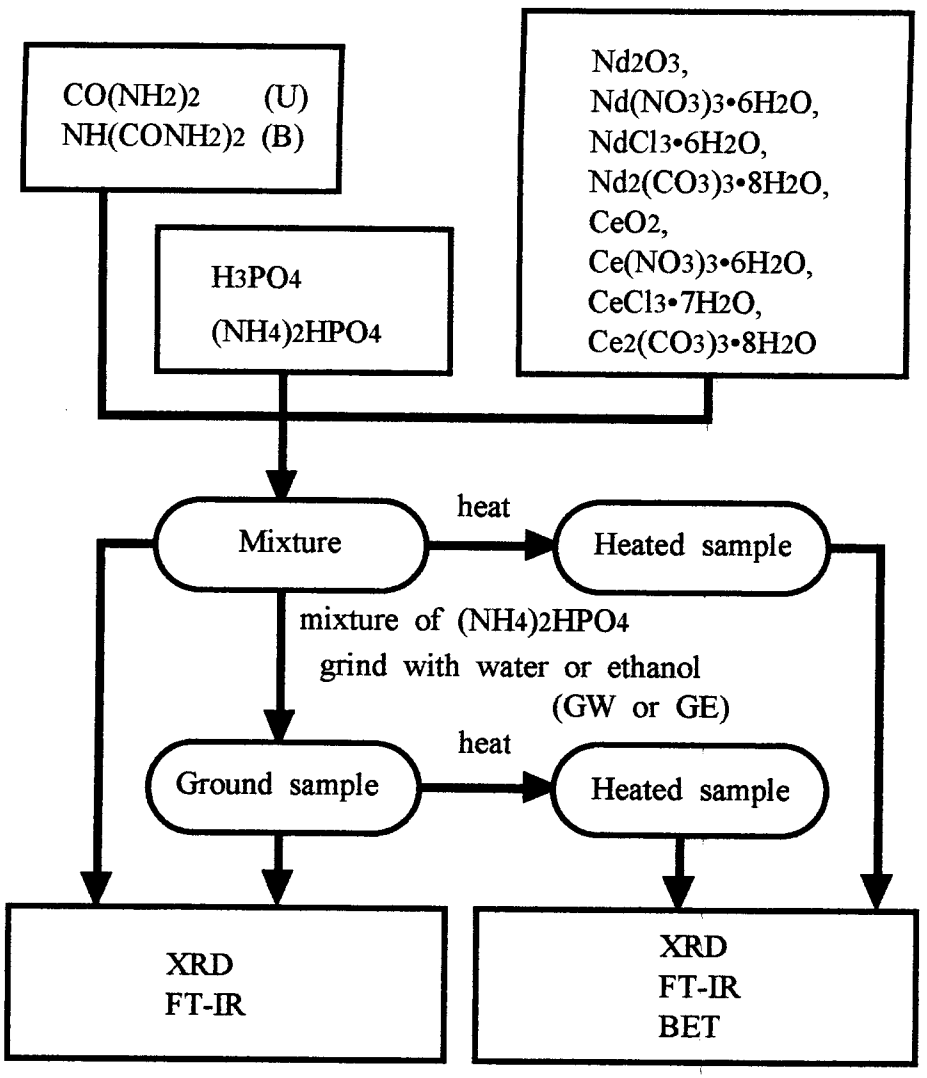

Fig. 4-1. Experimental procedure.

respectively. Furthermore, GW and GE are defined as samples ground with water and ethanol, respectively.

4.2.2. Analytical procedures

X-Ray diffraction patterns were recorded on a Rigaku Denki RINT 1200M X-Ray diffractometer using monochromated CuK α radiation. The IR spectra were recorded on a HORIBA FT-IR spectrometer FT-710 with a KBr disk method. The specific surface areas of samples were calculated from the amount of nitrogen gas adsorbed at the temperature of liquid nitrogen by five-points BET method (P/Po=0.10, 0.15, 0.20, 0.25, and 0.30) with Gemini-Micromeritics 2360 from Shimadzu Corp. Ltd. The grinding apparatus was an Ishikawa's grinder equipped with an agate motar.

4.3. Results and discussion

4.3.1. An additive / H_3PO_4 / a rare earth compound

In previous reports [7-10], the effects of addition of organic nitrogen compounds were studied in the phosphorus / cation ratio of *cyclo*-phosphates. Therefore, the author investigated the effects of addition of urea on formation of rare earth phosphates in the ratio of phosphorus / rare earth element (La, Ce, or Pr) = 3. The effects of addition were little observed because rare earth polyphosphates ($La(PO_3)_3$, $Ce(PO_3)_3$, and $Pr(PO_3)_3$) were easily formed. In this Chapter, the effects of addition of urea or biuret were investigated in the ratio of rare earth orthophosphate (P / Nd = 1 or P / Ce = 1).

Figure 4-2 shows typical XRD patterns of thermal products. Thermal products in the system of H_3PO_4-CeO_2 (NA, U1, U3, B1, and B3) were the mixture of CeO_2 and CeP_2O_7 (for example Fig. 4-2 (a)). In the system of H_3PO_4-CeO_2, Rhabdophane-type cerium phosphate was not formed with and without the addition of urea or

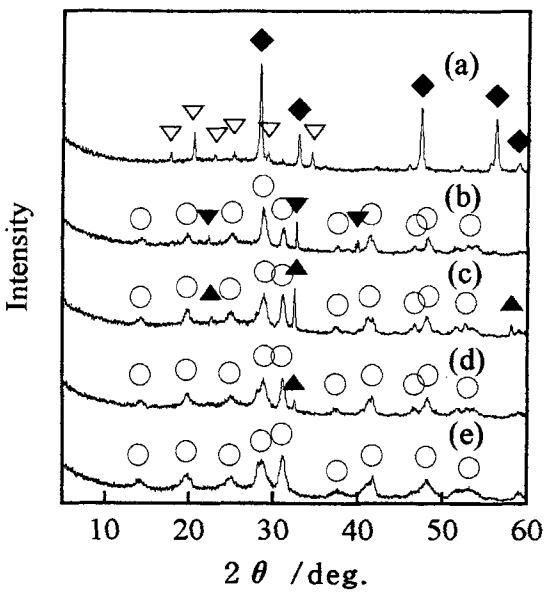

Fig. 4-2. XRD patterns of samples, (a) U3-H_3PO_4-CeO_2 300℃ 20 hours, (b) U3-H_3PO_4-$Ce(NO_3)_3$•$6H_2O$ 150℃ 20 hours, (c) U3-H_3PO_4-$CeCl_3$•$7H_2O$ 150℃ 20 hours, (d) B3-H_3PO_4-$CeCl_3$•$7H_2O$ 150℃ 20 hours, and (e) B3-H_3PO_4-$Ce_2(CO_3)_3$•$8H_2O$ 150℃ 20 hours, ◆; CeO_2, ▽; CeP_2O_7, ○; Rhabdophane-type $CePO_4$, ▼; NH_4NO_3, and ▲; NH_4Cl.

biuret. Samples of H_3PO_4-$Ce(NO_3)_3$•$6H_2O$, H_3PO_4-$CeCl_3$•$7H_2O$, and H_3PO_4-$Ce_2(CO_3)_3$•$8H_2O$ at 150℃ and 300℃ (NA, U1, U3, B1, and B3) indicated XRD peak patterns of Rhabdophane-type cerium phosphate (for example Fig. 4-2 (b)-(e)). Furthermore, the peaks of ammonium nitrate were also observed in XRD pattern of sample of U3-H_3PO_4-$Ce(NO_3)_3$•$6H_2O$ at 150℃ (Fig. 4-2 (b)). Samples of U3-H_3PO_4-$CeCl_3$•$7H_2O$ and B3-H_3PO_4-$CeCl_3$•$7H_2O$ at 150℃ had the peaks of ammonium chloride (Fig. 4-2 (c)(d)). Ammonium nitrate and ammonium chloride were decomposed and volatilized below 300℃. Urea and biuret worked not only as a

dispersing agent but also as a reactant. These reactions are formulated as follows;

$H_3PO_4+Ce(NO_3)_3+2(NH_2)_2CO+2H_2O \rightarrow CePO_4+3NH_4NO_3+2CO_2+NH_3$ (1)

$4NH_4NO_3 \rightarrow 4NH_3+4NO_2+2H_2O+O_2$ (2)

$H_3PO_4+CeCl_3+2(NH_2)_2CO+2H_2O \rightarrow CePO_4+3NH_4Cl+2CO_2+NH_3$ (3)

$NH_4Cl \rightarrow NH_3+HCl$ (4)

$H_3PO_4+CeCl_3+(NH_2CO)_2NH+2H_2O \rightarrow CePO_4+3NH_4Cl+2CO_2$ (5)

$NH_4Cl \rightarrow NH_3+HCl$ (4)

Urea and biuret were also decomposed simply at the same time by heating.

$(NH_2)_2CO+H_2O \rightarrow 2NH_3+CO_2$ (6)

$(NH_2CO)_2NH+2H_2O \rightarrow 3NH_3+2CO_2$ (7)

Figure 4-3 shows typical IR spectra of thermal products. IR spectrum of samples of

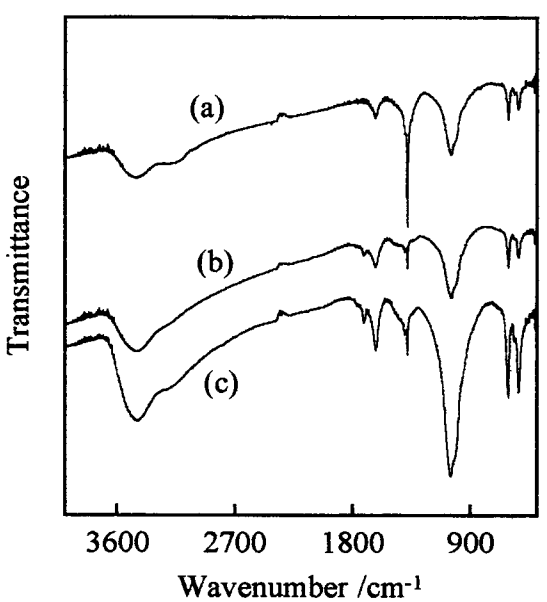

Fig. 4-3. IR spectra of samples at 150℃ for 20 hours, (a) U1-H_3PO_4-$Ce(NO_3)_3$•$6H_2O$, (b) U1-H_3PO_4-$CeCl_3$•$7H_2O$, and (c) U1-H_3PO_4-$Ce_2(CO_3)_3$•$8H_2O$.

H_3PO_4-CeO_2 was not shown because Rhabdophane-type cerium phosphate was not formed in these samples. Samples of H_3PO_4-$Ce(NO_3)_3 \cdot 6H_2O$ (NA, U1, U3, B1, and B3) at 150℃ had the strong absorption at about 1400cm^{-1} (for example Fig. 4-3 (a)). This absorption indicated the presence of nitrate anion in thermal product at 150℃ . Samples of H_3PO_4-$Ce(NO_3)_3 \cdot 6H_2O$, H_3PO_4-$CeCl_3 \cdot 7H_2O$, and H_3PO_4-$Ce_2(CO_3)_3 \cdot 8H_2O$ (U1, U3, B1, and B3) had the peaks at about 1400cm^{-1} and 3100cm^{-1} (for example Fig.4-3 (a)-(c)). These peaks were due to ammonium ion. These IR spectra agreed with the XRD results.

Rhabdophane-type neodymium phosphate was formed in all samples of H_3PO_4-Nd_2O_3, H_3PO_4-$Nd(NO_3)_3 \cdot 6H_2O$, H_3PO_4-$NdCl_3 \cdot 6H_2O$, and H_3PO_4-$Nd_2(CO_3) \cdot 8H_2O$ (NA, U1, U3, B1, and B3) by heating. XRD patterns of ammonium nitrate and ammonium chloride were also observed in the same fashion with cerium salts.

In previous reports, the influence of urea or biuret was discussed based on the nitrogen / phosphorus ratio [7,8,10]. Therefore, in this report, specific surface areas of Rhabdophane-type rare earth phosphates were also estimated on the N/P ratios. The N/P ratios of NA, U1, U3, B1, and B3 samples prepared from H_3PO_4 were 0, 2, 6, 3, and 9, respectively. Figure 4-4 shows specific surface areas of samples of H_3PO_4-$Nd(NO_3)_3 \cdot 6H_2O$, H_3PO_4-$NdCl_3 \cdot 6H_2O$, H_3PO_4-$Ce(NO_3)_3 \cdot 6H_2O$, and H_3PO_4-$CeCl_3 \cdot 7H_2O$ at 300℃. Specific surface areas of a large part of samples increased by the addition of urea or biuret. In the systems of H_3PO_4-$Nd(NO_3)_3 \cdot 6H_2O$, H_3PO_4-$Ce(NO_3)_3 \cdot 6H_2O$, and H_3PO_4-$CeCl_3 \cdot 7H_2O$, U3 samples (N/P=6) had large specific surface area. B3 samples (N/P=9) were considered to have too large N/P ratio. Specific surface areas had some relationship with the N/P ratios.

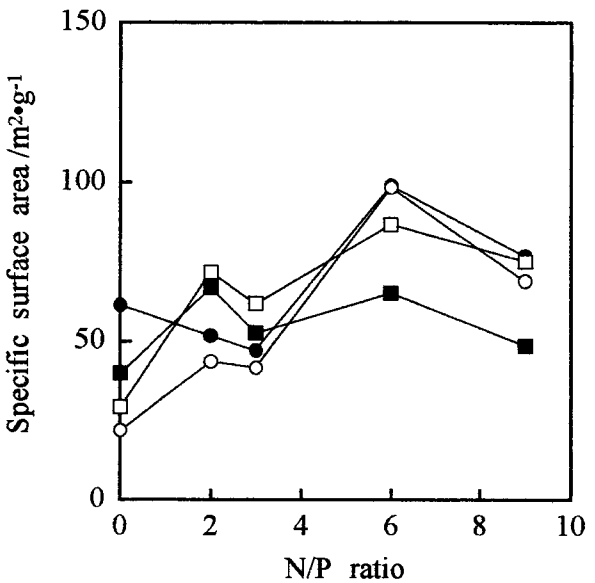

Fig. 4-4. Specific surface areas of samples of H_3PO_4-$Nd(NO_3)_3$•$6H_2O$ (●), H_3PO_4-$NdCl_3$•$6H_2O$ (■), H_3PO_4-$Ce(NO_3)_3$•$6H_2O$ (○), and H_3PO_4-$CeCl_3$•$7H_2O$ (□) at 300℃ for 20 hours.

4.3.2. An additive / $(NH_4)_2HPO_4$ / a rare earth compound

The changes in XRD patterns were observed by heating below 300℃ in the systems of $(NH_4)_2HPO_4$-$Nd(NO_3)_3$•$6H_2O$, $(NH_4)_2HPO_4$-$NdCl_3$•$6H_2O$, $(NH_4)_2HPO_4$-$Ce(NO_3)_3$•$6H_2O$, and $(NH_4)_2HPO_4$-$CeCl_3$•$7H_2O$. Rhabdophane-type neodymium or cerium phosphate was formed in the mixtures of $(NH_4)_2HPO_4$-$Nd(NO_3)_3$•$6H_2O$, $(NH_4)_2HPO_4$-$NdCl_3$•$6H_2O$, and $(NH_4)_2HPO_4$-$Ce(NO_3)_3$•$6H_2O$. Rhabdophane-type neodymium or cerium phosphate was not formed in the mixtures of $(NH_4)_2HPO_4$-Nd_2O_3, $(NH_4)_2HPO_4$-$Nd_2(CO_3)_3$•$8H_2O$, $(NH_4)_2HPO_4$-CeO_2, and $(NH_4)_2HPO_4$-$Ce_2(CO_3)_3$•$8H_2O$. There are some differences between the systems using $(NH_4)_2HPO_4$ and the systems using H_3PO_4. Diammonium hydrogenphosphate produces ammonia

by heating. Since the vapor of ammonia in the systems using $(NH_4)_2HPO_4$ was richer than that in the systems using H_3PO_4, NH_4NO_3 and NH_4Cl were easily formed. For this reason, some samples indicated the XRD peaks of NH_4NO_3 and NH_4Cl.

Figure 4-5 shows XRD peak patterns of samples prepared from $(NH_4)_2HPO_4$-$CeCl_3 \cdot 7H_2O$ at 300℃. Sample of NA-$(NH_4)_2HPO_4$-$CeCl_3 \cdot 7H_2O$ indicated XRD pattern of CeO_2. Sample of B1-$(NH_4)_2HPO_4$-$CeCl_3 \cdot 7H_2O$ had the peaks of cerium oxide and weak peaks of Rhabdophane-type cerium phosphate. Sample of B3-$(NH_4)_2HPO_4$-$CeCl_3 \cdot 7H_2O$ had single phase XRD pattern of Rhabdophane-type cerium phosphate. By heating, urea and biuret were decomposed into NH_3 and CO_2 with surrounding water (equ.(6)(7)). The NH_3 and CO_2 were considered to be the

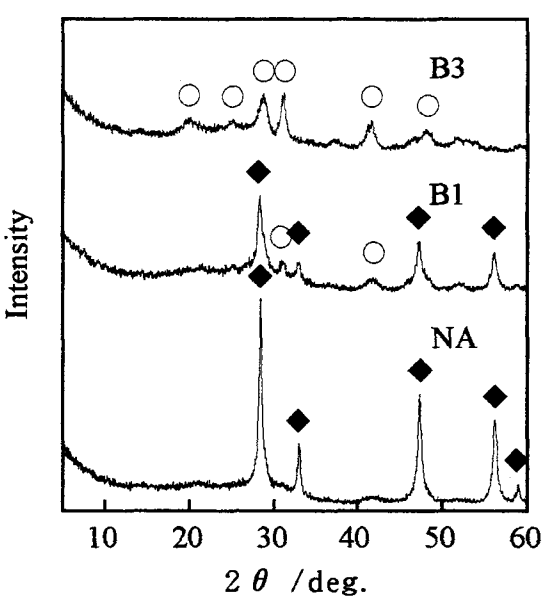

Fig. 4-5. XRD patterns of samples of $(NH_4)_2HPO_4$-$CeCl_3 \cdot 7H_2O$ heated at 300℃ for 20 hours, ○; Rhabdophane-type $CePO_4$ and ◆; CeO_2.

factors which made thermal products changed.

Specific surface areas of Rhabdophane-type neodymium and cerium phosphates were measured and estimated on the N/P ratios. The N/P ratios of NA, U1, U3, B1, and B3 samples prepared from $(NH_4)_2HPO_4$ were 2, 4, 8, 5, and 11, respectively. However, specific surface areas of Rhabdophane-type neodymium and cerium phosphates didn't have a regularity with these N/P ratios. As a factor of irregularity of specific surface areas, the mixing condition of solid materials could be considered. To increase the uniformity of the raw materials, mechanical treatment was performed.

4.3.3. Mechanochemical effects

To mix minutely and to react uniformly, mechanical treatment was occasionally used before heating [12]. From Section 4.3.2., if the mixtures of $(NH_4)_2HPO_4$-Nd_2O_3, $(NH_4)_2HPO_4$-$Nd_2(CO_3)_3 \cdot 8H_2O$, $(NH_4)_2HPO_4$-CeO_2, and $(NH_4)_2HPO_4$-$Ce_2(CO_3)_3 \cdot 8H_2O$ are treated mechanically before heating, Rhabdophane-type neodymium and cerium phosphates are unlikely to form. Therefore, in this Section 4.3.3., the systems of rare earth oxide and carbonate were not carried out. The mixtures of $(NH_4)_2HPO_4$-$Nd(NO_3)_3 \cdot 6H_2O$, $(NH_4)_2HPO_4$-$NdCl_3 \cdot 6H_2O$, $(NH_4)_2HPO_4$-$Ce(NO_3)_3 \cdot 6H_2O$, and $(NH_4)_2HPO_4$-$CeCl_3 \cdot 7H_2O$ were difficult to treat mechanically because of viscous solid. Therefore, water or ethanol was added to the mixtures of $(NH_4)_2HPO_4$-$Nd(NO_3)_3 \cdot 6H_2O$, $(NH_4)_2HPO_4$-$NdCl_3 \cdot 6H_2O$, $(NH_4)_2HPO_4$-$Ce(NO_3)_3 \cdot 6H_2O$, and $(NH_4)_2HPO_4$-$CeCl_3 \cdot 7H_2O$, and then treated with grinding-mill. The treatment with water or ethanol was expected to make surface energy decrease and to prevent the flocculation of materials.

Rhabdophane-type cerium and neodymium phosphates were not formed in purity in the systems of B1-, B3-$(NH_4)_2HPO_4$-$NdCl_3 \cdot 6H_2O$, NA-, U1-, U3-, and B1-

$(NH_4)_2HPO_4$-$CeCl_3 \cdot 7H_2O$. By grinding with water or ethanol before heating, Rhabdophane-type neodymium and cerium phosphates were produced in purity from XRD analyses in these samples.

Figure 4-6 shows specific surface areas of samples of $(NH_4)_2HPO_4$-$Nd(NO_3)_3 \cdot 6H_2O$-GW, $(NH_4)_2HPO_4$-$NdCl_3 \cdot 6H_2O$-GW, $(NH_4)_2HPO_4$-$Ce(NO_3)_3 \cdot 6H_2O$-GW, and $(NH_4)_2HPO_4$-$CeCl_3 \cdot 7H_2O$-GW. The N/P ratios of NA, U1, U3, B1, and B3 samples prepared from $(NH_4)_2HPO_4$ were 2, 4, 8, 5, and 11, respectively. In the systems of $(NH_4)_2HPO_4$-$NdCl_3 \cdot 6H_2O$-GW and $(NH_4)_2HPO_4$-$CeCl_3 \cdot 7H_2O$-GW, there was some extent relation between the specific surface areas and these N/P ratios. In

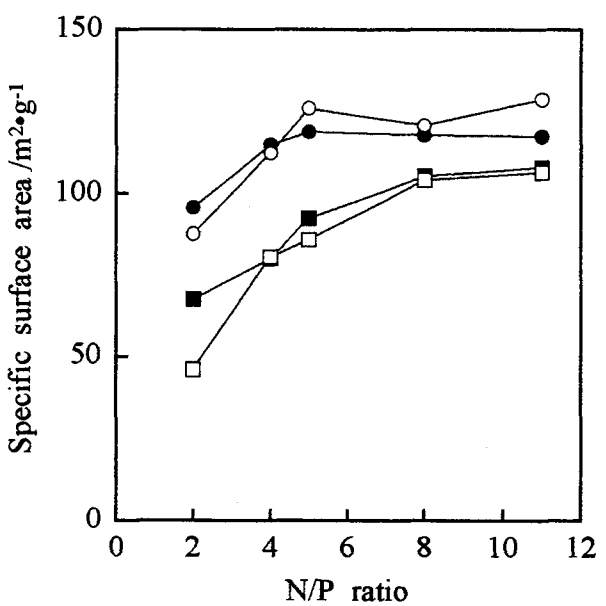

Fig. 4-6. Specific surface areas of samples of $(NH_4)_2HPO_4$-$Nd(NO_3)_3 \cdot 6H_2O$-GW (●), $(NH_4)_2HPO_4$-$NdCl_3 \cdot 6H_2O$-GW (■), $(NH_4)_2HPO_4$-$Ce(NO_3)_3 \cdot 6H_2O$-GW (○), and $(NH_4)_2HPO_4$-$CeCl_3 \cdot 7H_2O$-GW (□) at 300℃ for 20 hours.

the systems of $(NH_4)_2HPO_4$-$Nd(NO_3)_3 \cdot 6H_2O$-GW and $(NH_4)_2HPO_4$-$Ce(NO_3)_3 \cdot 6H_2O$-GW, specific surface areas became large by the addition of urea or biuret.

Specific surface areas of samples ground with ethanol were about $100 m^2/g$. These specific surface areas had little regularity with the NP ratios.

The addition of urea or biuret had influence on synthesis and specific surface areas of Rhabdophane-type neodymium and cerium phosphates.

4.4. References

[1] M. Tsuhako, S. Ikeuchi, T. Matsuo, I. Motooka, and M. Kobayashi, Bull. Chem. Soc. Jpn., **52**, 1034, (1979).

[2] I. A. Bonder, A. I. Domanskii, L. P. Mezentseva, M. G. Degen, and N. E. Kalinina, Russ. J. Inorg. Chem., **21**, 1126, (1976).

[3] S. Ohashi, Kogyo Kagaku Zasshi, **66**, 538, (1963).

[4] E. Thilo and I. Grunze, Z. Anorg. Allg. Chem., **290**, 209, (1957).

[5] R. C. L. Mooney, Acta Cryst., **3**, 337, (1950).

[6] H. Onoda, H. Nariai, A. Moriwaki, H. Maki, and I. Motooka, J. Mater. Chem., submitted (Chap.6).

[7] A. Takenaka, S. Kikui, I. Motooka, and H. Nariai, Nihon Kagaku Kaishi, **11**, 774, (1998).

[8] A. Takenaka, H. Sawa, M. Hirata, A. Yamamoto, I. Motooka, and H. Nariai, Phosphorus Res. Bull., **8**, 107, (1998).

[9] A. Takenaka, Y. Tsunoda, and H. Sawa, Phosphorus Res. Bull., **9**, 107, (1999).

[10] A. Takenaka and S. Yoshida, Phosphorus Res. Bull., **9**, 111, (1999).

[11] F. Cardellini, V. Contini, and G. Mazzone, J. Mater. Sci., **31**, 4175, (1996).

[12] P. Balaz, T. Havlik, Z. Bastl, J. Briancin, and R. Kammel, J. Mater. Sci. Letters, **15**, 1161, (1996).

[13] E. G. Avvakumov, E. T. Devyatkina, and N. V. Kosova, J. Solid State Chem., **113**, 379, (1994).

[14] N. Hashimoto, H. Yoden, and S. Deki, J. Am. Ceram. Soc., **76**, 438, (1993).

[15] W. Kim, Q. Zhang, and F. Saito, J. Mater. Sci., **35**, 5401, (2000).

[16] K. Kudaka, K. Iizuka, T. Sasaki, and H. Izumi, J. Am. Ceram. Soc., **83**, 2887, (2000).

[17] H. Nariai, M. Tada, M. Tsuhako, and I. Motooka, Phosphorus Res. Bull., **5**, 125, (1995).

[18] H. Nariai, S. Shibamoto, H. Maki, and I. Motooka, Phosphorus Res. Bull., **8**, 101, (1998).

Part Ⅱ
Thermal Behavior of Rare Earth Phosphates

Chapter 5.
Thermal behavior of various rare earth phosphates

Abstract

Thermal behavior of various rare earth phosphates synthesized from rare earth oxide and phosphoric acid in heating process was investigated by TG-DTA, XRD, FT-IR, and HPLC-FIA. Rhabdophane-type (light rare earth element) and Weinshenkite-type (heavy rare earth element) rare earth orthophosphates transformed to Monazite-type and Xenotime-type rare earth orthophosphates by heating, respectively. Rare earth polyphosphate and ultraphosphate changed to Monazite-type (light rare earth element) and Xenotime-type (heavy rare earth element) rare earth orthophosphates by losing P2O5. Rare earth *cyclo*-phosphate was not formed by heating the mixture of rare earth oxide and phosphoric acid. Then rare earth *cyclo*-octaphosphate and polyphosphate were synthesized in solution reaction and their thermal behaviors were also investigated. Rare earth *cyclo*-octaphosphate and polyphosphate synthesized in solution reaction were decomposed to ortho-, pyro-, tri-, and oligo-phosphates below 200℃. These phosphates were condensed to amorphous polyphosphate by heating. Then this amorphous polyphosphate was crystallized at specified temperature, which was related to ionic radius of rare earth element.

5.1. Introduction

As mentioned in General Introduction, phosphates condensed and hydrolyzed to other phosphates by heating. Consequently, to clarify thermal stability of phosphates as materials, and to find new phosphates, thermal behavior of various phosphates has been reported. However, thermal behavior of rare earth phosphates is not

satisfactory to be clarified. In this Chapter, thermal behavior was studied systematically about various rare earth phosphates synthesized from rare earth oxide and phosphoric acid by heating. However, rare earth *cyclo*-phosphates were not formed by heating [1]. Therefore, rare earth *cyclo*-octaphosphate and polyphosphate were synthesized in solution reaction and their thermal behaviors were also investigated [2].

5.2. Experimental

5.2.1. Thermal products

Rhabdophane-type rare earth orthophosphate was synthesized from rare earth oxide (La_2O_3, Pr_6O_{11}, Nd_2O_3, or Sm_2O_3) and phosphoric acid in P/R=1 at 150℃ for 20 hours. Rare earth oxide (Yb_2O_3 or Y_2O_3) was mixed with phosphoric acid in P/R=1 at < 5℃. Weinshenkite-type rare earth orthophosphate was obtained by heating this mixture at 80℃ for 20 hours. Monazite-type (La, Ce, Pr, Nd, and Sm) and Xenotime-type (Yb and Y) rare earth orthophosphates were synthesized from rare earth oxide and phosphoric acid in P/R=1 at 700℃ for 20 hours. Furthermore, Monazite-type and Xenotime-type rare earth orthophosphates were also synthesized from rare earth oxide and diammonium hydrogenphosphate at 1000℃ for 20 hours.

Rare earth polyphosphate was synthesized from rare earth oxide (La, Ce, Pr, Nd, Sm, Yb, or Y) - phosphoric acid or from rare earth oxide - diammonium hydrogenphosphate in P/R=3 at 700℃ for 20 hours.

The mixture of rare earth oxide (La_2O_3, CeO_2, Pr_6O_{11}, Nd_2O_3, or Sm_2O_3) - phosphoric acid or the mixture of rare earth oxide - diammonium hydrogenphosphate in P/R=10 was heated at 700℃ for 20 hours. Rare earth ultraphosphate was

obtained by washing this thermal product with water to remove excess phosphoric acid.

CeP_2O_7 and $Ce(PO_3)_4$, which were tetravalent cerium phosphate, were formed by heating the mixture of cerium oxide - phosphoric acid or the mixture of cerium oxide - diammonium hydrogenphosphate in P/Ce=2 and 4 at 700℃ for 20 hours, respectively.

5.2.2. Precipitates

Rare earth *cyclo*-octaphosphate was synthesized as follows. Slightly excess amount of each rare earth nitrate solution (rare earth element; Sc, Y, La ~ Lu, except for Pm) was mixed with sodium *cyclo*-octaphosphate solution [3,4]. The precipitates formed were filtered off, washed with water, and then dried in air. Phosphorus and rare earth elements in these precipitates were analyzed quantitatively by Molybdenum Blue Method and by back titration with EDTA and Zn standard solutions, respectively. The mole ratio of P/R (P: phosphorus, R: rare earth element) resulted in 3 except for scandium salt.

Rare earth polyphosphate was synthesized from rare earth nitrate solution (Pr, Nd, Yb, and Y) and sodium polyphosphate solution in the same manner with rare earth *cyclo*-octaphosphate [5].

5.2.3. Analytical procedures

Thermal behavior of various rare earth phosphates was investigated with thermogravimetry - differential thermal analyses (TG-DTA), X-ray diffraction (XRD), Fourier transform infrared spectroscopy (FT-IR), and high-performance liquid chromatography - flow injection analysis system (HPLC - FIA).

XRD patterns were recorded on a Rigaku Denki RINT 1200M X-Ray diffractometer

using monochromated CuK α 1 radiation. IR spectra were recorded on a HORIBA FT-IR spectrometer FT-710 with a KBr disk method. TG-DTA were carried out at a heating rate of 10℃/min, using a Rigaku Denki Thermo Plus TG8120. The phosphorus distribution in phosphates was determined with HPLC - FIA from TOSOH corp. Ltd. The separations were performed on a column (250×4.0mm I.D.) packed with a polystyrene - based anion exchanger (TSK gel SAX, dp=10 μm, Toyo Soda). The eluents for the chromatographic separation of phosphates were comprised of appropriate concentrations of potassium chloride and 0.1% (w/v) Na4EDTA (pH 10). The Mo(V) - Mo(VI) reagent for the analysis of phosphates was prepared by the method of F. Lucena - Conde and L. Prat [6]. The heteropoly blue complex thus formed was detected at 830 nm in the flow cell. The insoluble phosphate (high - polyphosphate) was determined after decomposition by heating with hydrochloric acid.

5.3. Results and discussion

5.3.1. Thermal products

Figure 5-1 shows TG-DTA curves of Rhabdophane-type (La, Pr, Nd, and Sm) and Weinshenkite-type (Yb and Y) rare earth orthophosphates synthesized from H_3PO_4. In cerium salts, these phosphates were not formed. DTA curves of Rhabdophane-type rare earth orthophosphates had two endothermic peaks at about 60℃ and 240 ℃. The endothermic peak at about 60℃ was due to adsorbed water, and the peak at about 240℃ corresponded to crystalline water. DTA curves of Weinshenkite-type rare earth orthophosphates had the peak at about 280℃. This peak was due to crystalline water. Gentle weight loss was observed in TG curve of itterbium salt,

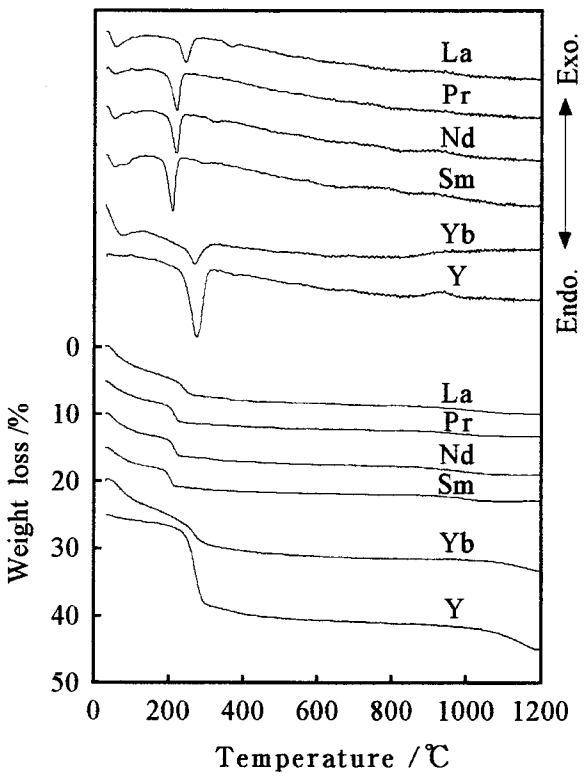

Fig. 5-1. TG-DTA curves of Rhabdophane-type (La, Pr, Nd, and Sm) and Weinshenkite-type (Yb and Y) rare earth orthophosphates.

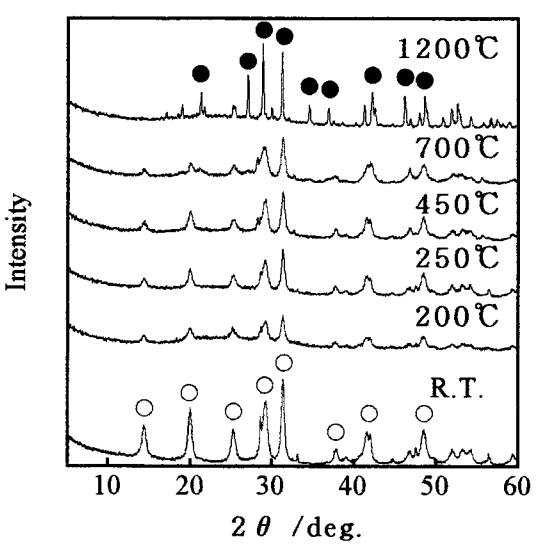

Fig. 5-2. XRD patterns of Rhabdophane-type $PrPO_4$ synthesized from Pr_6O_{11} and H_3PO_4 heated at several temperatures, ○; Rhabdophane-type $PrPO_4$ and ●; Monazite-type $PrPO_4$.

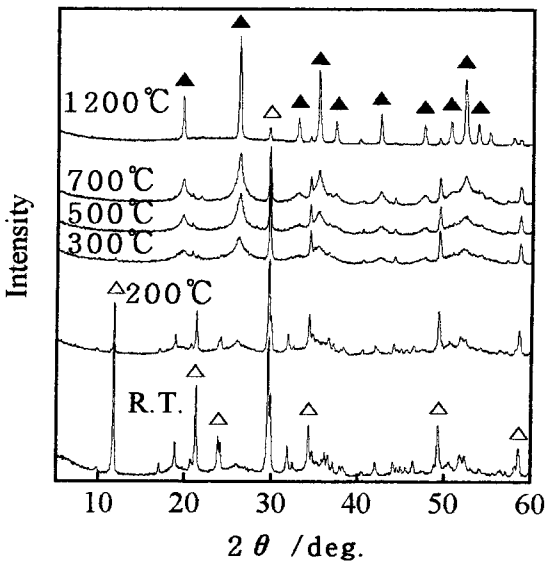

Fig. 5-3. XRD patterns of Weinshenkite-type $YbPO_4$ synthesized from Yb_2O_3 and H_3PO_4 heated at several temperatures, △; Weinshenkite-type $YbPO_4$ and ▲; Xenotime-type $YbPO_4$.

which was due to adsorbed water. Figures 5-2 and 5-3 show XRD patterns of Rhabdophane-type $PrPO_4$ and Weinshenkite-type $YbPO_4$ heated at several temperatures, respectively. Praseodymium salt heated at 700℃ indicated XRD pattern of Rhabdophane-type $PrPO_4$, and praseodymium salt heated at 1200℃ did XRD pattern of Monazite-type $PrPO_4$. On the other hand, Weinshenkite-type $YbPO_4$ transformed to Xenotime-type $YbPO_4$ at 300℃. Rhabdophane-type rare earth orthophosphate losed crystalline water with keeping their structure, however Weinshenkite-type rare earth orthophosphate losed crystalline water with decomposed their structure. These results were supported from IR spectra. Monazite-type and Xenotime-type rare earth orthophosphates had no change under 1200℃.

Rare earth (La, Pr, Nd, Sm, Yb, and Y) polyphosphates, $R(PO_3)_3$, transformed to Monazite-type (La, Pr, Nd, and Sm) and Xenotime-type (Yb and Y) rare earth

orthophosphates with volatilization of P_2O_5 above 700℃ [7,8]. Rare earth (La, Ce, Pr, Nd, and Sm) ultraphosphates, RP_5O_{14}, also changed to Monazite-type rare earth orthophosphates via polyphosphate with volatilization of P_2O_5 above 700℃. Thermal products in P/Ce=1, 2, 3, and 4 were the mixture of Monazite-type $CePO_4$, CeP_2O_7, $Ce(PO_3)_3$, $Ce(PO_3)_4$, and CeP_5O_{14}. These mixtures also changed to Monazite-type $CePO_4$ with volatilization of P_2O_5 above 700℃.

The kind of phosphorus raw materials (H_3PO_4 and $(NH_4)_2HPO_4$) had less influence on the thermal behaviors of Monazite-type and Xenotime-type rare earth orthophosphates, polyphosphate, and ultraphosphate.

5.3.2. Precipitates

Figure 5-4 shows TG-DTA curves of $Er_8(P_8O_{24})_3 \cdot nH_2O$. An endothermic peak at about 100℃ accompanied by weight loss and two exothermic peaks at about 200 ℃ and 790℃ were observed. The endothermic peak at about 100℃ was due to dehydration. The amount of water of crystallization and adsorbed water, n, was

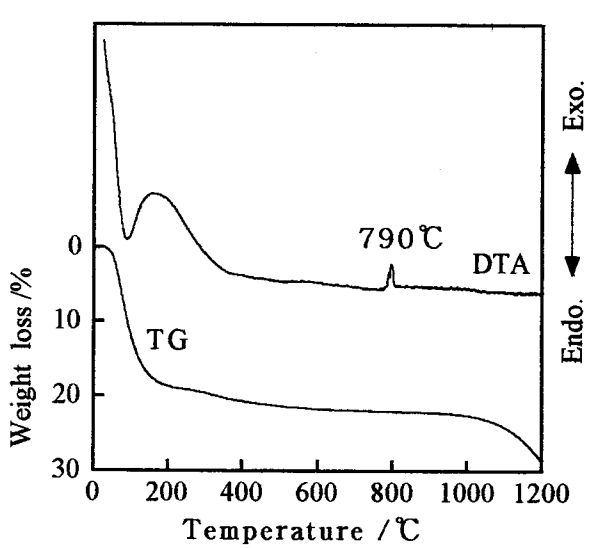

Fig. 5-4. TG-DTA curves of $Er_8(P_8O_{24})_3 \cdot nH_2O$.

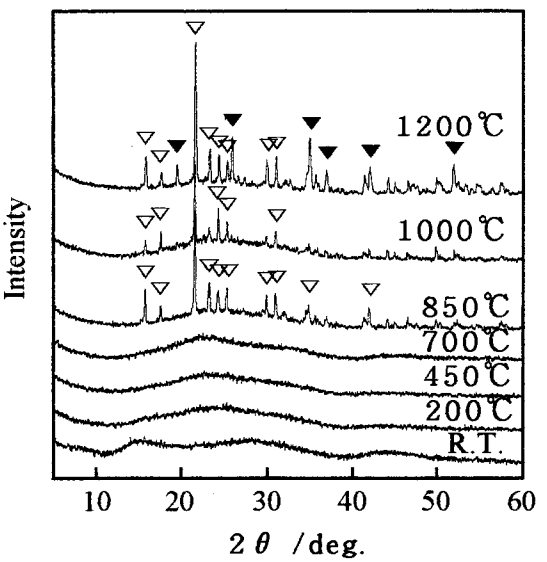

Fig. 5-5. XRD patterns of $Er_8(P_8O_{24})_3 \cdot nH_2O$ heated at several temperatures, ▽; $Er(PO_3)_3$ and ▼; Xenotime-type $ErPO_4$.

about 30 calculated from the weight loss in TG curve. Some of these water is coordinated to rare earth element. The ring structure of erbium *cyclo*-octaphosphate was decomposed with the removal of the water.

To clarify these thermal changes at each temperature, XRD and HPLC-FIA of the thermal products were performed. Figure 5-5 shows X-ray diffraction patterns of the products heated by TG-DTA apparatus. The original sample of erbium *cyclo*-octaphosphate was amorphous phase by XRD analysis. The diffraction patterns of the products heated below 700℃ also illustrated amorphous phases. On the other hand, those at 850℃ and 1000℃ showed the peaks of erbium polyphosphate, $Er(PO_3)_3$, and the product at 1200℃ was the mixture of erbium polyphosphate and Xenotime-type erbium orthophosphate, $ErPO_4$.

Table 5-1 shows the phosphorus distribution of products heated at several temperatures. At 200℃, a large portion of starting material (*cyclo*-octaphosphate)

Table 5-1 Changes of phosphorus distribution of $Er_8(P_8O_{24})_3 \cdot nH_2O$ heated at several temperatures / phosphorus %

Temp. /℃	P1	P2	P3	Poligo	P8m	Pinsol.
R.T.	0	0	2.0	3.4	94.6	0
200	4.9	5.9	7.4	54.3	13.8	13.7
450	1.2	0.6	1.4	43.1	0.9	52.8
700	0.7	0	0	9.6	0	89.7
850	0.3	0	0	1.3	0	98.4
1000	0	0	0	0.8	0	99.2

P1, P2, P3, Poligo, P8m, and Pinsol. represent ortho-, pyro-, tri-, oligo-(chain-length, n=4 ~ 20), *cyclo*-octa- and insoluble (high-poly-) phosphate, respectively.

changed already to short-chain phosphates and about 14% of *cyclo*-octaphosphate still remained. At 450℃, *cyclo*-octaphosphate almost disappered, and the half of the phosphorus changed to polyphosphate. Above 450℃, the polyphosphate increased, and at 850℃ almost of phosphates were polyphosphate.

Therefore, the endothermic peak at about 100℃ was due to dehydration, and the exothermic one at about 200℃ corresponds to hydrolysis. The endothermic peak seemed to be large peak because the exothermic peak overlapped to the endothermic peak. Heating above 200℃, sample gradually changed to amorphous polyphosphate, and crystallized at 790℃. Further heating, polyphosphate transformed into very stable orthophosphate losing P_2O_5 according to the following equation [7,8].

$$Er(PO_3)_3 \xrightarrow{> 1000℃} ErPO_4 + P_2O_5$$

Based upon the above results, the processes of the thermal behavior of rare earth *cyclo*-octaphosphate proceed in the following way.

cyclo-octaphosphate → ortho-, pyro-, tri- and oligo-phosphates

→ polyphosphate → orthophosphate (Monazite-type or Xenotime-type)

All of R8(P8O24)3•nH2O (R=Y, La ~ Lu, except for Pm) were examined in the same method, and showed similar results of TG-DTA, XRD, and HPLC-FIA. Figure 5-6 shows FT-IR spectrum of Er8(P8O24)3•nH2O. The intense absorption peaks present at about 1630, 1260, 945 and 510 cm^{-1} in all rare earth *cyclo*-octaphosphates [9]. Because the cyclic structure is formed for rare earth *cyclo*-octaphosphates by the synthetic process in water, water molecule in the structure is necessary to stabilize the salts, and the removal of structural water lead to the decomposition into the amorphous phase. As a results of the decomposition, *cyclo*-octaphosphates became amorphous phases composed of the mixture of ortho-, pyro-, tri-, and oligo-phosphates, followed by condensation to amorphous polyphosphate. These amorphous polyphosphates crystallized at the characteristic temperature of each rare earth element, e.g., 790℃ in erbium salts as shown in Fig. 5-4. These temperatures of

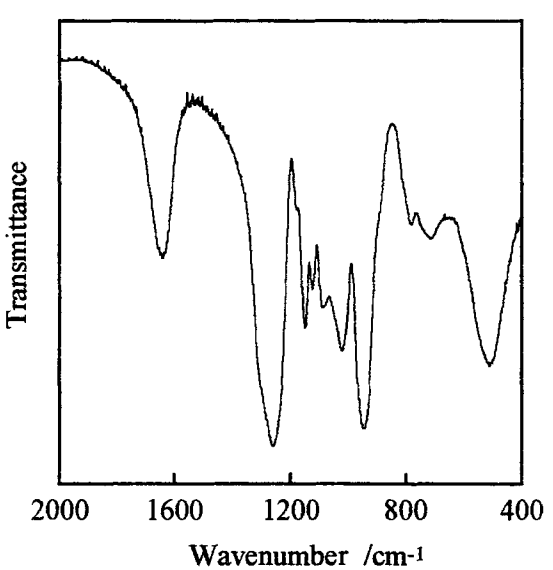

Fig. 5-6. IR spectrum of Er8(P8O24)3•nH2O.

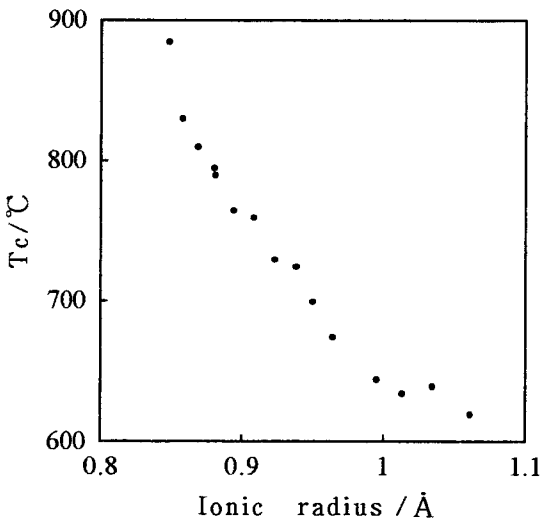

Fig. 5-7. Relationship between rare earth ionic radius (+ Ⅲ , Coor.No.6) and temperature of crystallization (Tc).

crystallization (Tc) in DTA curves had a little difference in rare earth elements.

Figure 5-7 shows the relationship between Tc and ionic radii of cations of which the coordination number is 6. The crystallization temperature increased with decreasing ionic radii of rare earth elements. This tendency was similar to those of glass transition point and melting point [10,11]. Therefore, it is clear that the crystallization of amorphous phase depends on glass transition point and melting point.

Rare earth polyphosphate synthesized in solution reaction was investigated in the same manner for reference. Rare earth polyphosphate synthesized in solution reaction had the similar themal behavior with rare earth *cyclo*-octaphosphate synthesized in solution reaction. TG-DTA curve of rare earth polyphosphate synthesized in solution reaction was the same with those of rare earth *cyclo*-octaphosphates. Table 5-2 shows HPLC - FIA results of praseodymium polyphosphate synthesized in solution reaction. Praseodymium polyphosphate was hydrolyzed to short - chain

Table 5-2 Changes of phosphorus distribution of $Pr(PO_3)_3 \cdot nH_2O$ heated at several temperatures

Temp. /℃	P1	P2	P3	Poligo.	Pinsol.
R.T.	1.1	0.3	0.2	0	98.4
200	10.4	8.7	6.4	25.1	49.4
400	2.9	1.5	1.9	7.6	86.1
600	0.9	0.5	0.5	2.0	96.1
800	0	0	0	0	100.0

P1, P2, P3, Poligo, and Pinsol. represent ortho-, pyro-, tri-, oligo-(chain-length, n=4 ~ 20), and insoluble (high-poly-) phosphate, respectively.

polyphosphate by heating. These phosphates were condensed to amorphous long-chain polyphosphate (insoluble phosphate). This amorphous rare earth polyphosphate crystallized at the characteristic temperature, which was the same with Fig. 5-7.

5.4. Conclusion

Rhabdophane-type and Weinshenkite-type rare earth orthophosphates were transformed to Monazite-type and Xenotime-type rare earth orthophosphates with volatilization of P_2O_5 by heating, respectively. Rare earth polyphosphate and ultraphosphate synthesized in thermal procedure changed to Monazite-type or Xenotime-type rare earth orthophosphate with volatilization of P_2O_5 by heating.

Rare earth *cyclo*-octaphosphates, $R_8(P_8O_{24})_3 \cdot nH_2O$ (R=Y, La~Lu, except for Pm), were synthesized by mixing rare earth nitrate solution with sodium *cyclo*-octaphosphate solution. Their thermal reactions proceeded in a similar process; *cyclo*-octaphosphate

changed to polyphosphate by way of ortho-, pyro-, tri-, and oligo-phosphates, and finally transformed to Monazite-type or Xenotime-type orthophosphate. The temperature of crystallization varied with rare earth element, and increased with the decrease of ionic radius of cation. Rare earth polyphosphate prepared in solution reaction was amorphous state, and had the similar thermal behavior with rare earth *cyclo*-octaphosphate.

5.5. References

[1] M. Tsuhako, S. Ikeuchi, T. Matsuo, I. Motooka, M. Kobayashi, Bull. Chem. Soc. Jpn., **52**, 1034, (1979).

[2] H. Nariai, J. Suenaga, M. Tsuhako, I. Motooka, Phosphorus Res. Bull., **4**, 99, (1994).

[3] U. Schülke, Z. Anorg. Allg. Chem., **360**, 231, (1968).

[4] G. Kura and T. Ueno, Polyhedron, **13**, 3105, (1994).

[5] T. Graham, Phil. Trans. Roy. Soc., **123A**, 253, (1833).

[6] F. Lucena-Conde and L. Prat, Anal. Chem. Acta, **16**, 473, (1957).

[7] I. L. Botto and E. J. Baran, Z. Anorg. Allg. Chem., **435**, 293, (1977).

[8] K. Byrappa and B. N. Litvin, J. Mater. Sci., **18(3)**, 703, (1983).

[9] S. Ohashi, G. Kura, Y. Shimada, and M. Hara, J. Inorg. Nucl. Chem. **39**, 1513, (1977).

[10] N. E. Topp, "Chemistry of the Rare-Earth Elements", edited by J. Shiokawa and G. Adachi, Kagakudojin, 1974.

[11] K. Matushita, "Kagakusousetsu", edited by the Chemical Society of Japan, Gakkai Shuppan Center, **41**, 95, (1983).

Part Ⅲ
Catalytic Properties of Rare Earth Phosphates

Chapter 6.
Catalytic characterization of various rare earth phosphates

Abstract

Various rare earth phosphates (rare earth elements; R=La, Ce, Pr, Nd, Sm, Yb, and Y, phosphate; Monazite-type, Xenotime-type, Rhabdophane-type, and Weinshenkite-type orthophosphates RPO_4, polyphosphate $R(PO_3)_3$, and ultraphosphate RP_5O_{14}) were synthesized by heating mixtures of each rare earth oxide and diammonium hydrogenphosphate or phosphoric acid. The compositions of rare earth phosphates were determined by XRD, FT-IR, and TG-DTA. Catalytic properties were studied as one of properties of various rare earth phosphates. Specific surface areas of samples were measured by the BET method. Acid strengths and amounts of acidic sites were measured using several indicators by n-butylamine titration. Acidic properties were also confirmed by adsorption of ammonia. Dehydration reaction of 2-propanol and cracking / dehydrogenation reaction of cumene in pulse method were studied as possible test reactions for estimation of these catalytic activities. Various rare earth phosphates were also characterized by catalytic activities on isomerization reaction of butene in circulation system. The characterization of catalysts was discussed from kind of rare earth elements (La, Ce, Pr, Nd, Sm, Yb, and Y), kind of phosphates (Monazite-type, Xenotime-type, Rhabdophane-type, and Weinshenkite-type orthophosphates, polyphosphate, and ultraphosphate), and kind of phosphorus resources ($(NH_4)_2HPO_4$ and H_3PO_4).

6.1. Introduction

Phosphates transform to various other phosphates with hydrolysis and dehydration

reactions by heating [1,2]. Phosphates have been used for ceramic materials, catalysts, fluorescent materials, dielectric substances, fuel cells, etc [3-12]. There is a little study about rare earth phosphates than other metal phosphates. Anhydrous rare earth orthophosphate is the main component of natural Monazite and Xenotime which are rare earth element ores. Rhabdophane-type rare earth orthophosphates have a specific structure with vacant spaces[13]. Polyphosphates have chain structures in which tetrahedral PO4 groups are linked together by oxygen bridges [14]. Rare earth ultraphosphates have the network structure which included the anion represented by $P5O14^{3-}$ [15]. A large part of ultraphosphate is not stable for hydrolysis reaction. However, rare earth ultraphosphate is stable.

The transformation of aliphatic primary and secondary alcohols to olefins and/or carbonyl compounds on acidic and basic catalysts has been studied [16-20]. The dehydration occurs on acidic sites, whereas the dehydrogenation is prefered in presence of basic or redox sites. Both dehydration and dehydrogenation reactions of 2-propanol occur on the acid and basic sites, respectively. Therefore, these reactions are used as proof of acidic or basic catalyst [3-9]. 2-propanol transforms to propylene on acidic catalysts and to acetone on basic catalysts. The conversion of 2-propanol to propylene is reported to be related to the amounts of acidic sites [3, 5, 9, 10].

On the other hand, cracking / dehydrogenation reaction of cumene is used to estimate Lewis and Brönsted acid sites of a catalyst from the product [9,10,21]. Cumene conversion gives cracking products as well as dehydrogenation products on acidic catalysts. Benzene and propylene are the cracking products mainly on Brönsted acid sites, whereas α -methylstyrene is a dehydrogenation product chiefly on Lewis acid sites.

The migration reaction of double bond and *cis - trans* isomerization reaction in

olefin molecule occur over many materials fields. Butene has minimum number of carbon atoms in olefin compounds that these both reactions could take place. Then isomerization reaction of n-butene is used as a representation of isomerization reaction of olefin [22-25].

In this Chapter, various rare earth phosphates (rare earth elements; R=La, Ce, Pr, Nd, Sm, Yb, and Y, phosphate; Monazite-type, Xenotime-type, Rhabdophane-type, and Weinshenkite-type orthophosphates, polyphosphate, and ultraphosphate) were investigated for catalytic aspects.

6.2. Experimental

6.2.1. Preparation of various rare earth phosphates

Various rare earth phosphates (rare earth elements; R=La, Ce, Pr, Nd, Sm, Yb, and Y, phosphate; Monazite-type, Xenotime-type, Rhabdophane-type, and Weinshenkite-type orthophosphates, polyphosphate, and ultraphosphate) were prepared by heating the mixtures of rare earth oxide and $(NH_4)_2HPO_4$ or H_3PO_4 in several ratios of phosphorus and rare earth elements (P/R) equal 1, 2, 3, 4, and 10. Thermal products were analyzed by X-ray diffractometry (XRD), Fourier transform infrared spectroscopy (FT-IR), and thermogravimetry - differential thermal analyses (TG-DTA). X-Ray diffraction patterns were recorded on a Rigaku Denki RINT 1200M X-Ray diffractometer, using monochromated Cu K α 1 radiation (λ =0.154nm). The IR spectra were recorded on a HORIBA FT-IR spectrometer FT-710 with a KBr disk method. TG-DTA were carried out at a heating rate of 10℃/min, using a Rigaku Denki Thermo Plus TG8120.

6.2.2. Estimation of surface properties

The surface areas of materials were calculated from the amount of nitrogen gas adsorbed at the temperature of liquid nitrogen by five-points BET method (P/Po=0.10, 0.15, 0.20, 0.25 and 0.30) with Gemini-Micromeritics 2360 from Shimadzu Corp. Ltd. Acidic properties (acidic strength and amount of acidic sites) were examined by n-butylamine titration using Hammett indicators because the pKa of an indicator is the factor which determines the level of acid strength of the titrated acid sites [26]. The Hammett indicators were Methyl red (pKa=+4.8), Dimethyl yellow (pKa=+3.3), Benzeneazodiphenylamine (pKa=+1.5), and Dicinnamalacetone (pKa = -3.0). Acidic properties were also confirmed by adsorption of ammonia. A 0.1g of a rare earth phosphate was heated at 150℃ for 2 hours under nitrogen gas, cooled to room temperature, and then placed in 3 ℓ of 1040 ppm ammonia gas baranced nitrogen gas for 24 hours. Then this phosphate was also analyzed by TG-DTA, XRD and FT-IR.

6.2.3. Dehydration reaction of 2-propanol

The conversion was calculated with dehydration reaction of 2-propanol on a gas chromatograph G-3000 from Hitachi Corp. Ltd. A column (ID. 3mm and length 2m) packed with Porapak Q and a thermocoupled detector were used. Helium was used as carrier gas in 20 mL/min flow rate. Pulse volume of 2-propanol was 0.8 μ L. Injected 2-propanol was vaporized and carried to catalyst phase. 2-propanol and catalytic products, propylene and water, were separated in column and detected.

A 0.2 g of a rare earth phosphate was mixed with about 2 mg of glass wool and then packed in a glass tube with about 10 mg of glass wool at both ends. Beforehand, glass wool was confirmed to have no activity in this reaction.

6.2.4. Cracking / dehydrogenation reaction of cumene

The conversion was calculated with cracking / dehydrogenation reaction of cumene on a gas chromatograph G-3900 from Hitachi Corp. Ltd. A column (ID. 3mm and length 2m) packed with 15%TCEP on Uniport B (GL Science) and a thermocouple detector were used. Helium was used as carrier gas in 20 mL/min flow rate. Pulse volume of cumene was 0.5 μ L. Other conditions were the same as for the system for dehydration of 2-propanol.

6.2.5. Isomerization reaction of butene

Catalytic reaction was carried out in a closed gas circulation system [27]. The 0.2g of phosphate was packed into the glass reaction tube, and then 1-butene (Tokyo Kasei) was introduced into the reaction system. The reaction gases were analyzed using a Yanaco G2800 gas chromatograph with a VZ-7 column, which was connected directly to the gas circulation system.

6.3. Results and discussion

6.3.1. Formation and surface properties

Monazite-type rare earth (La, Pr, Nd, and Sm) orthophosphates and Xenotime-type rare earth (Y and Yb) orthophosphates were synthesized by heating the mixture in P/R=1 at 1000℃ for 20 hours from (NH4)2HPO4, while Monazite-type and Xenotime-type rare earth orthophosphates were formed at 700℃ for 20 hours from H3PO4. Rhabdophane-type rare earth (La, Pr, Nd, and Sm) orthophosphates were obtained by heating the mixture in P/R=1 at 150℃ for 20 hours from H3PO4. Weinshenkite-

type rare earth (Yb and Y) orthophosphates were obtained by heating the mixture in P/R=1 at 80℃ for 20 hours from H_3PO_4. Rare earth (La, Ce, Pr, Nd, Sm, Yb, and Y) polyphosphates were prepared by heating the mixtures in P/R=3 at 700℃ for 20 hours. Lanthanum, cerium, praseodymium, neodymium, and samarium ultraphosphates were obtained by heating the mixtures in P/R=10 at 700℃ for 20 hours and then washing with water to remove the excess phosphoric acid. These rare earth phosphates except for cerium salts were determined to be single phase materials from XRD analyses.

Cerium salts in P/Ce=1, 2, 3, and 4 were the mixtures of various cerium phosphates, Monazite-type $CePO_4$, CeP_2O_7, $Ce(PO_3)_3$, $Ce(PO_3)_4$, and CeP_5O_{14} by heating at 700℃ for 20 hours. However, in this report, Monazite-type $CePO_4$, CeP_2O_7, $Ce(PO_3)_3$, and $Ce(PO_3)_4$ are defined as the samples prepared in P/Ce = 1, 2, 3, and 4, respectively.

TG-DTA, XRD, and FT-IR results indicated that Rhabdophane-type rare earth (La, Pr, Nd, and Sm) orthophosphates lost the crystalline water at about 240℃ with its structure maintained. However, Weinshenkite-type rare earth (Yb and Y) orthophosphates transformed to each Xenotime-type rare earth orthophosphate by losing crystalline water.

Table 6-1 shows specific surface areas of various rare earth phosphates. Specific surface areas of Monazite-type rare earth (La, Pr, Nd, and Sm) orthophosphates and Xenotime-type rare earth (Yb and Y) orthophosphates prepared from $(NH_4)_2HPO_4$ were smaller than 2 m^2/g, whereas those prepared from H_3PO_4 were about 20～30 m^2/g, except for cerium salts. It was considered that the synthetic temperature influenced the specific surface areas. Samples synthesized at 1000℃ from H_3PO_4 had similar specific surface areas to those of samples synthesized from $(NH_4)_2HPO_4$. Monazite-type cerium orthophosphate had a small specific surface area, which

Table 6-1 Specific surface areas of various rare earth phosphates /$m^2 \cdot g^{-1}$

		La	Ce	Pr	Nd	Sm	Yb	Y
M-RPO4	(NH4)2HPO4	0.9	0.5	1.7	0.7	0.8	---	---
	H3PO4	19.7	0.9	22.5	24.4	21.7	---	---
X-RPO4	(NH4)2HPO4	---	---	---	---	---	1.3	1.6
	H3PO4	---	---	---	---	---	20.7	29.2
R-RPO4	H3PO4	85.0	---	57.7	86.5	75.6	---	---
W-RPO4	H3PO4	---	---	---	---	---	16.8	17.8
RP2O7	(NH4)2HPO4	---	0.8	---	---	---	---	---
	H3PO4	---	0.3	---	---	---	---	---
R(PO3)3	(NH4)2HPO4	0.4	0.5	0.2	0.3	0.6	0.2	0.1
	H3PO4	2.1	0.5	0.1	0.2	0.4	0.1	0.2
R(PO3)4	(NH4)2HPO4	---	0.1	---	---	---	---	---
	H3PO4	---	0.1	---	---	---	---	---
RP5O14	(NH4)2HPO4	0.1	0.1	0.1	0.1	0.1	---	---
	H3PO4	0.2	0.3	0.3	0.2	0.2	---	---

M-, X-, R-, and W-RPO4 represented Monazite-type, Xenotime-type, Rhabdophane-type, and Weinshenkite-type orthophosphates, respectively.
---; This phosphate was not formed.

differed from other Monazite-type rare earth (La, Pr, Nd, and Sm) orthophosphates. Rare earth (La, Ce, Pr, Nd, Sm, Yb, and Y) polyphosphates and rare earth (La, Ce, Pr, Nd, and Sm) ultraphosphates had smaller specific surface areas than each rare earth orthophosphate. Since specific surface areas of these phosphates were very small, it is difficult to estimate catalytic activities based on specific surface areas. For this reason, the estimation of catalytic activities in this report was based on catalyst weight.

The acid strength of most rare earth phosphates was between -3.0 and +1.5 in pKa unit. The amount of acidic sites at $Ho \leqq +4.8$ was smaller than 3×10^{-4} mol• g^{-1}. Acid strength and amount of acidic sites were less influenced from kind of rare earth elements (La, Ce, Pr, Nd, Sm, Yb, and Y), kind of various phosphates (orthophosphate, polyphosphate, and ultraphosphate), and kind of phosphorus resources ($(NH_4)_2HPO_4$ and H_3PO_4). All rare earth phosphates in this Chapter adsorbed ammonia had no change in TG-DTA and XRD results. However, new IR absorption peaks appeared by adsorption of ammonia in the case of rare earth phosphates which have large specific surface area. Figure 6-1 shows IR spectra of Rhabdophane-type $NdPO_4$ absorbed NH_3. The adsorbtions were observed at about $1400cm^{-1}$ and $3100cm^{-1}$ which were considered to due to NH_4^+. These absorptions were disappered by heating. This indicated that a certain degree amount of acid sites existed on surface of materials.

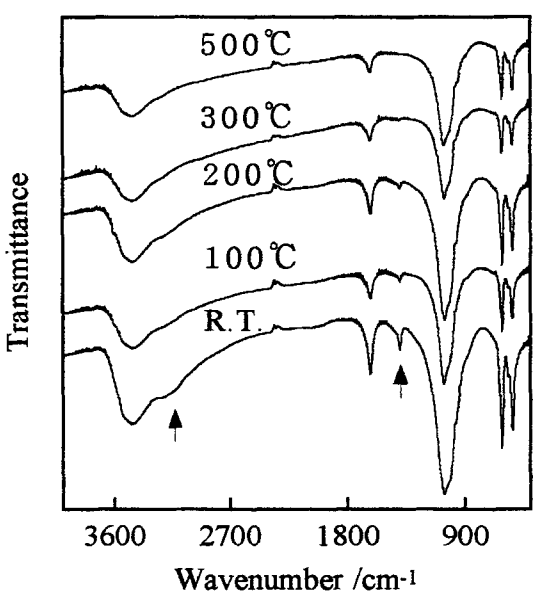

Fig. 6-1. IR spectra of Rhabdophane-type $NdPO_4$ adsorbed NH_3.

It was considered that catalytic activities of rare earth phosphates were influenced much by specific surface area less by acidic properties.

6.3.2. Dehydration reaction of 2-propanol

Table 6-2 shows conversion of 2-propanol to propylene over trivalent rare earth polyphosphates. 1.2-5.2% of 2-propanol transformed to propylene at 200℃, 3.6-13.4% at 225℃, and 14.0-32.1% at 250℃. No unique rare earth phosphate was observed in this table. Acetone was not detected in this Chapter. All rare earth phosphates had poor basic sites.

Table 6-2 Conversion of 2-propanol to propylene over various rare earth polyphosphates /%

rare earth element		Temperature /℃		
		200	225	250
La	(NH4)2HPO4	3.9	10.5	32.1
Ce	(NH4)2HPO4	3.5	8.7	23.2
Pr	(NH4)2HPO4	1.6	4.3	14.0
Nd	(NH4)2HPO4	2.3	5.6	13.9
Sm	(NH4)2HPO4	4.0	9.3	26.7
Yb	(NH4)2HPO4	1.2	3.9	12.2
Y	(NH4)2HPO4	1.3	3.6	15.0
La	H3PO4	2.6	6.5	16.6
Ce	H3PO4	4.7	11.0	25.7
Pr	H3PO4	2.5	10.6	17.3
Nd	H3PO4	2.1	6.9	15.3
Sm	H3PO4	2.6	7.3	18.9
Yb	H3PO4	3.0	9.0	28.3
Y	H3PO4	5.2	13.4	21.6

Table 6-3 shows conversion of 2-propanol over various neodymium phosphates. Monazite-type and Rhabdophane-type neodymium orthophosphates prepared from H_3PO_4 had higher catalytic activity than other neodymium phosphates. It was considered that small specific surface area of Monazite-type neodymium orthophosphate prepared from $(NH_4)_2HPO_4$ caused its low activity. Neodymium polyphosphates and ultraphosphates had low activity on dehydration reaction of 2-propanol.

Table 6-3 Conversion of 2-propanol to propylene over various neodymium phosphates /%

phosphate		Temperature /℃		
		200	225	250
M-$NdPO_4$	$(NH_4)_2HPO_4$*	0.2	1.0	1.0
	H_3PO_4	94.5	100.0	100.0
R-$NdPO_4$	H_3PO_4	100.0**	100.0	100.0
$Nd(PO_3)_3$	$(NH_4)_2HPO_4$	2.3	5.6	13.9
	H_3PO_4	2.1	6.9	15.3
NdP_5O_{14}	$(NH_4)_2HPO_4$	1.4	4.0	10.2
	H_3PO_4	0.9	1.6	5.2

M- and R-$NdPO_4$ represented Monazite-type and Rhabdophane-type $NdPO_4$, respectively. *; This phosphate was prepared at 1000℃ for 20 hours. **; Extreme tailing was observed.

Table 6-4 shows conversion of 2-propanol over cerium phosphates. Relatively high conversion was obtained in the case of Monazite-type cerium orthophosphate prepared from H_3PO_4. Monazite-type cerium orthophosphate (900℃ 20h, specific surface area; 0.15$m^2 \cdot g^{-1}$) and cerium ultraphosphate prepared from $(NH_4)_2HPO_4$

Table 6-4 Conversion of 2-propanol to propylene over various cerium phosphates /%

phosphate		Temperature /℃		
		200	225	250
M-$CePO_4$	$(NH_4)_2HPO_4$*	0.7	0.8	1.7
	H_3PO_4	6.3	25.9	47.8
CeP_2O_7	$(NH_4)_2HPO_4$	3.8	10.9	28.6
	H_3PO_4	3.5	9.1	19.7
$Ce(PO_3)_3$	$(NH_4)_2HPO_4$	3.5	8.7	23.2
	H_3PO_4	4.7	11.0	25.7
$Ce(PO_3)_4$	$(NH_4)_2HPO_4$	2.7	7.5	18.3
	H_3PO_4	1.9	5.8	20.4
CeP_5O_{14}	$(NH_4)_2HPO_4$	1.3	3.6	8.6
	H_3PO_4	5.0	10.9	24.8

M-$CePO_4$ represented Monazite-type $CePO_4$.

*; This phosphate was prepared at 900℃ for 20 hours.

indicated low conversion. The kind of phosphates had less influence on catalytic activity in cerium phosphates than other rare earth (La, Pr, Nd, Sm, Yb, and Y) phosphates.

6.3.3. Cracking / dehydrogenation reaction of cumene

Figure 6-2 shows conversion of cumene over rare earth polyphosphates prepared from H_3PO_4. Cerium polyphosphates had higher conversion than other rare earth (La, Pr, Nd, Sm, Yb, and Y) polyphosphates. Conversion over cerium polyphosphate had a maximum value at 450℃, whereas conversion over other rare earth (La, Pr, Nd, Sm, Yb, and Y) polyphosphates showed monotonous increasing with tempera-

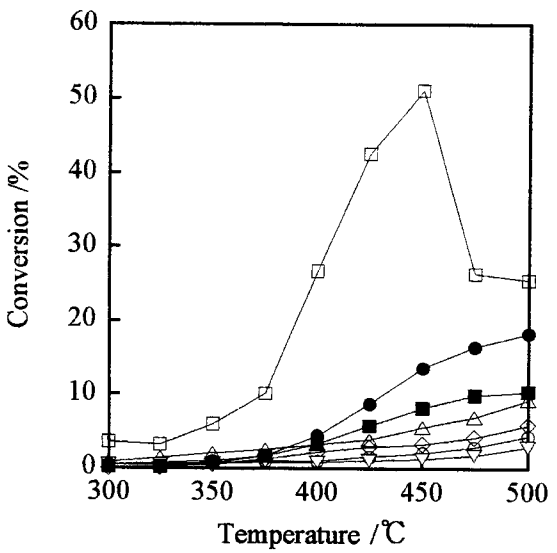

Fig.6-2. Conversion of cumene over $R(PO_3)_3$ prepared from H_3PO_4, ○; La, □; Ce, ◇; Pr, △; Nd, ▽; Sm, ■; Yb, and ●; Y.

ture rising. Figure 6-3 shows selectivity of cumene to benzene and propylene over these rare earth polyphosphates. 100% of selectivity means that cumene transformed to benzene and propylene by cracking reaction. 0% of selectivity means that cumene transformed to α-metylstylene by dehydrogenation reaction. Selectivity to benzene and propylene over rare earth polyphosphates generally increased with temperature. Lanthanum and samarium polyphosphates prepared from H_3PO_4 gave low selectivity to benzene and propylene. This indicated these catalysts had poor Brönsted acid sites. Other polyphosphate prepared from H_3PO_4 gave high selectivity. There are rich Brönsted acid sites on these catalysts. Almost all phosphates had maximum selectivity at about 450℃. Cerium phosphate had a large decrease of selectivity. Figure 6-4 shows yields of cracking products over various rare earth polyphosphates.

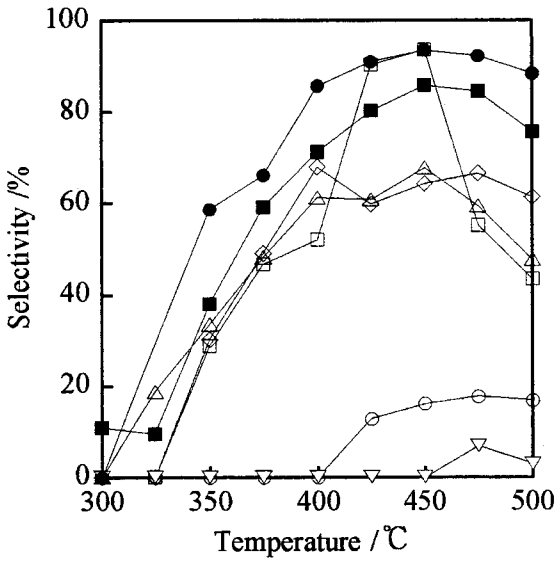

Fig. 6-3. Selectivity of cumene to benzene and propylene over $R(PO_3)_3$ prepared from H_3PO_4, ○ ; La, □ ; Ce, ◇ ; Pr, △ ; Nd, ▽ ; Sm, ■ ; Yb, and ● ; Y.

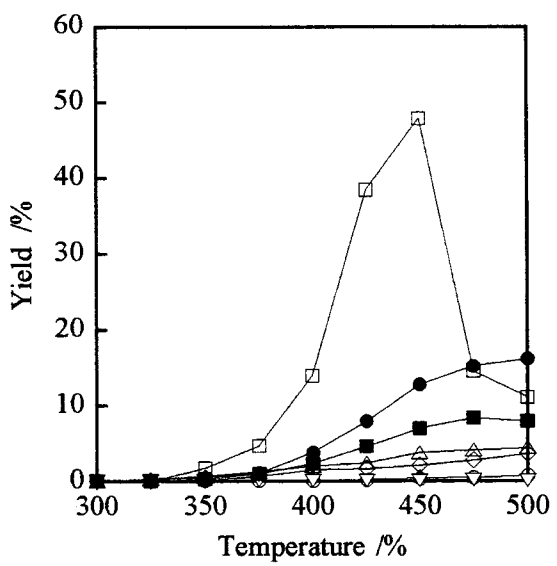

Fig. 6-4. Yields of cracking products over $R(PO_3)_3$ prepared from H_3PO_4, ○ ; La, □ ; Ce, ◇ ; Pr, △ ; Nd, ▽ ; Sm, ■; Yb, and ● ; Y.

This also indicated that cerium polyphosphate had different catalytic behavior with other rare earth (La, Pr, Nd, Sm, Yb, and Y) polyphosphates.

Figure 6-5 shows conversion of cumene over various neodymium phosphates. Monazite-type and Rhabdophane-type neodymium orthophosphates prepared from H_3PO_4 indicated high conversion of cumene and high selectivity to benzene and propylene. The retention time was long in the cases of Monazite-type and Rhabdophane-type neodymium orthophosphates prepared from H_3PO_4. Large specific surface areas of these phosphates were considered to lead to a long contact

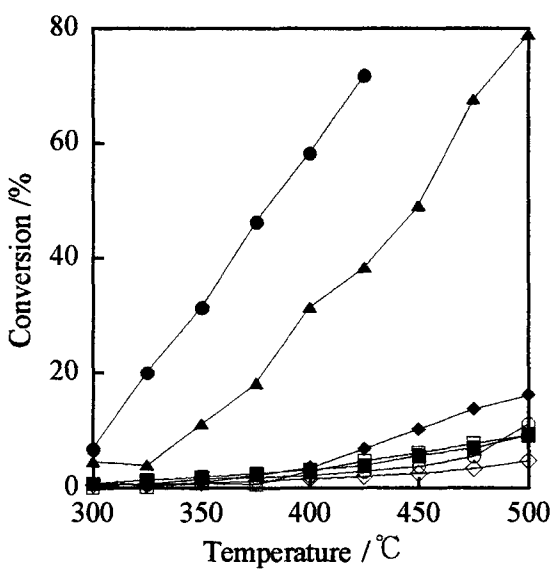

Fig. 6-5. Conversion of cumene over neodymium phosphates,
○; Monazite-type $NdPO_4$ prepared from $(NH_4)_2HPO_4$,
●; Monazite-type $NdPO_4$ prepared from H_3PO_4,
▲; Rhabdophane-type $NdPO_4$ prepared from H_3PO_4,
□; $Nd(PO_3)_3$ prepared from $(NH_4)_2HPO_4$,
■; $Nd(PO_3)_3$ prepared from H_3PO_4,
◇; NdP_5O_{14} prepared from $(NH_4)_2HPO_4$,
and ◆; NdP_5O_{14} prepared from H_3PO_4.

time by adsorption. A long contact time caused high conversion. At high temperature, the catalytic activity was not estimated due to tailing in the case of Monazite-type neodymium orthophosphate.

Monazite-type rare earth (La, Ce, Pr, Nd, and Sm) orthophosphate and Xenotime-type rare earth (Yb and Y) orthophosphates prepared from $(NH_4)_2HPO_4$ had low catalytic activity. Selectivity of cumene to benzene and propylene over Rhabdophane-type rare earth (La, Pr, Nd, and Sm) orthophosphates became small with temperature rising. The selectivity over rare earth (La, Pr, Nd, and Sm) ultraphosphates was much affected by temperature.

Figure 6-6 shows conversion of cumene over various cerium phosphates prepared from H_3PO_4. Conversion of cumene over cerium phosphates increased with temperature rising. CeP_2O_7 and $Ce(PO_3)_4$ gave maximum conversion at 425℃.

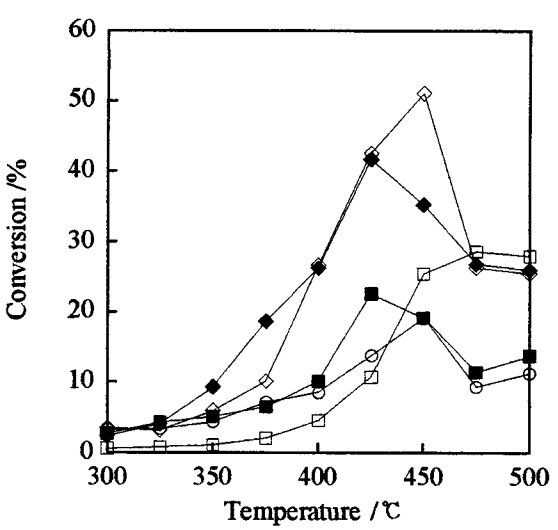

Fig. 6-6. Conversion of cumene over cerium phosphates prepared from H_3PO_4, ○; Monazite-type $CePO_4$, ■; CeP_2O_7, ◇; $Ce(PO_3)_3$, ◆; $Ce(PO_3)_4$, and □; CeP_5O_{14}.

Monazite-type $CePO_4$ and $Ce(PO_3)_3$ gave maximum conversion at 450℃. Above 475℃, the large decrease of conversion was observed except for CeP_5O_{14}. Figure 6-7 shows selectivity of cumene to benzene and propylene over these cerium phosphates prepared from H_3PO_4. The selectivity over CeP_2O_7 and $Ce(PO_3)_4$ had the maximum value at 400℃. Monazite-type $CePO_4$ and $Ce(PO_3)_3$ had maximum selectivity at 450℃. Monazite-type $CePO_4$ had lower catalytic activity than other Monazite-type rare earth (La, Pr, Nd, and Sm) orthophosphates. $Ce(PO_3)_3$ and $Ce(PO_3)_4$ had high activity. Cerium ultraphosphate indicated same tendency as other rare earth (La, Pr, Nd, and Sm) phosphates. Figure 6-8 shows yields of cracking products over cerium phosphates. The yields over $Ce(PO_3)_3$ had large decrease with temperature rising.

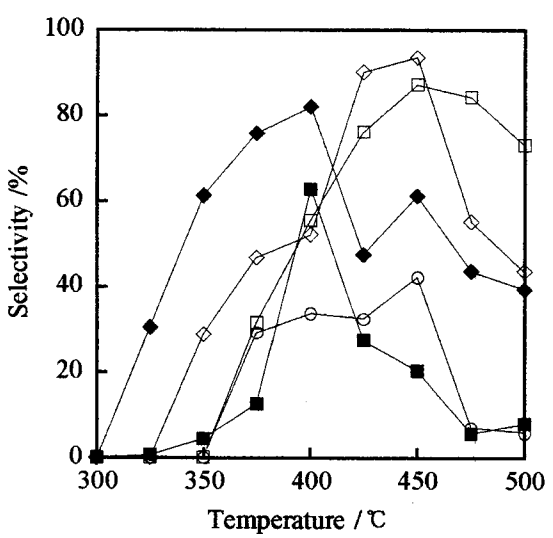

Fig. 6-7. Selectivity of cumene to benzene and propylene over cerium phosphates prepared from H_3PO_4, ○ ; Monazite-type $CePO_4$, ■ ; CeP_2O_7, ◇ ; $Ce(PO_3)_3$, ◆ ; $Ce(PO_3)_4$, and □ ; CeP_5O_{14}.

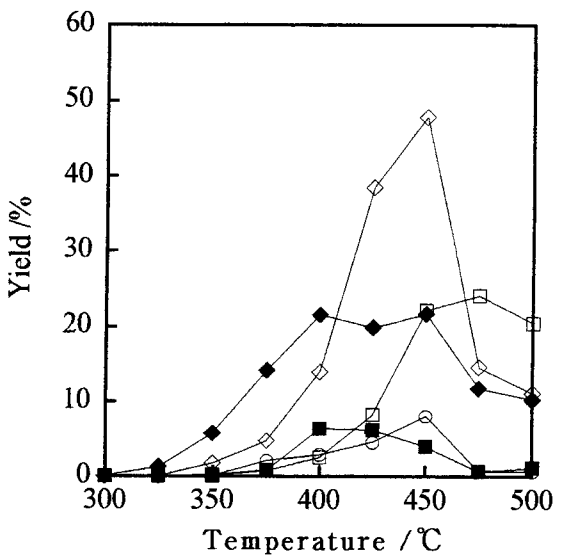

Fig. 6-8. Yields of cracking products from cumene over cerium phosphates prepared form H_3PO_4, ○; Monazite-type $CePO_4$, ■; CeP_2O_7, ◇; $Ce(PO_3)_3$, ◆; $Ce(PO_3)_4$, and □; CeP_5O_{14}.

Figures 6-9 and 6-10 show XRD peak patterns of cerium phosphates prepared from H_3PO_4 before and after catalytic reaction. The sample in P/Ce=3 before catalytic reaction is a mixture of $Ce(PO_3)_3$ and CeP_2O_7. The sample in P/Ce=3 before catalytic reaction is a mixture of $Ce(PO_3)_3$ and CeP_2O_7. The sample in P/Ce=10 before and after catalytic reaction indicated the XRD peak pattern of CeP_5O_{14}. The peaks of CeP_2O_7 and $Ce(PO_3)_4$ became small in XRD results of samples after catalytic reaction. These results indicated that Ce(Ⅳ) phosphates were reduced to Ce(Ⅲ) phosphates by use as a catalyst in cracking / dehydrogenation reaction of cumene. Cerium phosphates were considered to be reduced by the

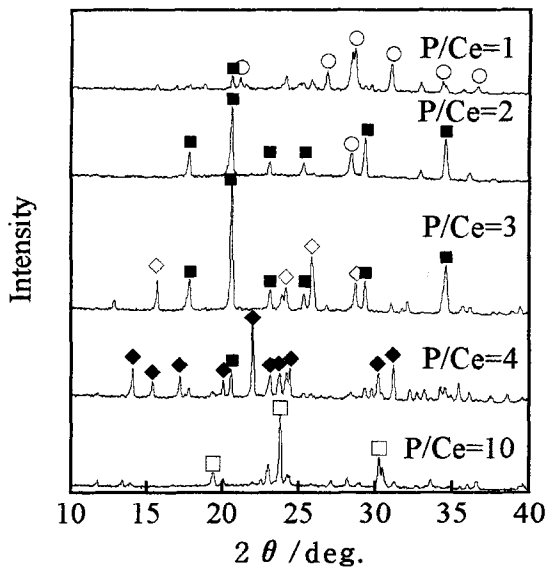

Fig. 6-9. XRD patterns of cerium phosphates prepared from H_3PO_4 before catalytic reaction, ○ ; Monazite-type $CePO_4$, ■ ; CeP_2O_7, ◇ ; $Ce(PO_3)_3$, ◆ ; $Ce(PO_3)_4$, and □ ; CeP_5O_{14}.

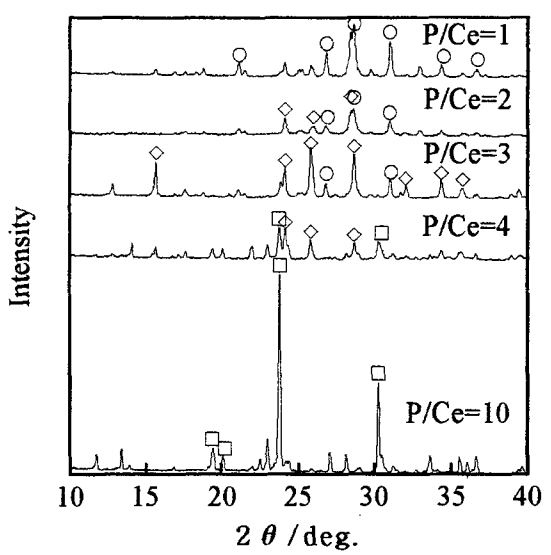

Fig. 6-10. XRD patterns of cerium phosphates prepared from H_3PO_4 after catalytic reaction, ○ ; Monazite-type $CePO_4$, ◇ ; $Ce(PO_3)_3$, and □ ; CeP_5O_{14}.

following equations.

$$2CeP_2O_7 \rightarrow CePO_4+Ce(PO_3)_3+1/2O_2$$

$$2Ce(PO_3)_4 \rightarrow Ce(PO_3)_3+CeP_5O_{14}+1/2O_2$$

The oxygen produced from these reactions attacked to cumene in oxidative dehydrogenation. Cerium phosphates were reduced at about 400～425℃ and cumene was oxidated to α -methylstylene by oxidative dehydrogenation reaction. All cerium phosphates were unchanged by heating under air condition below 700℃ from XRD analyses. These reactions caused low selectivity of cumene to benzene and propylene. Conversion of cumene over cerium phosphates became small by transformation from Ce(Ⅳ) phosphates to Ce(Ⅲ) salts. It was considered that Ce(Ⅳ) phosphates had higher catalytic activity than Ce(Ⅲ) salts.

The oxidative dehydrogenation reaction of cumene to α -methylstylene was thought to cause the reduction of cerium phosphate. It was interesting that cerium phosphate reduced in the presence of cumene at 400～450℃.

6.3.4. Isomerization reaction of butene

Figure 6-11 shows conversion of 1-butene, selectivities to *cis*-2-butene and *trans*-2-butene, and the ratio of *cis-/trans*-2-butene at several temperatures over Monazite- and Nd_2O_3. Conversion of 1-butene increased with temperature rising, however the ratio of *cis-/trans*-2-butene decreased. Because *trans*-2-butene was more thermodynamically stable than *cis*-2-butene, 1-butene was considered to transform to *trans*-2-butene selectively at higher temperature. Figure 6-12 shows results of isomerization reaction of butene over the above Monazite-type $NdPO_4$ on several contact times. In the case of BPO_4, conversion of 1-butene was reported to have little change on contact time [16]. However, conversion of 1-butene over Monazite-type $NdPO_4$ rised with contact time increasing. The ratio of *cis-/trans*-2-butene was less influenced on

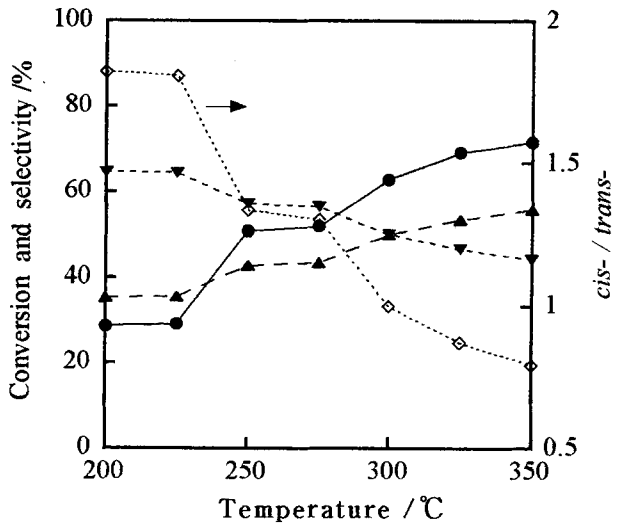

Fig. 6-11. Conversion of 1-butene(●), selectivities to *cis*-2-butene (▼) and *trans*-2-butene(▲), and the ratio of *cis-/trans*-2-butene(◇) at several temperatures over Monazite-type NdPO4 prepared from H3PO4 (15.8 mg•min•ml^{-1}, 200 torr).

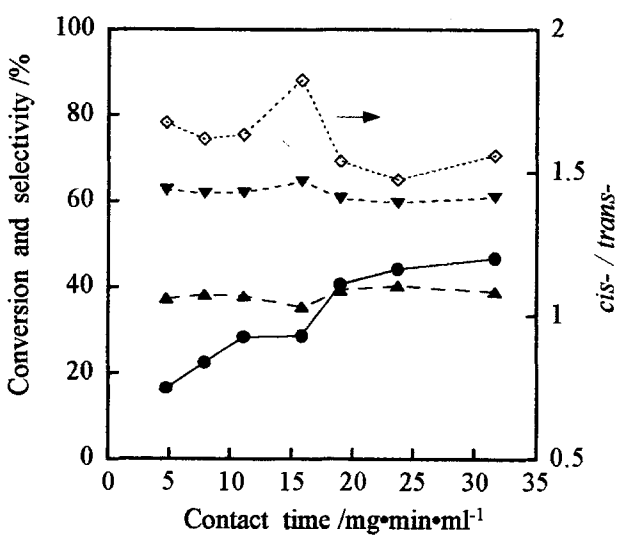

Fig. 6-12. Conversion of 1-butene(●), selectivities to *cis*-2-butene (▼) and *trans*-2-butene(▲), and the ratio of *cis-/trans*-2-butene(◇) over Monazite-type NdPO4 prepared from H3PO4 on several contact time (200℃, 200 torr).

contact time. Figure 6-13 shows results of isomerization reaction of butene over the Monazite-type NdPO4 on several butene-pressures. By an increase of amount of induced 1-butene molecule, conversion of 1-butene decreased a little. The ratio of *cis-/trans*-2-butene had less change by amount of butene molecule.

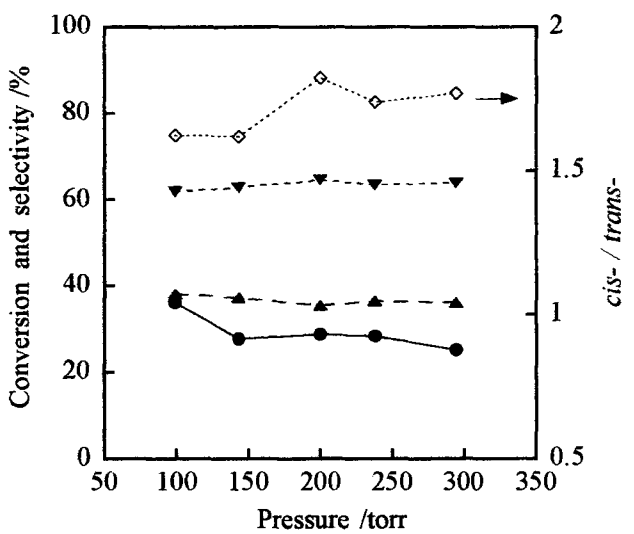

Fig. 6-13. Conversion of 1-butene(●), selectivities to *cis*-2-butene (▼) and *trans*-2-butene(▲), and the ratio of *cis-/trans*-2-butene(◇) over Monazite-type NdPO4 prepared from H3PO4 on several butene-pressure (200℃, 15.8 mg•min•ml^{-1}).

Table 6-5 shows results of isomerization reaction of butene over Monazite-type rare earth (La, Ce, Pr, Nd, and Sm) orthophosphates and Xenotime-type rare earth (Yb and Y) orthophosphates prepared from H3PO4. Monazite-type cerium orthophosphate indicated lower conversion of 1-butene than other rare earth (La, Pr, Nd, Sm,

Table 6-5 Results of isomerization reaction of butene over Monazite-type rare earth (La, Ce, Pr, Nd, and Sm) orthophosphates and Xenotime-type rare earth (Yb and Y) orthophosphates prepared from H_3PO_4 (300℃, 15.8 mg•min•ml^{-1}, 200 torr)

rare earth element	Conversion / %	Selectivity *cis-* /%	*trans-* /%	*cis-/trans-* -
La	66.9	45.9	54.1	0.849
Ce	21.5	50.0	50.0	1.000
Pr	59.0	43.5	56.5	0.771
Nd	62.7	50.0	50.0	1.000
Sm	73.5	41.5	58.5	0.709
Yb	74.1	40.7	59.3	0.687
Y	77.8	40.6	59.4	0.685

cis- = *cis*-2-butene, *trans-* = *trans*-2-butene.

Yb, and Y) orthophosphates. Table 6-6 shows results over various neodymium phosphates. Monazite-type and Rhabdophane-type neodymium orthophosphates prepared from phosphoric acid had high conversion of 1-butene. Neodymium polyphosphates and ultraphosphates prepared from $(NH_4)_2HPO_4$ and H_3PO_4 produced *cis*-2-butene selectively. Table 6-7 shows results over various cerium phosphates. As mentioned above, cerium orthophosphate had lower conversion than other rare earth (La, Pr, Nd, Sm, Yb, and Y) phosphates. However, cerium condensed

Table 6-6 Results of isomerization reaction of butene over various neodymium phosphates (300℃, 15.8 mg•min•ml^{-1}, 200 torr)

phosphate		Conversion / %	Selectivity *cis-* /%	*trans-* /%	*cis-/trans-* -
M-NdPO4	(NH4)2HPO4*	6.5	46.5	53.6	0.867
	H3PO4	62.7	50.0	50.0	1.000
R-NdPO4	H3PO4	62.5	46.5	53.5	0.868
Nd(PO3)3	(NH4)2HPO4	29.5	58.9	41.1	1.431
	H3PO4	8.7	61.9	38.1	1.624
NdP5O14	(NH4)2HPO4	1.6	55.6	44.4	1.250
	H3PO4	11.5	69.2	30.8	2.250

M- and R-NdPO4 represented Monazite-type and Rhabdophane-type NdPO4, respectively. *cis-* = *cis*-2-butene, *trans-* = *trans*-2-butene. *; This phosphate was prepared at 1000℃ for 20 hours. Other phosphates were prepared at 700℃ for 20 hours.

phosphates (CeP2O7, Ce(PO3)3, Ce(PO3)4, and CeP5O14) indicated the similar conversion of 1-butene and the ratio of *cis-/trans*-2-butene with other rare earth (La, Pr, Nd, Sm, Yb, and Y) polyphosphates and ultraphosphates. Cerium condensed phosphates (CeP2O7, Ce(PO3)3, Ce(PO3)4, and CeP5O14) prepared from H3PO4 had the similar selectivities of 1-butene to *cis*-2-butene and *trans*-2-butene. The kind of phosphorus resource ((NH4)2HPO4 and H3PO4) gave some influence on catalytic activities for isomerization reaction of butene.

Table 6-7 Results of isomerization reaction of butene over various cerium phosphates (300℃, 15.8 mg•min•ml^{-1}, 200 torr)

phosphate		Conversion / %	Selectivity *cis-* /%	*trans-* /%	*cis-/trans-* -
M-CePO4	(NH4)2HPO4*	0	-	-	-
	H3PO4**	21.5	50.0	50.0	1.000
CeP2O7	(NH4)2HPO4	21.8	59.9	40.1	1.493
	H3PO4	1.8	58.1	41.9	1.384
Ce(PO3)3	(NH4)2HPO4	24.0	50.5	49.5	1.021
	H3PO4	15.4	59.0	41.0	1.441
Ce(PO3)4	(NH4)2HPO4	9.9	62.4	37.6	1.658
	H3PO4	13.4	60.7	39.3	1.542
CeP5O14	(NH4)2HPO4	0	-	-	-
	H3PO4	1.1	59.0	41.0	1.441

M-CePO4 represented Monazite-type CePO4. *cis-* = *cis*-2-butene, *trans-* = *trans*-2-butene. *; This phosphate was prepared at 900℃ for 20 hours. **; This phosphate was prepared at 600℃ for 20 hours. Other phosphates were prepared at 700℃ for 20 hours.

6.4. Conclusion

Various rare earth phosphates (rare earth elements; R=La, Ce, Pr, Nd, Sm, Yb, and Y, phosphate; Monazite-type, Xenotime-type, Rhabdophane-type, and

Weinshenkite-type orthophosphates, polyphosphate, and ultraphosphate) were obtained by heating the mixtures of rare earth oxide - $(NH_4)_2HPO_4$ and rare earth oxide - H_3PO_4 in several ratios of phosphorus and rare earth elements. Rare earth orthophosphates prepared from H_3PO_4 had larger specific surface area than rare earth polyphosphates and ultraphosphates. All rare earth phosphates works as acidic catalysts, not as basic catalysts. Catalytic activities of rare earth phosphates verified from kind of rare earth elements (La, Ce, Pr, Nd, Sm, Yb, and Y), kind of phosphates (Monazite-type, Xenotime-type, Rhabdophane-type, and Weinshenkite-type orthophosphates, polyphosphate, and ultraphosphate), and kind of phosphorus resources ($(NH_4)_2HPO_4$ and H_3PO_4). Especially, cerium phosphates had characteristic catalytic activities.

6.5. References

[1] M. Tsuhako, S. Ikeuchi, T. Matsuo, I. Motooka, and M. Kobayashi, Bull. Chem. Soc. Jpn., **52**, 1034, (1979).

[2] A. F. Selevich, A. S. Lyakhov, and A. I. Lesnikovich, Phosphorus Res. Bull., **10**, 171, (1999).

[3] H. Nariai, H. Taniguchi, H. Maki, and I. Motooka, Phosphorus Res. Bull., **8**, 119, (1998).

[4] H. Onoda, H. Nariai, H. Maki, and I. Motooka, Phosphorus Res. Bull., **9**, 69, (1999).

[5] M. R. Mostafa and A. M. Youssef, Mater. Lett., **34**, 405, (1998).

[6] K. Yamamoto and Y. Abe, J. Am. Ceram. Soc., **81**, 2201, (1998).

[7] E. A. El-Sharkawy, M. R. Mostagfa, and A. M. Youssef, Coll. Surf. A; Physicochem. Eng. Asp., **157**, 211, (1999).

[8] J. J. Jimenez, P. M. Maireles, A. J. Lopez, and E. R. Castellon, J. Solid State Chem., **147**, 664, (1999).

[9] T. Mishra, K. M. Parida, and S. B. Rao, Appl. Catal. A: General, **166**, 115, (1998).

[10] A. C. B. dos Santos, W. B. Kover, and A. C. Faro, Appl. Catal. A: General, **153**, 83, (1997).

[11] Y. Takita, K. Sano, T. Muroya, H. Nishiguchi, N. Kawata, M. Ito, T. Akbay, and T. Ishihara, Appl. Catal. A: General, **170**, 23, (1998).

[12] Y. Takita, M. Ninomiya, H. Miyake, H. Wakamatsu, Y. Yoshinaga, and T. Ishihara, Phys. Chem., Chem. Phys., **1**, 4501, (1999).

[13] R. C. L. Mooney, Acta Cryst., **3**, 337, (1950).

[14] H. Y-P. Hong, Acta Cryst., **B30**, 468, (1974).

[15] D. Stachel and A. Olbertz, Phosphorus Res. Bull., **10**, 70, (1999).

[16] J. B. Moffat, Catal. Rev-sci. Eng., **18**, 199, (1978).

[17] Y. Sakai and H. Hattori, J. Catal., **42**, 37, (1976).

[18] R. F. Vogel and G. Marcelin, J. Catal., **80**, 492, (1983).

[19] A. Schmidmeyer and J. B. Moffat, J. Catal., **96**, 242, (1985).

[20] H. Itoh, A. Tada, H. Hattori, and K. Tanabe, J. Catal., **115**, 244, (1989).

[21] M. A. Aramendia, V. Borau, C. Jimenez, J. M. Marinas, F. J. Romero, and J. R. Ruiz, J. Coll. Interface Sci., **202**, 456, (1998).

[22] A. Waghray and E. I. Ko, Catal. Today, **28**, 41, (1996).

[23] S. Gao and J. B. Moffat, J. Catal., **180**, 142, (1998).

[24] R. A. Boyse and E. I. Ko, Catal. Lett., **38**, 225, (1996).

[25] P. Meriaudeau, A. V. Tuan, N. L. Hung, and G. Szabo, Catal. Lett., **47**, 71,

(1997).

[26] O. Johnson, J. Phys. Chem., **59**, 827, (1955).

[27] K. Nakamura, K. Eda, S. Hasegawa, and N. Sotani, Appl. Catal. A: General, **178**, 167, (1999).

Chapter 7.
Reforming by mechanochemical treatment of rare earth ultraphosphates for catalytic properties

Abstract

Rare earth ultraphosphates, RP_5O_{14}, were synthesized, and their mechanochemical effects due to grinding were investigated by using TG-DTA, XRD, FT-IR and SEM. When the ultraphosphates were ground, their XRD peaks became smaller, their particles were flocculated to be paste, and their P-O-P bondings were cleaved to form P-O-H bondings. The P-O-H bondings formed by mechanical treatment were expected to raise catalytic activities of rare earth ultraphosphates. The ultraphosphates reformed by grinding enlarged the surface areas, the acid strength, amount of acidic sites, and catalytic activity on dehydration reaction of 2-propanol and cracking / dehydrogenation reaction of cumene.

7.1. Introduction

One of the features of rare earth phosphates is to form specific crystal structure because the ionic radii of rare earth elements are larger than those of other metals. Ultraphosphates have the network structure which consists of the anions represented by $[P_{(n+2)}O_{(3n+5)}]^{n-}$ (n=2, 3, 4, 6). Because these anions contain more P-O-P bondings than chain and ring phosphates [1], ultraphosphates are generally unstable for hydrolysis, accordingly there are few stable salts except for rare earth salts. Consequently, there has been few reports about ultraphosphates.

In Chapter 6, rare earth ultraphosphate indicated low catalytic activities. The reforming of solid surface gives the powder higher functional properties. There are some kinds of reforming by coating, topochemical method, mechanical treatment,

ultraviolet irradiation, etc [2,3].

In this Chapter, the mechanochemical effects of some rare earth ultraphosphates by grinding were studied, and their mechanical reformings were attempted in order to use them as a solid acid catalyst. Furthermore, the influence of grinding media, water and ethanol, was also investigated in the same way with Chapters 1, 3, and 4.

7.2. Experimental

Each of rare earth oxides (La_2O_3, CeO_2, and Nd_2O_3) was mixed with phosphoric acid in the molar ratio of P/R=10, and then the mixture was heated at 700℃ for 20 hours [4]. Rare earth (La, Ce, and Nd) ultraphosphates were obtained by washing the thermal products with water to remove the excess phosphoric acid and dried in air.

Rare earth ultraphosphates (LaP_5O_{14}, CeP_5O_{14}, and NdP_5O_{14}) were treated with grinding-mill, and ground samples were taken out at the prescribed time interval for analyses [5,6]. Samples before and after mechanical treatment were analyzed by X-Ray diffractometry (XRD), fourier transform infrared spectroscopy (FT-IR), thermogravimetry - differential thermal analysis (TG-DTA), and scanning electron micrograph (SEM). Rare earth ultraphosphates were also ground with water or ethanol in the ratio of liquid (water or ethanol) / solid (rare earth ultraphosphate) equal about 5 ml/g, and then analyzed in the same methods. X-ray diffraction patterns were recorded on a Rigaku Denki RINT1200M X-Ray diffractometer using monochromated CuK α 1 radiation. The IR spectra were recorded on a HORIBA FT-IR spectrometer, FT-710 with a KBr disk method. TG-DTA were measured with a Rigaku Denki Thermo Plus TG8120. 15 ~ 20mg of sample was placed in a

platinum pan. Thermal analyses were carried out at 10℃/min. SEM images were observed using S2500 Hitachi Corp. Ltd. Scanning Electron Micrograph. The grinding apparatus was an Ishikawa's grinder equipped with an agate motor.

The ground samples were also estimated for catalytic properties. The surface areas of samples were calculated from the amount of nitrogen molecules adsorbed at the temperature of liquid nitrogen by five-points BET method (P/Po=0.10, 0.15, 0.20, 0.25 and 0.30) with a Gemini-Micromeritics 2360 from Shimadzu Corp. Ltd. [7]. Acidic properties (acidic strength and amount of acidic sites) were examined by n-butylamine titration using Hammett indicators in benzene [8]. The Hammett indicators were Methyl red (pKa=+4.8), Dimethyl yellow (pKa=+3.3), Benzeneazodiphenylamine (pKa=+1.5), and Dicinnamalacetone (pKa=-3.0).

A 0.2 g of a sample was mixed with about 2 mg of glass wool and then packed in a glass tube with about 10 mg of glass wool at both ends. Beforehand, glass wool was confirmed to have no activity for dehydration reaction of 2-propanol and cracking / dehydrogenation reaction of cumene.

The conversion was measured with a gas chromatograph G-3000 from Hitachi Corp. Ltd. during dehydration reaction of 2-propanol [9]. A column (ID. 3mm and length 2m) packed with Porapak Q and a thermocoupled detector were used. Helium was used as a carrier gas (20 cm^3/min). Injection volume of 2-propanol was 0.8 μ l. Injected 2-propanol was vaporized and carried to catalyst surface. 2-propanol, propylene and water were separated in the column and detected.

The conversion was estimated on a gas chromatograph G-3900 from Hitachi Corp. Ltd. on cracking / dehydrogenation reaction of cumene. A column (ID. 3mm and length 2m) packed with 15%TCEP on Uniport B (GL Science) and a thermo-couple detector were used. Helium was used as carrier gas in 20 mL/min flow rate. Pulse volume of cumene was 0.5 μ L. Other conditions were the same as for the

system for dehydration reaction of 2-propanol.

7.3. Results and discussion

7.3.1. Mechanochemical effects

As shown in Fig. 7-1, X-ray diffraction peaks of neodymium ultraphosphate became smaller with the increasing of grinding time, and then the sample treated for 7 days was amorphous. Figure 7-2 shows the changes of infrared spectra of NdP_5O_{14} due to grinding. IR spectra of treated samples contained two new peaks at about 1640 and 3300 cm^{-1}. These peaks were assigned to O-H stretching vibration [10] based on adsorbed water.

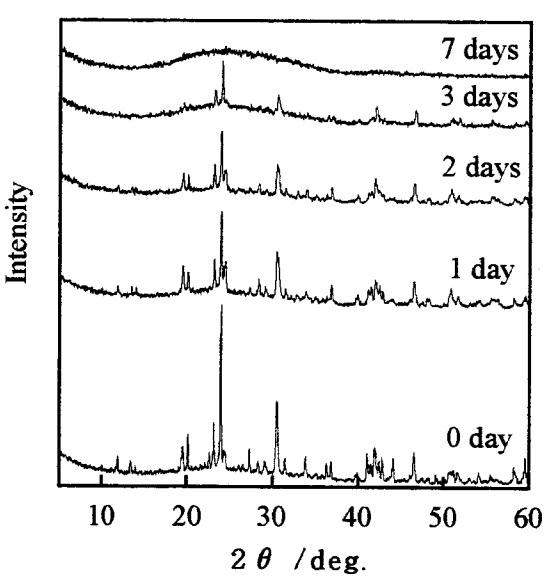

Fig. 7-1. XRD patterns of NdP_5O_{14} treated with grinding-mill for several days.

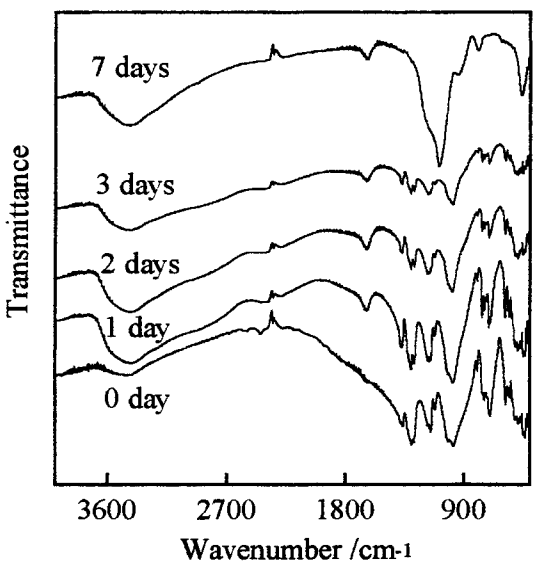

Fig. 7-2. IR spectra of NdP_5O_{14} treated with grinding-mill for several days.

Figure 7-3 shows TG-DTA curves of NdP_5O_{14} treated with grinding-mill. Treated phosphates had an endothermic peak at $< 100℃$ in DTA curves. Although the untreated sample didn't have weight loss in TG curves, the treated samples have the weight loss caused by adsorbed water. The samples ground for 2 and 3 days have some endothermic peaks accompanied with the weight loss at $350 \sim 400℃$. This result indicated that the P-O-H bonding produced by grinding was condensed to P-O-P bonding. In XRD results of heated products, the peaks of neodymium polyphosphate were observed with those of neodymium ultraphosphate. The endothermic peak by condensation of the sample treated for 1 day wasn't observed, because it had little P-O-H bonding.

Figure 7-4 shows SEM photographs of neodymium ultraphosphate treated for

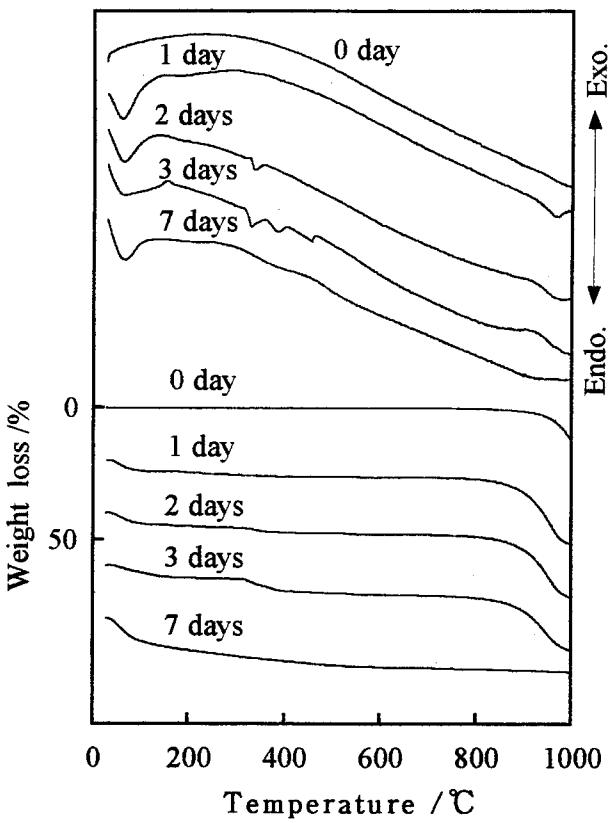

Fig. 7-3. TG-DTA curves of NdP5O14 treated with grinding-mill for several days.

several days. The flocculation of samples occurred by grinding and the size of their particles became larger. The hydrogen bonding formed by the P-O-H groups served as a cohesive force.

The mechanochemical effects of LaP5O14 and CeP5O14 were similar to those of NdP5O14.

It was found from the above results that rare earth ultraphosphates were affected greatly by mechanical treatment, that is, the grinding destroyed their crystal structure and triggered the cleavage of P-O-P bonding.

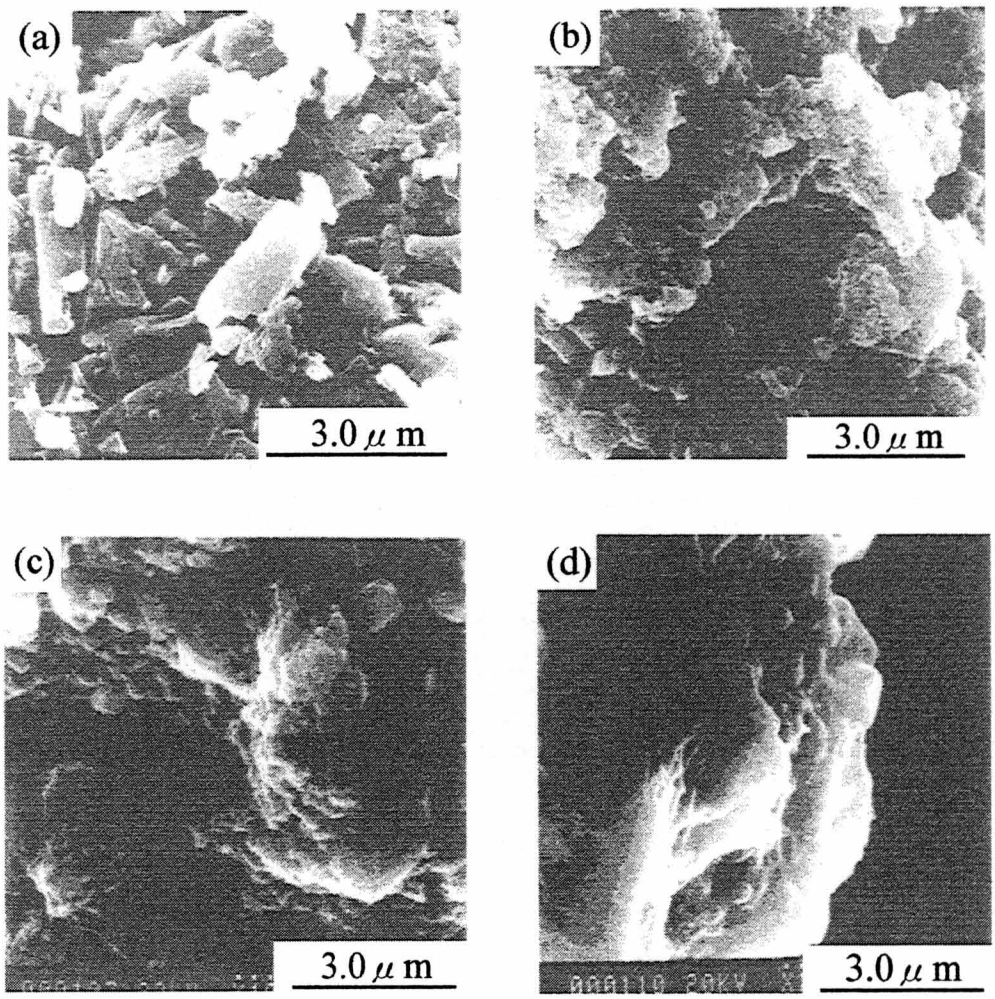

Fig. 7-4. SEM images of NdP_5O_{14} treated with grinding-mill for several days, (a) 0 day, (b) 1 day, (c) 2days, and (d) 3 days.

7.3.2. Catalytic properties

The formation of P-O-H bonding is expected to improve the ability of rare earth ultraphosphate as solid acid catalyst. When rare earth ultraphosphates were ground for long time, their particles aggregated and their surface areas became smaller, and the ground samples became paste. Therefore, the surface areas, acidic properties and the catalytic activity of the samples treated for short time were investigated.

Figure 7-5 shows the changes of the surface areas of ground neodymium ultraphosphates. The surface areas of NdP_5O_{14} became larger with increase of grinding time. The treatment of more long time made the measurement of surface area difficult because samples flocculated and became paste.

Figure 7-6 shows the changes of the acid strength and amount of acidic sites due to grinding. The acid strength of untreated material was between +3.3 and +1.5 in pKa unit, and its amount of acidic sites was very small. In contrast, the acid strength of sample treated for 6 hours became stronger than -3.0, and the amounts of acidic sites remarkably increased. The acidic strength and amount of the sample treated for 12 hours became lower. Figure 7-7 shows the conversion of 2-propanol to propylene over neodymium ultraphosphates at 200℃, 225℃ and 250℃. Although at 250℃ the ultraphosphate untreated converted 5.2% of 2-propanol into propylene, the sample treated for 1 hour transformed 80.2% of 2-propanol into propylene. The sample treated for 6 hours had the best catalytic activities.

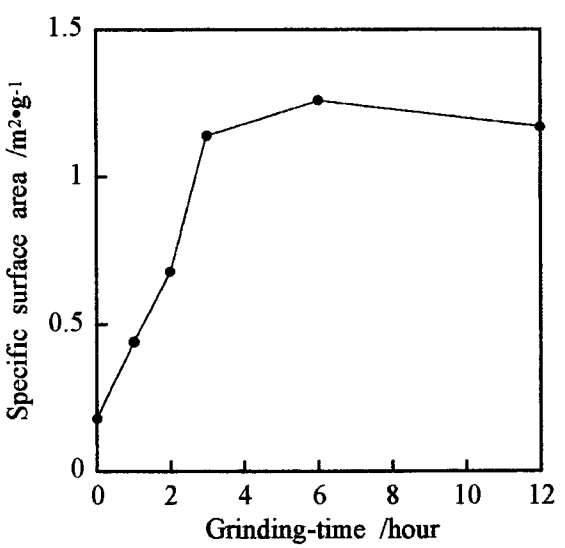

Fig. 7-5. Specific surface area of NdP_5O_{14} ground for several hours.

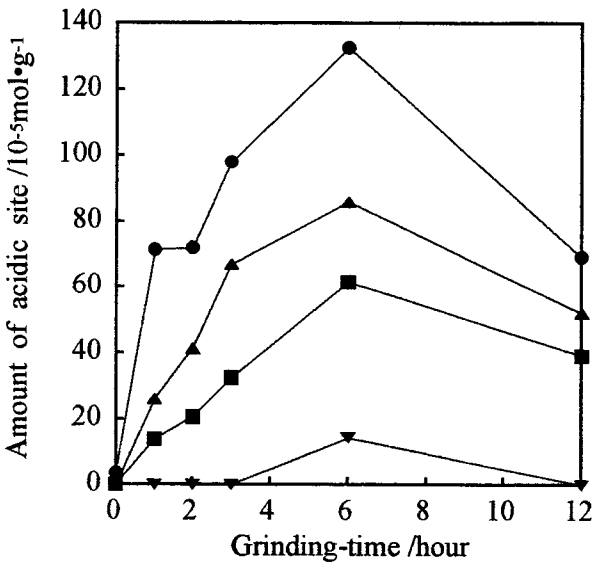

Fig. 7-6. Acid strength and amount of acidic sites on NdP5O14 ground for several hours, ●; Ho ≦ +4.8, ▲; Ho ≦ +3.3, ▼; Ho ≦ +1.5, and ◆; Ho ≦ -3.0.

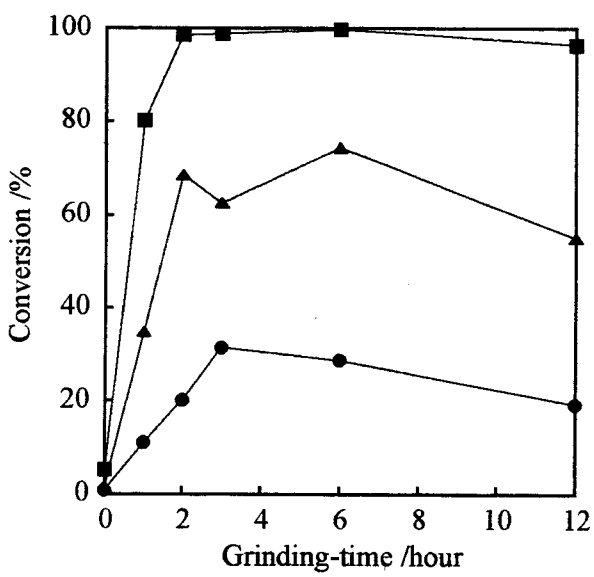

Fig. 7-7. Conversion of 2-propanol to propylene over NdP5O14 ground for several hours, ●; 200℃, ▲; 225℃, and ■; 250℃.

The catalytic properties of LaP_5O_{14} and CeP_5O_{14} were examined in the same method, and obtained similar results. Only CeP_5O_{14} treated for 12 hours produced a little acetone with propylene.

7.3.3. Grinding media

As mentioned in Chapters 1, 3, and 4, water and ethanol improved mechanochemical effect as grinding media. The influence of grinding media, water and ethanol, was also investigated on reforming of rare earth ultraphosphate. Little change was observed in XRD, FT-IR, and TG-DTA results between samples treated with and without grinding media. Table 7-1 shows specific surface areas of neodymium ultraphosphates in several conditions. Samples ground with ethanol had large specific surface area. This result was corresponded with that in Chapter 3 (Table 3-1). Grinding with ethanol was effective way to obtain large specific surface area both as pretreatment before thermal synthesis and as reforming of rare earth phosphate. These effects were considered to be suffered from prevention for flocculation by ethanol. Figure 7-8 shows acid strength and amount of acidic sites of NdP_5O_{14}.

Table 7-1 Specific surface area of NdP_5O_{14} in several conditions, (a); non-ground, (b); ground for 6 hours, (c); ground with water for 6 hours, and (d); ground with ethanol for 6 hours

condition	specific surface area /$m^2 \cdot g^{-1}$
(a)	0.18
(b)	1.26
(c)	1.28
(d)	1.39

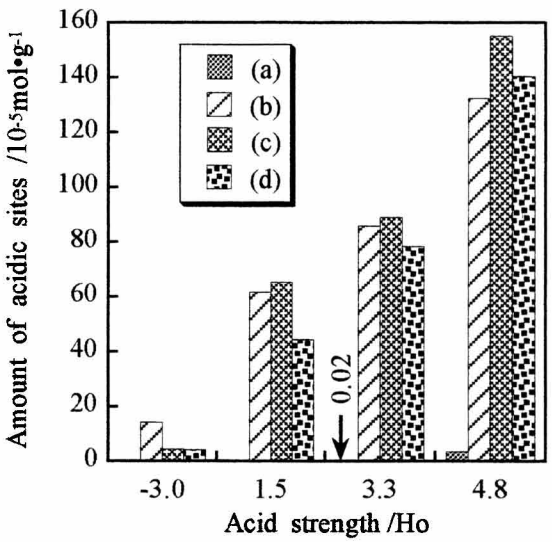

Fig. 7-8. Acid strength and amount of acidic sites of NdP5O14 in several conditions, (a); non-ground, (b); ground for 6 hours, (c); ground with water for 6 hours, and (d); ground with ethanol for 6 hours.

Amount of acidic sites became larger by mechanochemical treatment with water. Figure 7-9 shows the conversion of 2-propanol to propylene over NdP5O14. The difference was little observed between samples milled with and without grinding media. Figure 7-10 shows conversion of cumene over NdP5O14 at several conditions. Ground sample indicated high conversion, whereas sample ground with water had low conversion. Figure 7-11 shows selectivity of cumene to benzene and propylene over NdP5O14. All ground samples had higher selectivity than non treated sample. Figure 7-12 shows yields of cracking products over NdP5O14. Ground sample and sample ground with ethanol had advantage to obtain cracking products. Lanthanum and cerium salts had each tendency on mechanochemical effects for catalytic properties.

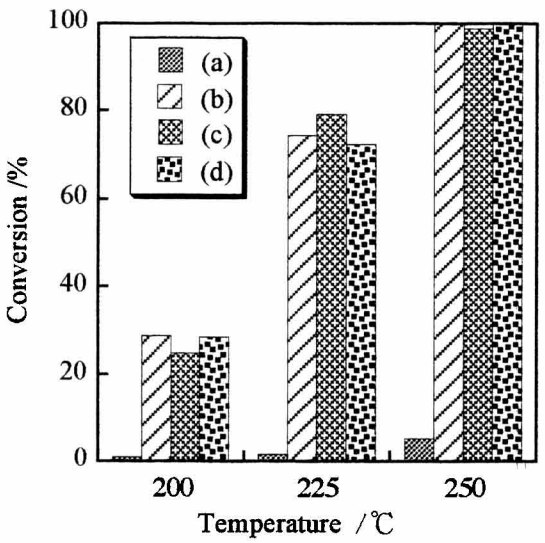

Fig. 7-9. Conversion of 2-propanol to propylene over NdP_5O_{14} in several conditions, (a); non-ground, (b); ground for 6 hours, (c); ground with water for 6 hours, and (d); ground with ethanol for 6 hours.

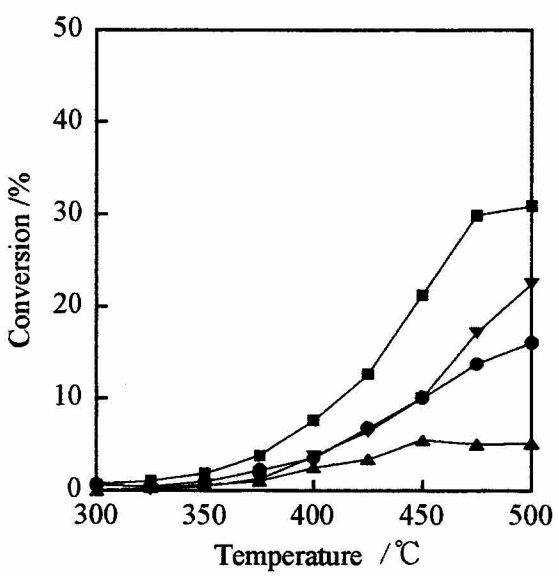

Fig. 7-10. Conversion of cumene over NdP_5O_{14} in several conditions, ●; non-ground, ■; ground for 6 hours, ▲; ground with water for 6 hours, and ▼; ground with ethanol for 6 hours.

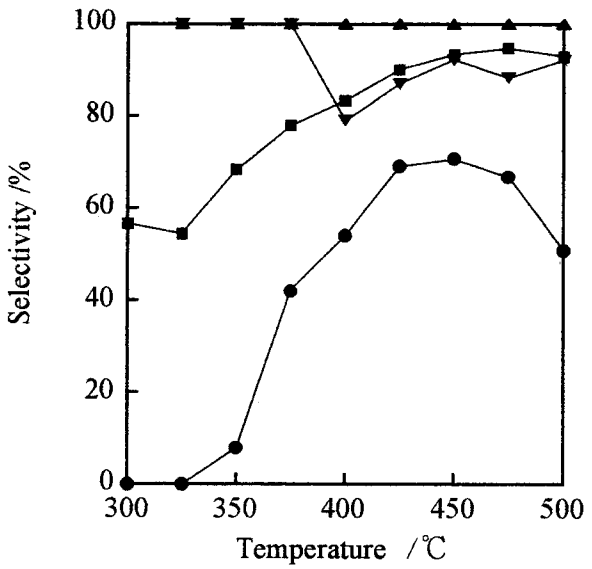

Fig. 7-11. Selectivity of cumene to cracking products over NdP5O14 in several conditions, ●; non-ground, ■; ground for 6 hours, ▲; ground with water for 6 hours, and ▼; ground with ethanol for 6 hours.

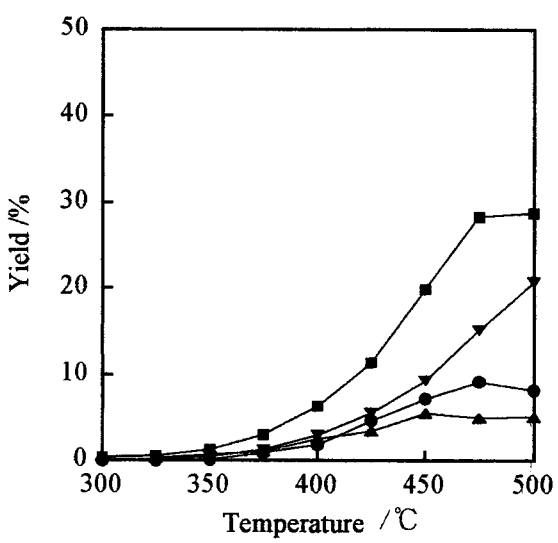

Fig. 7-12. Yields of cracking products over NdP5O14 in several conditions, ●; non-ground, ■; ground for 6 hours, ▲; ground with water for 6 hours, and ▼; ground with ethanol for 6 hours.

7.4. Conclusion

By grinding, the intensity of X-ray diffraction lines of ultraphosphate became smaller and its P-O-P bonding changed to P-O-H bonding. The reforming based on these mechanochemical effects enlarged the catalytic abilities of rare earth ultraphosphates. Grinding media (water and ethanol) were effective on mechanochemical reforming of rare earth ultraphosphate.

7.5. References

[1] A. Durif, "CRYSTAL CHEMISTRY OF CONDENSED PHOSPHATES", Chap. 6, pp. 359-374, Plenum Publishing Corp., New York, 1995.

[2] H. Honda, J. Soc. Mat. Sci., Jpn., **46**, 703, (1997).

[3] T. Kubo, "Mechanochemistry Gairon", Chap. 9, Sec. 5, pp. 176-190, Tokyo kagaku dojin, Tokyo, 1978.

[4] M. Tsuhako, S. Ikeuchi, T. Matsuo, I. Motooka, and M. Kobayashi, Bull. Chem. Soc. Jpn., **52**, 1034, (1979).

[5] Y. Hikichi, T. Sasaki, K. Murayama, T. Nomura, and M. Miyamoto, J. Am. Ceram. Soc., **72(6)**, 1073, (1989).

[6] H. Nariai, I. Motooka, M. Doi, and M. Tsuhako, Bull. Chem. Soc. Jpn., **58**, 379, (1985).

[7] S. Kondo, T. Ishikawa, and I. Abe, "Science of Adsorption", Chap. 3, Sec. 2, pp. 33-58, Maruzen Ltd., Tokyo, 1991.

[8] O. Johnson, J. Phys. Chem., **59**, 827, (1955).

[9] H. Nariai, H. Taniguchi, H. Maki, and I. Motooka, Phosphorus Res. Bull., **8**, 119, (1998).

[10] D. E. C. Corbridge and E. J. Lowe, J. Chem. Soc., **493**, 4555, (1954).

Chapter 8.
Synthesis and catalytic properties of copper and magnesium *cyclo*-tetraphosphates containing rare earth elements

Abstract

Basic copper or magnesium carbonate was mixed with phosphoric acid in the mole ratio of P/M=2 (M; Cu or Mg). Each mixture was transformed to *cyclo*-tetraphosphate by heating. A part of the basic copper or magnesium carbonate was replaced with a rare earth oxide (La_2O_3, CeO_2, Pr_6O_{11}, Nd_2O_3, Sm_2O_3, Yb_2O_3, or Y_2O_3) in this system. These mixtures containing one of the rare earth oxides were heated, and then the products were analyzed by XRD, FT-IR, and TG-DTA. It was observed in copper system that the product changed from *cyclo*-tetraphosphate to pyrophosphate by the addition of rare earth oxide used in this study. In magnesium system, magnesium *cyclo*-tetraphosphate was formed in spite of the addition of rare earth oxide. Surface properties, specific surface area, acid strength and amount of acid sites, catalytic activity for dehydration reaction of 2-propanol and cracking / dehydrogenation reaction of cumene, were measured to clarify the role of rare earth element in magnesium *cyclo*-tetraphosphate.

8.1. Introduction

Phosphates are transformed to other phosphates in hydrolysis and dehydration reactions at elevated temperatures [1-3]. There are polyphosphate, *cyclo*-phosphate, and ultraphosphate in a group of condensed phosphates. Polyphosphate has a chain structure in which PO_4 unit shares two oxygen atoms, *cyclo*-phosphate has a cyclic structure, and ultraphosphate has a network structure [4].

Orthophosphate, polyphosphate, and ultraphosphate of rare earth elements were formed by heating a mixture of a rare earth oxide and phosphoric acid in P/R ratio = 1, 3, and 10 (R: rare earth element), respectively [1]. However a rare earth *cyclo*-phosphate wasn't formed by only heating. It was formed from a sodium *cyclo*-phosphate solution and a rare earth nitrate solution [5,6]. This salt was decomposed to ortho-, pyro-, triphosphate, and so on above 100℃. For this reason, there is few study about surface properties of rare earth *cyclo*-phosphates.

Previously, magnesium, manganese, cobalt, nickel, copper, and zinc *cyclo*-tetraphosphates were synthesized and investigated on their surface properties and catalytic activities for the dehydration reaction of 2-propanol [7]. The transformation of aliphatic primary and secondary alcohols to olefins and / or carbonyl compounds has been studied over various catalysts [8-12]. The dehydration occurs over acidic site, whereas the dehydrogenation occurs over basic or reducing sites. It is known that both dehydration and dehydrogenation occur in a 2-propanol conversion reaction over metal oxides and so on. 2-propanol is transformed to propylene over acid sites of materials and to acetone over basic sites [7,13-18]. Therefore, these reactions of 2-propanol are used as a probe to characterize both acidic and basic properties. On the other hand, cumene cracking / dehydrogenation reaction is used to estimate Lewis and Brönsted acid sites on metal oxides and so on [18-20]. Benzene and propylene are the cracking products mainly on Brönsted acid sites, whereas α-methylstyrene is a dehydrogenation product chiefly over Lewis acid sites.

The addition of rare earth elements gives higher functional properties to the material [21]. In this work, formation of binary *cyclo*-tetraphosphate was studied by replacing of copper or magnesium with rare earth elements in synthesis of *cyclo*-tetraphosphates. Furthermore, surface properties of the mixed phosphates were investigated to clarify the role of rare earth elements.

8.2. Experimental

8.2.1. Synthesis

A rare earth oxide (La_2O_3, CeO_2, Pr_6O_{11}, Nd_2O_3, Sm_2O_3, Yb_2O_3, or Y_2O_3) was mixed with a basic metal carbonate in the mole ratio of M/R = 100/0, 99/1, 97/3, 95/5, and 90/10 (M: Cu or Mg, R: La, Ce, Pr, Nd, Sm, Yb, or Y). Phosphoric acid was added to these mixtures in the mole ratio of P/(2M+3R)=1. Then the mixtures were heated at 420℃ for 1 hour, washed with water, and dried in air [4,8]. The products were analyzed by X-ray diffraction (XRD), Fourier transform infrared spectroscopy (FT-IR), and thermogravimetry - differential thermal analyses (TG-DTA). X-ray diffraction patterns were recorded on a Rigaku Denki RINT1200M X-Ray diffractometer using monochromated CuK α radiation. The IR spectra were recorded on a HORIBA FT-IR spectrometer, FT-710, with a KBr disk method. TG-DTA were performed with a Rigaku Denki Thermo Plus TG8120.

8.2.2. Specific surface area and acidic properties

The surface areas of samples were calculated from the amount of nitrogen molecules adsorbed at the temperature of liquid nitrogen by five-points BET method (P/Po=0.10, 0.15, 0.20, 0.25 and 0.30) with a Gemini-Micromeritics 2360 from Shimadzu Corp. Ltd. Acidic properties (acidic strength and amount of acidic sites) were examined by n-butylamine titration using Hammett indicators in benzene [22]. The Hammett indicators were Methyl red (pKa=+4.8), Dimethyl yellow (pKa=+3.3), Benzeneazodiphenylamine (pKa=+1.5), and Dicinnamalacetone (pKa=-3.0).

8.2.3. Dehydration reaction of 2-propanol

A 0.2 g of a sample was mixed with about 2 mg of glass wool and then packed

in a glass tube with about 10 mg of glass wool at both ends. Beforehand, glass wool was confirmed to have no activity for dehydration reaction of 2-propanol.

The conversion was measured with a gas chromatograph G-3000 from Hitachi Corp. Ltd. during dehydration reaction of 2-propanol. A column (ID. 3mm and length 2m) packed with Porapak Q and a thermocoupled detector were used. Helium was used as a carrier gas (20 cm^3/min). Injection volume of 2-propanol was 0.8 μ l. Injected 2-propanol was vaporized and carried to catalyst surface. 2-propanol, propylene and water were separated in the column and detected.

8.2.4. Cracking / dehydrogenation reaction of cumene

The conversion was estimated on a gas chromatograph G-3900 from Hitachi Corp. Ltd. on cracking / dehydrogenation reaction of cumene. A column (ID. 3mm and length 2m) packed with 15%TCEP on Uniport B (GL Science) and a thermo-couple detector were used. Helium was used as carrier gas in 20 mL/min flow rate. Pulse volume of cumene was 0.5 μ L. Other conditions were the same as for the system for dehydration reaction of 2-propanol.

8.3. Results and discussion

8.3.1. Synthesis

Figure 8-1 shows XRD results of samples in Cu-Sm system. Samples with Cu/Sm=100/0 and 99/1 indicated the peaks of copper *cyclo*-tetraphosphate, $Cu_2P_4O_{12}$, while a sample with Cu/Sm=90/10 showed a XRD pattern of copper pyrophosphate, $Cu_2P_2O_7$. Samples with Cu/Sm=97/3 and 95/5 were the mixture of copper *cyclo*-tetraphosphate and pyrophosphate. With decreasing the Cu/Sm ratio, the peaks of

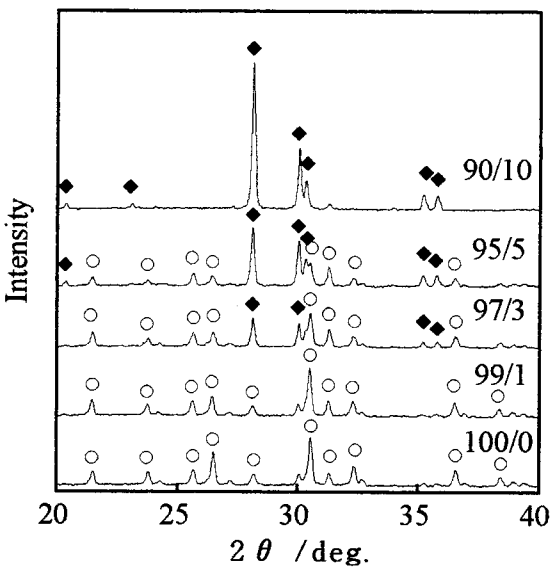

Fig. 8-1. XRD patterns of samples of Cu/Sm=100/0, 99/1, 97/3, 95/5, and 90/10, ○; Cu2P4O12 and ◆; Cu2P2O7.

copper *cyclo*-tetraphosphate became weaker, and the peaks of copper pyrophosphate became stronger. The addition of samarium changed the product from copper *cyclo*-tetraphosphate to pyrophosphate. The peaks of samarium compound were not observed in XRD patterns. The structure of copper *cyclo*-tetraphosphate was collapsed by replacing copper with samarium. On the other hand, the ratio of P/Cu in copper *cyclo*-tetraphosphate is 2, and that in copper pyrophosphate is 1. Copper pyrophosphate was formed in spite of this ratio (P/(2M+3R)=1) for formation of *cyclo*-tetraphosphate. The excess phosphoric acid which was caused from the formation of pyrophosphate was removed by washing with water.

Table 8-1 shows XRD results of mixed phosphates of copper and various rare earth elements. The peak which was due to any rare earth compound wasn't observed by XRD analyses. A sample with Cu/Pr=95/5 indicated the peaks of

Table 8-1 XRD analysis of samples of different Cu/R=(100 − α)/ α

	La	Ce	Pr	Nd	Sm	Yb	Y
ionic radius* /pm	116.0	114.3	112.6	110.9	107.9	98.5	101.9
α = 0	P4m	P4m	P4m	P4m	P4m	P4m	P4m
1	P4m	P4m	P4m	P4m	P4m	P4m	P2
3	P4m	P4m	P4m	P4m	P4m+P2	P4m+P2	P2
5	P2	P2+P4m	P4m	P2+P4m	P2+P4m	P4m+P2	P2
10	P2	P2+P4m	P4m+P2	P2	P2	P4m+P2	P2

*; coordination number 8, R. D. Shannon, Acta Cryst., **A32**, 751, (1976). P4m; $Cu_2P_4O_{12}$ and P2; $Cu_2P_2O_7$.

copper *cyclo*-tetraphosphate. On the other hand, a sample with Cu/Y=99/1 had the peaks of copper pyrophosphate. The ability to change the products from *cyclo*-tetraphosphate to pyrophosphate depends on the kind of rare earth cations. The ability of yttrium was stronger than others. Transformation of the products depended less on ionic radius of rare earth elements.

All mixed salts of magnesium and rare earth element indicated XRD peaks assigned to magnesium *cyclo*-tetraphosphate. There was no diffraction peak due to a rare earth compound. IR spectra of these samples had the doublet at about 770 cm^{-1} which was caused from *cyclo*-tetraphosphate [23]. The results of TG-DTA indicated that all samples were stable at temperature from room temperature to 500℃.

The reason that copper system differed from magnesium system is that copper pyrophosphate is easy to form. Furthermore, the structure of copper *cyclo*-tetraphosphate was differed from structures of magnesium, manganese, cobalt, nickel, copper, and zinc *cyclo*-tetraphosphates [7].

8.3.2. Catalytic properties

Magnesium *cyclo*-tetraphosphate was formed even in the system of Mg/R=90/10. Surface properties were also investigated to clarify the role of rare earth element in magnesium *cyclo*-tetraphosphate.

Figure 8-2 shows specific surface areas of mixed *cyclo*-tetraphosphates of magnesium and lanthanum. All samples had small specific surface areas. Specific surface areas of the samples weren't much effected by the addition of rare earth elements.

Figure 8-3 shows the acid strengths and the amounts of acidic sites of mixed *cyclo*-tetraphosphate of magnesium and lanthanum. The maximum acid strength of magnesium *cyclo*-tetraphosphate was between +1.5 and -3.0. As contrasted, those of samples with Mg/La=95/5 and 90/10 were stronger than -3.0. A sample with Mg/La=99/1 had small amount of acidic sites. With increasing the content of lanthanum,

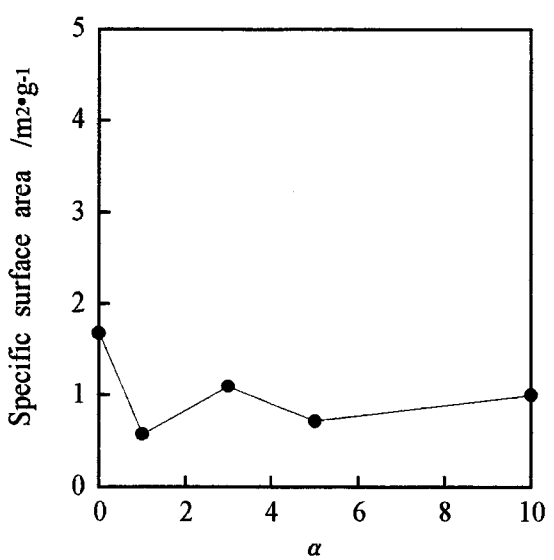

Fig. 8-2. Specific surface areas of mixed *cyclo*-tetraphosphates with Mg/La=(100- α)/ α .

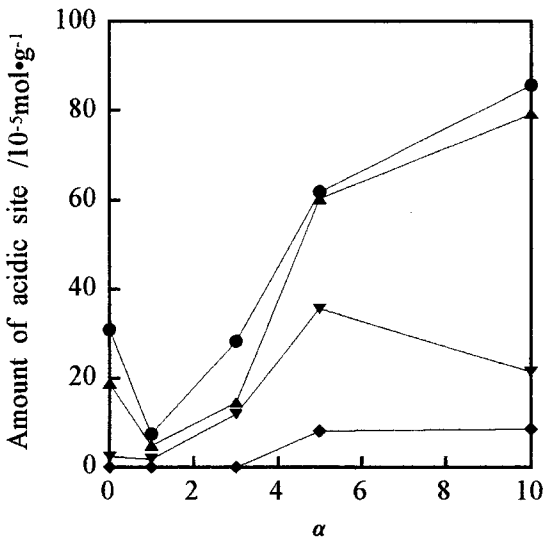

Fig. 8-3. Acid strengths and the amounts of acidic sites of mixed *cyclo*-tetraphosphates with Mg/La=(100- α)/ α , ●; Ho≦+4.8, ▲; Ho ≦ +3.3, ▼; Ho ≦ +1.5, and ◆; Ho ≦ -3.0.

the samples had large amounts of acidic sites. The addition of other rare earth element indicated the similar results. Rare earth element in *cyclo*-tetraphosphate was thought to improve the amount of acidic sites.

In this experiment, 2-propanol transformed to propylene without dehydrogenation product, acetone, over all mixed *cyclo*-tetraphosphates. These mixed *cyclo*-tetraphosphates worked as an acidic catalyst not as a basic catalyst. Figure 8-4 shows the conversion of 2-propanol to propylene over mixed *cyclo*-tetraphosphate of magnesium and lanthanum at 200℃, 225℃, and 250℃. The conversion of 2-propanol became large with increasing the α value. It was reported that the dehydration of 2-propanol to propylene was related to the amounts of acid sites at pKa≦+4.8 [7]. The promoted conversion obtained in this study was explained by the above relationship.

Figure 8-5 shows the conversion of cumene over mixed *cyclo*-tetraphosphate of

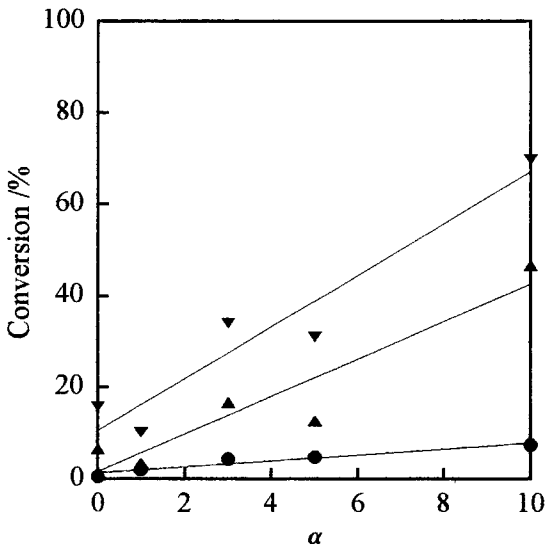

Fig. 8-4. Conversion of 2-propanol to propylene over mixed *cyclo*-tetraphosphates with Mg/La=(100- α)/ α , ●; 200℃, ▲; 225℃, and ▼; 250℃.

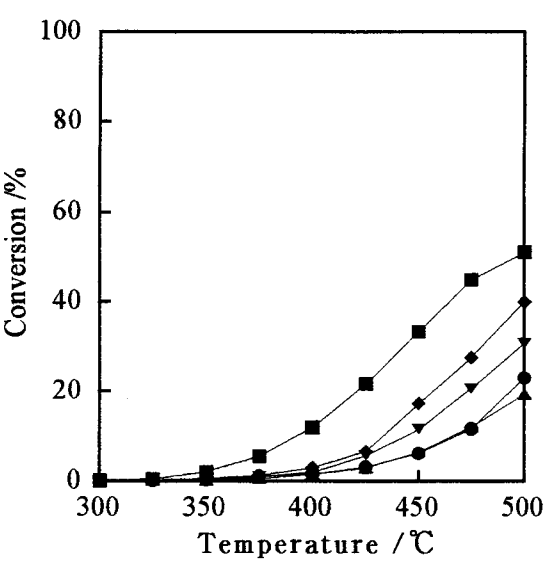

Fig. 8-5. Conversion of cumene over mixed *cyclo*-tetraphosphates of magnesium and lanthanum, ●; Mg/La=100/0, ▲; 99/1, ▼; 97/3, ◆; 95/5, and ■; 90/10.

magnesium and lanthanum at several temperatures. Magnesium *cyclo*-tetraphosphate had about 23% of cumene conversion at 500℃. The conversion of cumene increased with an increase in α value. The increase in amount of acidic sites also gave influence on the conversion of cumene. Figure 8-6 shows the selectivity of cumene to benzene and propylene over mixed *cyclo*-tetraphosphates of magnesium and lanthanum. At low temperatures, the selectivity of cumene to cracking products varied widely because of low conversion. Mixed *cyclo*-tetraphosphate of magnesium and lanthanum indicated high selectivity of cumene to benzene and propylene at high temperatures. The selectivity was raised slightly with increasing of the ratio of lanthanum. The addition of lanthanum into magnesium *cyclo*-tetraphosphate caused the increase in Brönsted acid sites.

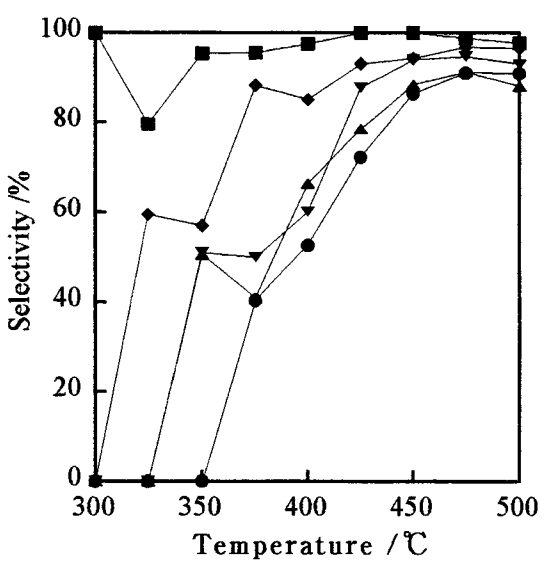

Fig. 8-6. Selectivity of cumene to benzene and propylene over mixed *cyclo*-tetraphosphates of magnesium and lanthanum, ●; Mg/La=100/0, ▲; 99/1, ▼; 97/3, ◆; 95/5, and ■; 90/10.

To take results of other rare earth elements into account, the kind of rare earth elements had a little influence on catalytic activities. The addition of a rare earth element improved amount of acidic sites on magnesium *cyclo*-tetraphophate. The conversions of 2-propanol and cumene were raised by the increasing of acid sites. Mixed *cyclo*-tetraphosphate of magnesium and a rare earth element had high activity as acidic catalyst than rare earth polyphosphate or ultraphosphate. *Cyclo*-phosphate was considered to be improved the catalytic activities by rare earth element.

8.4. Conclusion

The experimental results obtained in this Chapter are summarized as follows.

1. The thermal products were changed from *cyclo*-tetraphosphate to pyrophosphate by the addition of rare earth element in preparation of copper *cyclo*-tetraphosphate. Whereas, magnesium *cyclo*-tetraphosphate was formed in spite of the addition of rare earth element.

2. By the addition of rare earth element to magnesium *cyclo*-tetraphosphate, the increases of the amounts of acidic sites, the conversion of 2-propanol to propylene, and the conversion of cumene were observed.

8.5. References

[1] M. Tsuhako, S. Ikeuchi, T. Matsuo, I. Motooka, and M. Kobayashi, Bull. Chem. Soc. Jpn., **52**, 1034, (1979).

[2] A. F. Selevich, A. S. Lyakhov, and A. I. Lesnikovich, Phosphorus Res. Bull., **10**, 171, (1999).

[3] E. Thilo and I. Grunze, Z. Anorg. Allg. Chem., **290**, 209, (1957).

[4] H. Y-P. Hong, Acta Cryst., **B30**, 468, (1974).

[5] H. Nariai, J. Suenaga, M. Tsuhako, and I. Motooka, Phosphorus Res. Bull., **4**, 99, (1994).

[6] H. Onoda, H. Nariai, H. Maki, and I. Motooka, Mem. Grad. School Sci. & Technol., Kobe Univ., **18-A**, 39, (2000).

[7] H. Nariai , H. Taniguchi , H. Maki , and I. Motooka, Phosphorus Res. Bull., **8**, 119, (1998) .

[8] J. B. Moffat, Catal. Rev-sci. Eng., **18**, 199, (1978).

[9] Y. Sakai and H. Hattori, J. Catal., **42**, 37, (1976).

[10] R. F. Vogel and G. Marcelin, J. Catal., **80**, 492, (1983).

[11] A. Schmidmeyer and J. B. Moffat, J. Catal., **96**, 242, (1985).

[12] H. Itoh, A. Tada, H. Hattori, and K. Tanabe, J. Catal., **115**, 244, (1989).

[13] H. Onoda, H. Nariai, H. Maki, and I. Motooka, Phosphorus Res. Bull., **9**, 69, (1999).

[14] M. R. Mostafa and A. M. Youssef, Mater. Lett., **34**, 405, (1998).

[15] K. Yamamoto and Y. Abe, J. Am. Ceram. Soc., **81**, 2201, (1998).

[16] E. A. El-Sharkawy, M. R. Mostagfa, and A. M. Youssef, Coll. Surf. A; Physicochem. Eng. Asp., **157**, 211, (1999).

[17] J. J. Jimenez, P. M. Maireles, A. J. Lopez, and E. R. Castellon, J. Solid State Chem., **147**, 664, (1999).

[18] T. Mishra, K. M. Parida, S. B. Rao, Appl. Catal. A: General, **166**, 115, (1998).

[19] A. C. B. dos Santos, W. B. Kover, and A. C. Faro, Appl. Catal. A: General, **153**, 83, (1997).

[20] M. A. Aramendia, V. Borau, C. Jimenez, J. M. Marinas, F. J. Romero, and J. R. Ruiz, J. Coll. Interface Sci., **202**, 456, (1998).

[21] N. E. Topp, "Chemistry of the Rare Earth Elements", p.184, edited by J. Shiokawa and G. Adachi, Kagakudojin, Kyoto, 1974.

[22] O. Johnson, J. Phys. Chem., **59**, 827, (1955).

[23] D. E. C. Corbridge and E. J. Lowe, J. Chem. Soc., **493**, 4555, (1954).

Summary

In this work, some factors were discussed on formation of various rare earth phosphates. Then, thermal behavior of various rare earth phosphates was investigated to support the knowledge of formation of rare earth phosphates. Furthermore, thermostable rare earth phosphates were estimated for catalytic aspects.

In Chapter 1, mixing conditions of rare earth oxide and diammonium hydrogenphosphate were picked up on formation of various rare earth phosphates. The mixture of rare earth oxide and diammonium hydrogenphosphate was homogenized and activated by mechanical treatment. Water and ethanol worked as effective grinding media in mixing process of raw materials on formation of Monazite-type rare earth orthophosphate. Mechanical treatment and grinding media (water and ethanol) had the influence on formation of rare earth condensed phosphates in the manner as Monazite-type rare earth orthophosphate.

In Chapter 2, some rare earth compounds were used with phosphoric acid and diammonium hydrogenphosphate for formation of various rare earth phosphates. Rhabdophane-type cerium orthophosphate was not formed in the system using cerium oxide, however this phosphate was formed in the systems using cerium nitrate, chloride, and carbonate. The formation temperature and crystallinity of various rare earth phosphates were affected from raw rare earth compounds.

In Chapter 3, mechanochemical effects were investigated in the mixture of a rare earth compound (nitrate, chloride, or carbonate) and diammonium hydrogenphosphate.

Composition of thermal products and formation temperatures of rare earth phosphates were affected by mechanochemical treatment. The crystallinity of Rhabdophane-type rare earth phosphate was affected by mechanochemical treatment. The crystallinity of Rhabdophane-type rare earth phosphate was high in samples ground with water. Samples ground with ethanol had large specific surface areas.

In Chapter 4, urea or biuret was added into the thermal synthetic system of rare earth phosphate. The mixture of a rare earth compound (oxide, nitrate, chloride, or carbonate), a phosphorus compound (H_3PO_4 or $(NH_4)_2HPO_4$), and an additive (urea or biuret) was heated and the thermal products were analyzed. Urea and biuret worked not only as a dispersing agent but also as a reactant. The addition of urea or biuret was affected on compositions and specific surface areas of thermal products.

In Chapter 5, thermal behavior of various rare earth phosphates was investigated. Rare earth polyphosphate and ultraphosphate synthesized in thermal procedure changed to Monazite-type or Xenotime-type rare earth orthophosphate with volatillization of P_2O_5 by heating. Rare earth polyphosphate and *cyclo*-octaphosphate synthesized in solution reaction changed to polyphosphate by way of ortho-, pyro-, tri-, and oligo-phosphates, and finally transformed to Monazite-type or Xenotime-type rare earth orthophosphate.

In Chapter 6, catalytic characterization was studied as one of properties of various thermostable rare earth phosphates. Various rare earth phosphates were determined by use as catalyst on dehydration reaction of 2-propanol, cracking / dehydrogenation reaction of cumene, and isomerization reaction of butene. These results indicated

specificity of cerium phosphate with other rare earth phosphates. Catalytic properties verified from kind of rare earth elements and kinds of phosphates (ortho-, poly-, and ultra-phosphate.

Rare earth poly- and ultra-phosphates indicated low catalytic activity in Chapter 6. Therefore, in Chapter 7, the reforming of surface by mechanochemical treatment was tried for rare earth ultraphosphate. Rare earth ultraphosphate was treated mechanically, and then investigated on catalytic properties. By grinding, the intensity of X-ray diffraction lines of rare earth ultraphosphate became smaller and its P-O-P bonding changed to P-O-H bonding. The reforming based on these mechanochemical effects enlarged the catalytic abilities of rare earth ultraphosphates. Grinding media (water and ethanol) were effective on mechanochemical reforming of rare earth ultraphosphate.

Rare earth *cyclo*-phosphate was clarified to decompose easily by heating in Chapter 5. Therefore, catalytic activity of rare earth *cyclo*-phosphate was not investigated in Chapter 6. In Chapter 8, formation and catalytic properties of *cyclo*-phosphate containing rare earth element were studied. The thermal products were changed from *cyclo*-tetraphosphate to pyrophosphate by the addition of rare earth element in preparation of copper *cyclo*-tetraphosphate. Whereas, magnesium *cyclo*-tetraphosphate was formed in spite of the addition of rare earth element. By the addition of rare earth element to magnesium *cyclo*-tetraphosphate, the increases of the amounts of acidic sites, the conversion of 2-propanol to propylene, and the conversion of cumene were observed.

List of publications

Chapter 1.

H. Onoda, H. Nariai, H. Maki, and I. Motooka,

"Mixing Conditions of Raw Materials on Formation of Various Rare Earth Phosphates"

in preparation.

Chapter 2.

H. Onoda, H. Nariai, H. Maki, and I. Motooka,

"Syntheses of Various Rare Earth Phosphates from Some Rare Earth Compounds"

Materials Chemistry and Physics, **73**, 19, (2002).

Chapter 3.

H. Onoda, H. Nariai, H. Maki, and I. Motooka,

"Mechanochemical Effects on Synthesis of Rhabdophane-type Neodymium and Cerium Phosphates"

Materials Chemistry and Physics, submitted.

Chapter 4.

H. Onoda, H. Nariai, H. Maki, and I. Motooka,

"Addition of Urea or Biuret on Synthesis of Rhabdophane-type Neodymium and Cerium Phosphates"

Journal of Materials Synthesis and Processing, to be submitted.

Chapter 5.

H. Onoda, H. Nariai, H. Maki, and I. Motooka,

"Thermal Behavior of Rare-Earth *cyclo*-Octaphosphates"

Memoirs of Graduate School of Science & Technology, Kobe University,

18-A, 39, (2000).

Chapter 6.

H. Onoda, H. Nariai, A. Moriwaki, H. Maki, and I. Motooka,

"Formation and Catalytic Characterization of Various Rare Earth Phosphates"

Journal of Materials Chemistry, submitted.

Chapter 7.

H. Onoda, H. Nariai, H. Maki, and I. Motooka,

"Mechanochemical Effects of Some Rare-Earth Ultraphosphates and Reforming of Their Surface for Catalytic Properties"

Phosphorus Research Bulletin, **9**, 69, (1999).

Chapter 8.

H. Onoda, H. Nariai, H. Maki, and I. Motooka,

"Synthesis and Surface Properties of Copper and Magnesium *cyclo*-Tetraphosphates Containing Rare Earth Elements"

Phosphorus Research Bulletin, **12**, 139, (2001).

Acknowledgement

The author would like to express their sincere gratitude to Professor Itaru Motooka and Dr. Hiroyuki Nariai for their encouragement and suggestion thoughout this work.

The author also wishes to thanks Professor Mitsutomo Tsuhako, Dr. Hirokazu Nakayama, Ms. Hideko Inoue and Ms. Aki Hayashi of Kobe Pharmaceutical University and Dr. Atsushi Takenaka of Yonago National College of Technology for their valuable discussion and advise.

The author would like to thank to Professor Noriyuki Sotani, Dr. Kazuo Eda, and Dr. Takashi Suzuki for measurement of catalytic activity on isomerization reaction of butene. The author also would like to express sincere thanks to Professor Kimiaki Yamamura, Dr. Hideyoshi Miyake, Mr. Hideshi Maki, Ms. Kazuko Azumi, and Ms. Kazumi Nakazaki for their encouragement.

The author would like to express sincere gratitude to the colleagues of the Laboratory of Inorganic Polymer and Analytical Chemistry, Department of Chemical Science and Engineering, Kobe University, in particular, Ms. Ai Moriwaki, for their considerable assistance.

Finally, the author wishes to express his greatest gratitude to his grandparents and his parents for their hearty help, dedication and support throughout these years, without whom this work would not have been made possible.

Hiroaki Onoda

January, 2002